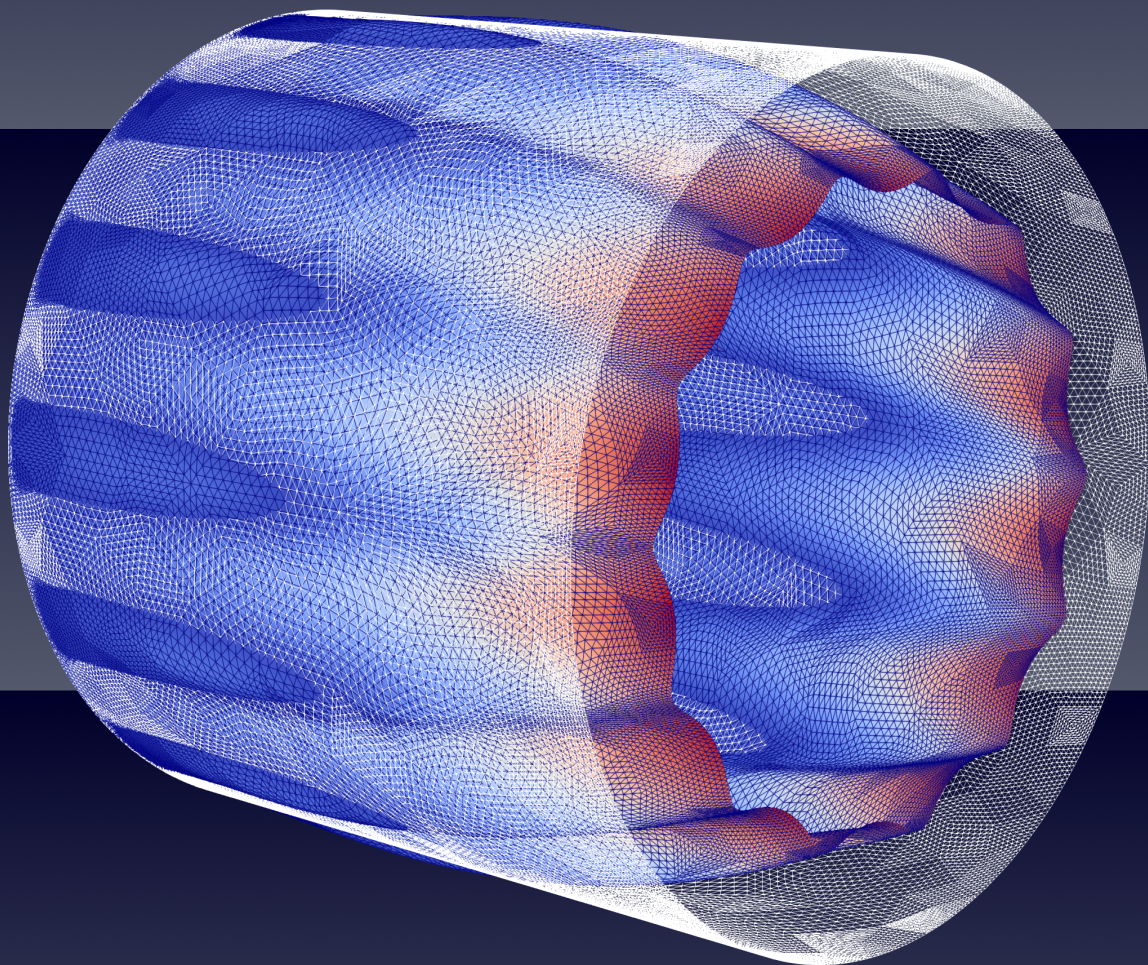


# Department of Precision and Microsystems Engineering

## On the use of Modal Derivatives in Nonlinear Dynamics.

Hessel Tijsseling

Report no : 2024.046  
Coach : Farbod Alijani and Alejandro Aragón  
Professor : Ron van Ostayen  
Specialisation : Engineering Dynamics  
Type of report : Master of Science Thesis  
Date : 9 July 2024



# Preface

The report that you are about to read, "On the use of Modal Derivatives in Nonlinear Dynamics", is the culmination of my career as a student of the Technical University of Delft. This thesis deals mainly on the use cases and limitations of modal derivatives-based model order reduction methods in dynamic analysis of thin-walled structures. As I could not have completed this on my own, I would like to thank a few people.

Firstly, I thank my supervisors Alejandro Aragón and Farbod Alijani for their commitment to the project. While the eventual road to completion was certainly not as we had initially planned, they took time out of their schedule to support me anyway. Secondly, I would like to thank Paolo Tiso, for offering his time and knowledge at a point in the project where I was stuck and did not see a way forward. His help in clarifying my assumptions on modal derivatives-based methods was invaluable in continuing the project.

Thirdly, this thesis report was not only made possible by myself and my supervisors, but also those who worked on this topic before me. Both Koen Markestein and Yogesh Pilia did remarkable work on implementing first tensor-decomposition based model order reduction and then, additionally, modal derivatives into the Hybrida codebase. I would like to thank them for their help: in the case of Yogesh with meetings and e-mailed support long after his thesis had ended, and in the case of Koen for his thorough commenting and set-up of the coded methods.

Furthermore, I would like to thank all the people that asked me about my thesis during my 2,5 year "leave of absence". In the end, you've pestered me enough and won as I seem to have completed it, although I definitely will not admit that this was an important factor in any other conversation. Lastly, I would like to thank my girlfriend Anne, for not knowing how to help me but doing it anyway.

Amsterdam, July 9, 2024

H. Tijsseling

# Contents

List of Symbols	4
List of Abbreviations	5
<b>1 Introduction</b>	<b>1</b>
1.1 The Curse of Dimensionality in FE-based Nonlinear Dynamics	2
1.1.1 Geometric nonlinearities	2
1.2 Model order reduction	3
1.3 Model-based model order reduction methods	4
1.3.1 Static condensation	4
1.3.2 Component mode synthesis	5
1.3.3 Reduced basis projections	5
1.4 Accounting for nonlinearities in model-based ROMs	7
1.4.1 Stiffness evaluation procedure	8
1.4.2 Modal Derivatives	8
1.4.3 Selection of Modal Derivatives	12
1.4.4 Quadratic manifold	14
1.4.5 Nonlinear normal modes	15
1.4.6 Spectral submanifolds	16
1.5 Data-driven model order reduction methods	17
1.6 Research goals	18
<b>2 Modal Derivatives-based Model Order Reduction for Nonlinear Structural Analysis</b>	<b>19</b>
2.1 Verification of triangular shell finite element	19
2.2 Verification of static modal derivatives	24
2.3 SMD-based Model Order Reduction in Non-linear Dynamics	27
2.3.1 Simply supported square plate, immovable edges	27
2.3.2 Simply supported square plate, movable edges	28
2.3.3 Vertical Cantilever	30
2.3.4 MEMS Double Clamped Beam	33
2.3.5 Single-curved circular cylindrical shell	34
2.3.6 Double curved shallow shell	35
2.4 Conclusions	39
2.4.1 Verification of finite element implementation	39
2.4.2 Verification of static modal derivative implementation	39
2.4.3 SMD-based model order reduction for nonlinear dynamics	39
2.5 Discussion	40
2.6 Recommendations	40
<b>3 Process Reflection</b>	<b>41</b>
<b>A Model Order Reduction implementation in Hybrid</b>	<b>45</b>
A.1 Finite Element implementation	45
A.2 Construction of the reduction basis $\mathbf{R}$	46
A.2.1 Vibration modes	46
A.2.2 Static Modal Derivatives	48
A.2.3 Post-processing the Reduction Basis	51

A.3	Reduction of Equations of Motion . . . . .	52
A.3.1	Reduction of linear System Matrices . . . . .	52
A.3.2	Tensor Decomposition and Reduction of Nonlinear Stiffness Matrix . .	53
A.3.3	Post-processing the Reduced Equations of Motion . . . . .	55
A.4	Dynamic nonlinear solution procedures . . . . .	56
A.5	Static nonlinear solution procedures . . . . .	56
A.5.1	Hybrid Incremental-iterative solver for nonlinear static analysis . . . .	58
<b>B</b>	<b>Parameters and data used in numerical experiments</b>	<b>60</b>
B.1	Parameters for statics benchmarking tests . . . . .	60
B.2	Parameters for verification of Modal Derivatives . . . . .	64
B.3	Parameters for model order reduction for nonlinear dynamics . . . . .	65

## List of Symbols

$A$	Area of finite element
$D$	Discrete strain-displacement relations
$D_{bw}$	Coefficient matrix used in $D$ ; $f(a,b,\lambda)$
$D_{b\phi}$	Coefficient matrix used in $D$ ; $f(a,b,\lambda)$
$G$	Geometric stiffness matrix
$Q_{ij}$	Local to global transformation matrix
$R_{ij}$	Global to local transformation matrix
$S$	Constitutive relations
$a, b$	Shell element side vector coefficients
$c_i$	Second-order derivatives of $a, b$
$d_i$	First-order derivatives of $a, b$
$k_e$	Element stiffness matrix
$l_v$	Number of elements
$m_e$	Element mass matrix
$\lambda$	Length of element side vector
$\phi_i$	$i^{\text{th}}$ Vibration mode
$\theta_{ij}^{ST}$	Static modal derivative of $\phi_i$ with regards to $\phi_j$

## List of Abbreviations

CAD	computer-aided design
CMS	component mode synthesis
DoFs	degrees of freedom
DNF	direct normal form
EoMs	equations of motion
FE	finite element
FEM	finite element modelling
FRF	frequency response function
HBFEM	harmonic balance finite element method
LDRV	load-dependent Ritz vector
MAPE	mean average percentage error
MD	modal derivatives
MOR	model order reduction
ODE	ordinary differential equation
POD	proper orthogonal decomposition
QM	quadratic manifold
RAM	random access memory
ROM	reduced-order model
RRQR	rank-revealing QR
SMD	static modal derivative
SSM	spectral submanifold
STEP	stiffness evaluation procedure
SVD	singular value decomposition
TS	tangent stiffness (matrix)
VM	vibration mode

# 1 Introduction

In more and more industries, there is a push towards lightweight, slender designs. Especially in aerospace and automotive engineering, fields naturally subject to strict weight requirements, thin-walled structures are everywhere. The problem is, however, that these structures can vibrate in unpredictable ways even when subjected to relatively moderate-intensity dynamic loads. Understanding these vibrations in order to predict fatigue, creep, or even failure of these structures is the topic of concern of the field of structural dynamics.

Understanding vibrations is essentially an energy question: how does the outside energy, acting upon the structure as forces, get absorbed or dissipated within the structure? This question can be answered in multiple ways. Before computers, variational methods like the Rayleigh-Ritz [1] or least-squares [2] methods were used for simple cases, where the expressions could be made to satisfy all the present boundary conditions. These methods assume the solution is a combination of a finite number of functions, thus discretizing the problem and reducing the infinite number of degrees of freedom (DoFs) into a finite number.

Since the advent of computers, however, structural dynamics has shifted more and more to using the Finite Element method. In this method, first, computer-aided design (CAD) models are made of the structure under consideration. finite element modelling (FEM) is then used to discretize the CAD drawing into a discrete "mesh" of subdomains or "elements" with small, finite dimensions [23]. Applying the element kinematics of a certain finite element on each subdomain results in a set of equations of motion (EoMs) which can then be solved to find the mechanical behaviour of the entire structure.

Performing finite-element based dynamic analysis for thin-walled structures runs into an issue, however. As these structures tend to behave nonlinearly rather quickly, the set of EoMs must be recomputed regularly to reflect the changing geometry of the structure. This can be very computationally costly, as the size of the system of equations of motion depends on the amount of DoFs in the finite element discretization. model order reduction (MOR) methods attempt to avoid this issue by reducing the required computational cost of performing dynamic analysis of the model under consideration (Figure 1).

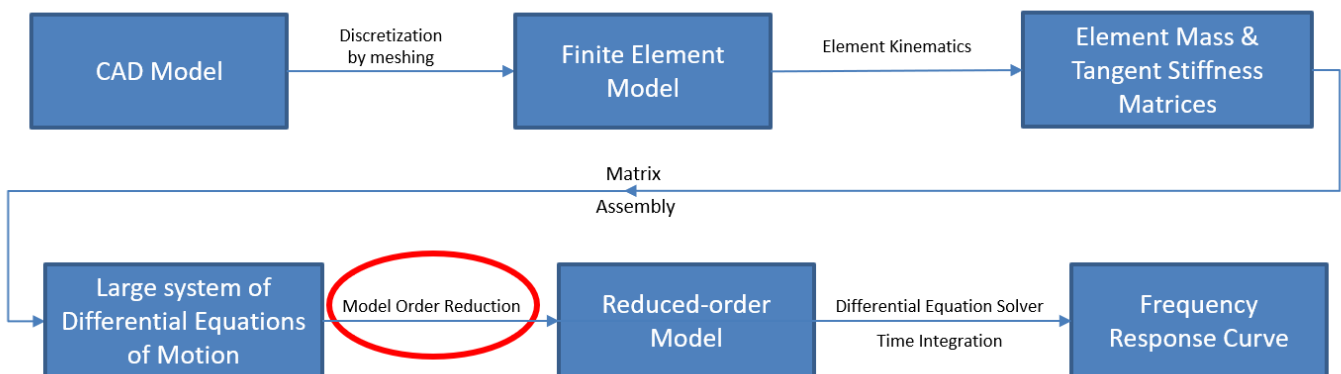


**Figure 1:** Generalized block diagram of an example workflow of finite element-based analysis of structural dynamics, including model order reduction, which is highlighted as the focus of this thesis.

Most MOR methods aim to reduce the cost of (re)computation of the EoMs by reducing the size of a model, thus avoiding the "curse of dimensionality" (Bellman, 1956) [3].

## 1.1 The Curse of Dimensionality in FE-based Nonlinear Dynamics

When using finite elements to investigate forced structural dynamics specifically, we obtain a set of time-dependent second-order differential equations of motion from our mesh:

$$\mathbf{M}\ddot{\mathbf{u}}(t) + \mathbf{C}\dot{\mathbf{u}}(t) + \mathbf{K}\mathbf{u}(t) = \mathbf{F}(t) \quad (1)$$

with  $\mathbf{M}$ ,  $\mathbf{C}$ , and  $\mathbf{K} \in \mathbb{R}^{N \times N}$  as the mass, damping and stiffness matrices, respectively. The vector  $\mathbf{u}(t) \in \mathbb{R}^N$  represents the displacements of the nodes of the finite element mesh as they change through time. Note that, owing to the use of linear finite elements, none of the system matrices exhibit any dependency on the configuration  $\mathbf{u}$  of the structure. For a more detailed review of the mathematics behind Finite Element discretization, I refer to Newland (1965) [9].

The dimensionality  $N$  of the full model is equal to the amount of degrees of freedom in the finite element mesh, that is, a finer mesh results in a larger  $N$  [75]. The number of DoFs of complete finite element models, also known as the dimensionality or "order" of the model, can run into the millions [39, 42, 46]. As this order or dimensionality of a system of equations of motion increases, the required computational effort for recomputation (which is necessary for dynamic calculations) scales quadratically with it.

### 1.1.1 Geometric nonlinearities

A second complication in the FEM process described above arises when the thin-walled structures of interest display nonlinear behaviour. One example of nonlinearity is geometric nonlinearity, where the relations between kinematic quantities (e.g. displacements, rotations, or strains) are nonlinear:

$$\epsilon(x) = \frac{du}{dx} + \frac{1}{2}\left(\frac{du}{dx}\right)^2 \quad (2)$$

If  $\frac{du}{dx}$  is small, the quadratic term tends to zero and we get the linear strain approximation:

$$\epsilon(x) \approx \frac{du}{dx} \quad (3)$$

Because thin-walled structures can flex easily, however, strains and rotations are finite, and the  $\left(\frac{du}{dx}\right)^2$  term is non-zero. These nonlinearities often cannot be set aside: they arise in a myriad of different situations and often have dramatic effects. To demonstrate this we take a look at two simple static bending cases analyzed with both linear and nonlinear finite elements (Figure 2).

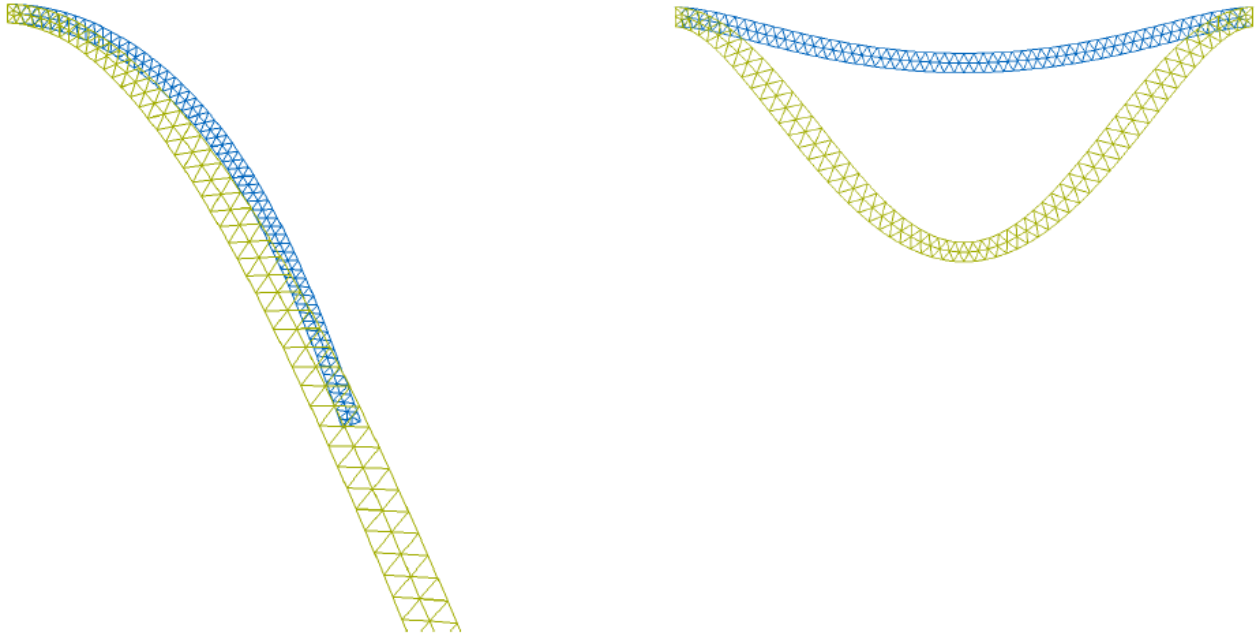


**Figure 2:** Static simulations of a cantilever (left) and clamped-clamped beam (right) using linear (green) and nonlinear (blue) finite elements. Reprinted from J. B. Rutzmoser (2018) [75].

As shown, the linear finite elements (green) overestimate the deformation of both beams. This is due to non-realistic behaviour, as the linear elements stretch and take up more volume than they originally did. Additionally, the linear finite element analysis does not account for stiffening effects caused by the present geometric nonlinearity of the beams. This means that when large rotations and/or displacements occur, including geometric nonlinearities in a model is imperative in order to accurately describe its deformation. This can be done, for instance, by including geometric nonlinear terms on the element level in the tangent stiffness and mass matrices [26]. After assembly of the full system, the geometric nonlinearities are reflected in the dependence of the stiffness matrix  $\mathbf{K}$  on the displacement vector  $\mathbf{u}$ :

$$\mathbf{M}\ddot{\mathbf{u}} + \mathbf{C}\dot{\mathbf{u}} + \mathbf{K}(\mathbf{u})\mathbf{u} = \mathbf{F} \quad (4)$$

Finding the displacements  $\mathbf{u}$  of nonlinear models of this size under static loads  $\mathbf{F}$  can be costly, but is usually within the realm of possibility. A problem arises, however, when the nonlinear dynamic behaviour of a large model is of interest. Accurately capturing this behaviour requires solving the "statics" problem for a lot of small time steps, and updating the model configuration and system matrices after each step. This is computationally very costly and thus takes a lot of time, which often makes this approach unfeasible as a whole.

## 1.2 Model order reduction

Model order reduction (MOR) methods can be used to reduce the amount of degrees of freedom in the equations of motion, thus reducing the size of the  $\mathbf{M}$ ,  $\mathbf{C}$ , and  $\mathbf{K}$  matrices. After this reduction, solving or performing time integration on the system of differential equations is computationally much cheaper, allowing for faster analysis of structures or use of the reduced equations of motion in real-time control loops.

To reduce the dimensionality of a model, two overarching strategies can be chosen:

- one can attempt to reduce the size of the model without ever computing the solution of the full model. This is known as simulation-free or "model-based" MOR, as the only information available to construct the reduced-order model (ROM) is that which is present in the full model;
- one can solve the full model, and then work backwards to try and find the best reduced-order model that produces (almost) the same results as the full model. This is known as "data-driven" MOR, as the data produced by solving the full model is also available as a basis for the reduced model.

As model-based MOR methods attempt to reduce the dimensionality of the problem at hand without ever computing the full solution, they are usually computationally cheaper than data-driven methods, but the downside of their predictive nature is that they lack the information generated by fully solving the problem. Data-driven approaches, however, defeat the original purpose of model order reduction of not having to solve the full problem under consideration.

Model-based model order reduction methods can be further split up into non-intrusive methods, which do not require access to the underlying finite element framework, and intrusive methods that do need this access. As non-intrusive methods can be applied more easily to models resulting from commercial software packages (which often do not grant access to the underlying nonlinear system matrices), non-intrusiveness is generally seen as a desirable trait for MOR methods [61].

In subsection 1.3, a short overview of some popular model-based model order reduction methods is given. In subsection 1.5 an often used data-driven approach, proper orthogonal decomposition (POD), is treated.

## **1.3 Model-based model order reduction methods**

In this subsection a short overview of (the development of) model-based MOR methods and their most important characteristics is given. For a more detailed overview, I refer to van Woerkom [20], Noor [31], Qu [49], Rutzmoser [75], and Pilania [87].

### **1.3.1 Static condensation**

The method of static condensation is one of the oldest ways of reducing the number of degrees of freedom in a finite element mesh, proposed in 1965 by Guyan & Irons [6, 8]. It achieves the order reduction by deleting the unwanted internal "slave" DoFs, and forcing them to follow the external "master" DoFs. Because this disregards the dynamic effects of the internal DoFs, this method is only valid for the frequency range up to the "cut frequency", which is the lowest frequency of the full model with all its master DoFs grounded (i.e., fixed) [24]. The accuracy of the static condensation-based reduction is then dependent on the ratio of the cut frequency to the frequency of interest [49].

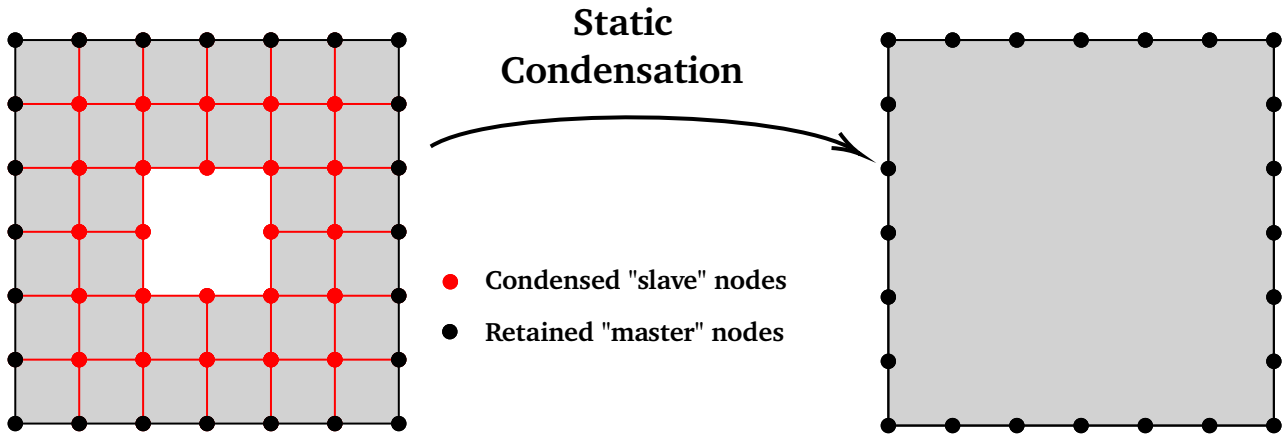


**Figure 3:** Static condensation reduces the inner nodes of a structure by forcing them to follow the "master" outer nodes. Adapted from Wu et al. (2019) [80].

### 1.3.2 Component mode synthesis

component mode synthesis (CMS) or "dynamic substructuring" relies on partitioning the complete meshed structure into separate components or "substructures". Each component can then be separately analyzed or reduced, and afterwards assembled back into a global model. This achieves a couple of things:

- Reduction of the required computational effort, by splitting up a large dynamic problem into several smaller problems;
- Parallel analysis of multiple substructures becomes possible;
- Repeated analysis of the full structure is not necessary when only a small part of it is changed.

Component mode synthesis methods can broadly be divided into three categories: fixed-interface methods, free-interface methods, and hybrid methods. This division rests upon if the mode shapes used for the substructures are obtained by leaving their respective master DoFs fixed, free, or a mix of both [49].

Hurty was the first to propose component mode substructuring [7]. His method was quickly simplified by Craig and Bampton, whose names thus became permanently connected to this fixed-interface CMS technique. Goldman and Hou went in a different direction, by leaving the component master DoFs free [11]. Macneal subsequently combined their two approaches in his hybrid CMS method [12]. One of the more influential contributions came from Rubin [13], who extended the method of Macneal by including second-order residual effects of modes deleted from the final set of substructure normal modes. For a more detailed description of component mode synthesis methods, see Pilia [87].

### 1.3.3 Reduced basis projections

A key observation in the field of structural dynamics is that the actual dimension of a dynamic problem is generally much smaller than the dimensionality of the full model resulting from a FEM discretization. This is because the structure can only exhibit physically possible or "admissible" configurations, which represent a small part of the total number of configurations. The MOR methods detailed in this subsection all exploit this observation to construct a reduced basis and then use this basis to project the full model down onto a smaller subspace.

## Linear modal truncation & superposition

The method of modal coordinate reduction posits that the smaller subspace containing all the physically feasible configurations is spanned by  $m$  modal basis vectors, also known as eigenvectors, mode shapes, or vibration modes. These mode shapes  $\phi_i$  are the solution to the linear eigenvalue problem:

$$(\mathbf{K}_{\text{eq}} - \omega_i^2 \mathbf{M})\phi_i = 0 \quad (5)$$

and in this reduction method are taken to form the columns of the reduction basis  $\mathbf{R}$ :

$$\mathbf{R} = \left[ \phi_1|_{\text{eq}} \quad \phi_2|_{\text{eq}} \quad \dots \quad \phi_m|_{\text{eq}} \right]. \quad (6)$$

Generally, the number of solutions to this eigenvalue problem (and thus the number of vibration modes) is as large as the dimensionality  $N$  of the full model. The modal coordinate reduction method assumes, however, that the basis can be "truncated": the nodal displacements  $\mathbf{u}$  can be represented as a linear combination or superposition of a small number  $m$  of low-frequency modes. This can be stated as

$$\Delta \mathbf{u} = \sum_{i=1}^N \phi_i \mathbf{q}_i \approx \sum_{i=1}^m \phi_i \mathbf{q}_i \quad (7)$$

where  $\mathbf{q}_i$  represents the amplitudes of the mode shapes, also known as the generalized modal coordinates, and  $m \ll N$ .

This transformation onto a reduced basis, consisting of eigenmodes or "spectral subspaces" that exist in the phase space, can be visualized as projecting onto surfaces in Euclidean space as shown in Figure 4. The full solution (in red) can be approximated, for example, by a linear superposition (shown in blue) of the first two eigenmodes. This holds for geometrically linear systems, where the mode shapes or eigenvectors spanning this space are independent of each other or "invariant". This means that they do not influence each other: if we only excite one mode, the other modes stay quiet.

With the transformation to the modal space from Equation 7 done, we can now write our system of equations of motion as

$$\hat{\mathbf{M}}\ddot{\mathbf{q}} + \hat{\mathbf{C}}\dot{\mathbf{q}} + \hat{\mathbf{K}}\mathbf{q} = \hat{\mathbf{F}} \quad (8)$$

where  $\hat{\mathbf{M}}$ ,  $\hat{\mathbf{C}}$ , and  $\hat{\mathbf{K}} \in \mathbb{R}^{m \times m}$  represent the reduced modal mass, damping and stiffness matrices, and  $\hat{\mathbf{F}}$  represents the reduced force vector, all denoted by the hat superscript:

$$\hat{\mathbf{M}} = \mathbf{R}^T \mathbf{M} \mathbf{R} \quad (9)$$

$$\hat{\mathbf{C}} = \mathbf{R}^T \mathbf{C} \mathbf{R} \quad (10)$$

$$\hat{\mathbf{K}} = \mathbf{R}^T \mathbf{K} \mathbf{R} \quad (11)$$

$$\hat{\mathbf{F}} = \mathbf{R}^T \mathbf{F} \quad (12)$$

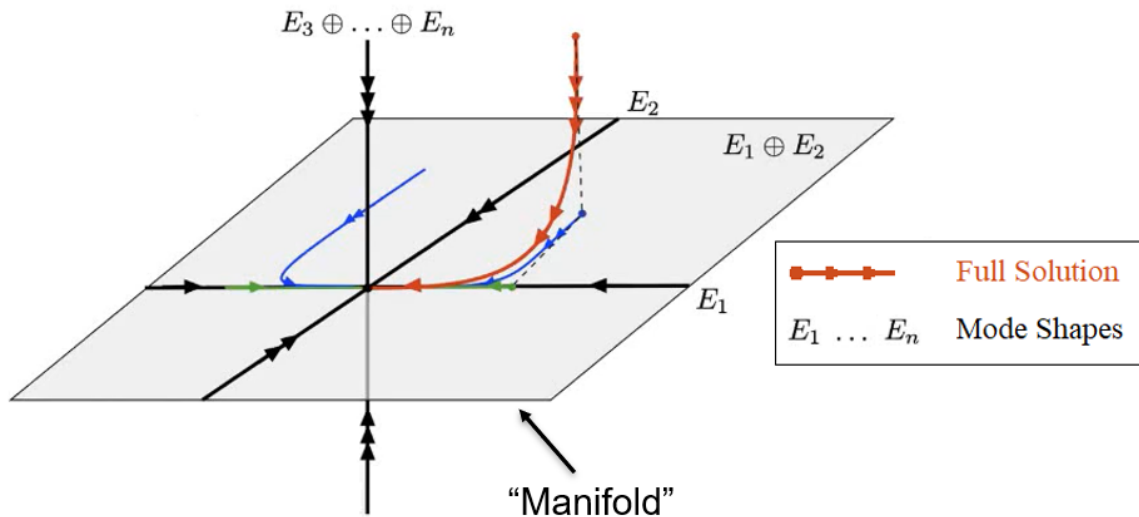


**Figure 4:** Linear reduction methods are often based around a projection onto a smaller subspace, in this example spanned by eigenvectors or "mode shapes". Adapted from G. Haller: "Fast reduction of nonlinear finite-element models to spectral submanifolds", NODYCON 2021.

The number of degrees of freedom in the equations of motion is thus reduced from  $N$  to  $m$ , and with that the computational cost of the associated solve of the system of differential equations is also reduced.

### Ritz-Wilson methods

The Ritz-Wilson method, also called the method of load-dependent Ritz vectors (LDRVs), was proposed in 1982 by Wilson, Yuan and Dickens [15]. Their theory was based on the seminal paper on determining frequencies and mode shapes by Ritz from 1909 [1]. In their method the information of the forces or "loading" on the structure is used to efficiently generate a sequence of Ritz vectors that span the reduced basis. This can be more accurate than exact eigenvectors, in the case that eigenvectors orthogonal to the loads aren't excited even though their eigenfrequencies lie within the frequency bandwidth of the loading [49]. Apart from this, the Ritz-Wilson technique has another major advantage: the basis vectors are usually cheaper to compute than modal basis vectors, as there is no need for a computationally expensive eigensolve.

However, as the Ritz-Wilson reduced model is dependent on the specific loading pattern, the Ritz vectors have to be computed again if the loading pattern changes. Thus, when using the Ritz-Wilson technique, use must be made of an incremental-iterative formulation in order to maintain an accurate solution. There have been many extensions to the method of Wilson, which can be grouped into static Ritz vector methods [17, 19] and quasi-static Ritz vector methods [38, 62].

## 1.4 Accounting for nonlinearities in model-based ROMs

Model order reduction methods are often based on assumptions that have to be valid in order for the reduction to produce good results. Static condensation, for example, assumes that the in-plane dynamics of the interior degrees of freedom can be neglected, and reduced basis projections assume that the dynamics of a structure can be closely approximated by a linearly

invariant combination of a small set of basis vectors. However, when displacements are large and we enter the geometrically nonlinear regime, these assumptions are often not valid anymore. Large displacements can, for example, cause the assumption that the basis vectors in a reduced basis projection are linearly independent to no longer hold true. Model order reduction methods deal with complications resulting from nonlinear behaviour in multiple ways, which are described in more detail in this section.

### 1.4.1 Stiffness evaluation procedure

The stiffness evaluation procedure (STEP) was proposed in 2003 by Muravyov & Rizzi [45]. Its core principle is writing the EoMs of a system in modal coordinates and then accounting for the nonlinear stiffness force components by writing them as second and third order modal displacements multiplied by (at first unknown) coefficients. By then prescribing displacement fields they create a set of linear and nonlinear static problems, which can be solved to determine the unknown coefficients of nonlinearity.

The STEP is not a model order reduction method; rather, it's a way of finding the nonlinear geometric stiffness components present in a system of equations of motion. However, by applying the STEP after a modal basis reduction, for example, it can be applied to reduced-order models as well. This procedure is non-intrusive in the sense that no access to the underlying FEM implementation or code is required in order to determine the nonlinear stiffness components. This is a great advantage of the STEP over other methods, such as the analytical derivation method described in [21]. For a more thorough review of this method, I refer to Mignolet & Rizzi [61] and Givois et al. [77].

### 1.4.2 Modal Derivatives

Idelsohn and Cardona were the first to propose modal derivatives (MDs) as an extension of the modal basis vector reduction methods described in section 1.3.3 [18]. They argued that, as the eigenmodes  $\phi_i$  are found by solving the eigenvalue problem

$$(\mathbf{K}_{\text{eq}} - \omega_i^2 \mathbf{M})\phi_i = 0, \quad (13)$$

that if  $\mathbf{K}$  is dependent on displacements, this dependence should also exist for  $\phi_i$ . This would change the linear superposition of basis vectors that we derived in Equation 7:

$$\Delta \mathbf{u} \approx \sum_{i=1}^m \phi_i \mathbf{q}_i = \sum_{i=1}^m \phi_i(\mathbf{q}) \mathbf{q}_i \quad (14)$$

Therefore, as the displacements  $\Delta \mathbf{u}$  depend on  $\mathbf{q}$ , we can use a Taylor expansion to approximate them around the equilibrium configuration [18, 87]:

$$\Delta \mathbf{u} = \Delta \mathbf{u}(\mathbf{q}_i) \approx \left. \frac{\partial \Delta \mathbf{u}}{\partial \mathbf{q}_i} \right|_{\text{eq}} \mathbf{q}_i + \left. \frac{\partial^2 \Delta \mathbf{u}}{\partial \mathbf{q}_i \partial \mathbf{q}_j} \right|_{\text{eq}} \frac{\mathbf{q}_i \mathbf{q}_j}{2} + \mathcal{O}^3 + \dots \quad (15)$$

We see that the first Taylor term signifies the linear vibration modes, as it describes how the

configuration changes when we excite a mode shape. The second, quadratic term is comprised of the modal derivatives, which tell us how a change in configuration will change the linear vibration modes. This information predicts the nonlinear behaviour of our model without requiring the reduction basis to be updated after some steps of a time integration scheme.

The method of modal derivatives was subsequently further elaborated upon by Slaats et al. [33]. In recent years, work by Wu, Tiso and others has revived interest in the method as a valid approach to nonlinear model order reduction [60, 66, 76, 79, 86]. The method promises to improve modal reduction-based approximations of geometrically nonlinear systems, which cannot be properly described solely by linear vibration modes, by adding to the reduction basis second-order terms that include information on in-plane displacements.

Slaats et al. showed that these second-order terms show great promise when used in combination with vibration modes to approximate geometrically nonlinear truss problems (Figure 5). Figure 6 shows that adding modal derivatives results in a significantly reduced approximation error. The computation time required for each of the reductions in Figure 6 was about 20 times less than for the full solution. This reduction in computation time can be even greater when the number of DoFs in the original problem is increased, as certain "overhead" costs slow down reduction methods when used for small problems.

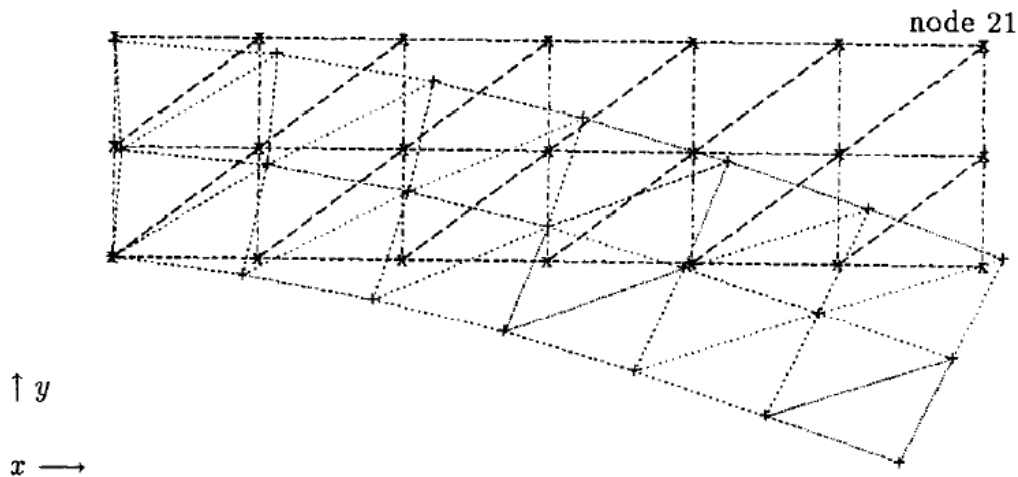


**Figure 5:** Geometrically nonlinear truss problem with 39 degrees of freedom. Reprinted from Slaats et al. (1995) [33].

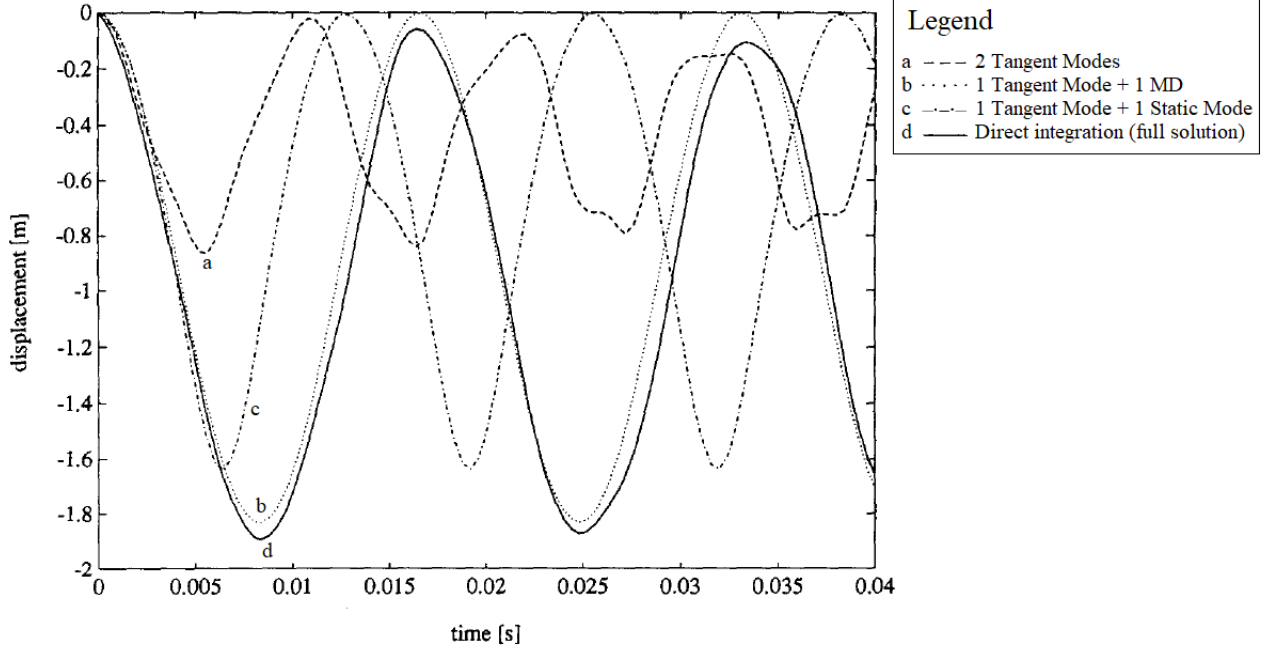


**Figure 6:** Full solution of the structure in Figure 5 compared to various approximations based on tangent modes, static modes and modal derivatives. Adapted from Slaats et al. (1995) [33].

### Static vs. original Modal Derivatives

A distinction must be made between the original modal derivatives, as intended by Idelsohn and Cardona in their 1985 paper, and the later simplification of "static" modal derivatives. Modal derivatives (the quadratic terms in Equation 15) can be computed by taking the derivative of the linear vibration modes with regards to the modal amplitudes  $q$  [87]:

$$\frac{\partial}{\partial q_j} ((\mathbf{K}_{eq} - \omega_i^2 \mathbf{M}) \phi_i) = 0 \quad (16)$$

Using the product rule for differentiation:

$$(\mathbf{K}_{eq} - \omega_i^2 \mathbf{M}) \frac{\partial \phi_i}{\partial q_j} + \left( \frac{\partial \mathbf{K}_{eq}}{\partial q_j} - \frac{\partial \omega_i^2}{\partial q_j} \mathbf{M} \right) \phi_i = 0 \quad (17)$$

In Equation 17 the term  $\frac{\partial \phi_i}{\partial q_j} = \theta_{ij}$  signifies the modal derivative of the  $i^{\text{th}}$  mode w.r.t. the  $j^{\text{th}}$  mode. At this point, we could try to solve for this term; however, a problem arises as the coefficients matrix  $(\mathbf{K}_{eq} - \omega_i^2 \mathbf{M})$  is singular [18, 87], which cannot be solved exactly in an instant fashion. Additional constraints are required, like imposing the requirement that the derivative of the mass normalization condition remains zero [75]:

$$\frac{\partial}{\partial q_j} (\phi_i^T \mathbf{M} \phi_i) = 0 \quad (18)$$

which signifies that the norm of an eigenmode  $\phi_i$  remains constant throughout a change in geometry in the direction of mode  $q_j$ . This additional constraint, together with Equation 17, then forms a system of equations:

$$\begin{bmatrix} \mathbf{K}_{\text{eq}} - \omega_1^2 \mathbf{M} & -\mathbf{M}\phi_i \\ -(\mathbf{M}\phi_i)^T & 0 \end{bmatrix} \begin{bmatrix} \theta_{ij} \\ \frac{\partial \omega_1^2}{\partial q_j} \Big|_{q=0} \end{bmatrix} = \begin{bmatrix} \frac{\partial \mathbf{K}^{\text{NL}}}{\partial q_j} \Big|_{q=0} \phi_i \\ 0 \end{bmatrix}. \quad (19)$$

This system of equations can be solved to find the modal derivatives of a system. Alternatively, approximate procedures like the pseudo inverse method, Nelson's method, or other methods can be used to solve Equation 17 [27, 29, 56].

A second issue with the "classic" Idelsohn & Cardona MDs from Equation 19 is that they are not symmetric:  $\theta_{ij} \neq \theta_{ji}$ . Therefore, every modal derivative has to be calculated independently, and for each calculation a new factorization of the coefficients matrix is required [75]. This is associated with a large increase in computation time, even more so because, as the modal derivatives are second-order derivatives of the modes with respect to each other, the number of MDs associated with a certain amount of linear normal modes increases quadratically (see Figure 7).

Therefore, in most literature on modal derivatives the authors choose to disregard the mass terms in Equation 19. This leads to a simpler computation of the modal derivatives, which now also become symmetric  $\theta_{ij}^{\text{ST}} = \theta_{ji}^{\text{ST}}$ :

$$\theta_{ij}^{\text{ST}} = \frac{\partial \phi_i}{\partial q_j} = -\mathbf{K}_{\text{eq}}^{-1} \frac{\partial \mathbf{K}^{\text{NL}}}{\partial q_j} \Big|_{q=0} \phi_i \quad (20)$$

These are known as static modal derivatives (SMDs), denoted by the superscript "ST", which can then be added to the reduction basis from Equation 6:

$$\mathbf{R} = \left[ \phi_1|_{\text{eq}} \phi_2|_{\text{eq}} \dots \phi_i|_{\text{eq}} \theta_{11}^{\text{ST}} \theta_{12}^{\text{ST}} \dots \theta_{ij}^{\text{ST}} \right]. \quad (21)$$

### Computation of Modal Derivatives

The modal derivatives in Equation 20 can be computed in two ways: either by using a finite difference method to capture the change of the nonlinear stiffness matrix around the equilibrium configuration, or by analytically delving into the element stiffness formulation and differentiating those matrix elements dependent on displacements. The first method is non-intrusive; that is, no deeper access to the source code of the underlying FEM package is required. The second method, in contrast, is always considered intrusive. Both methods are described in more detail in Appendix A.

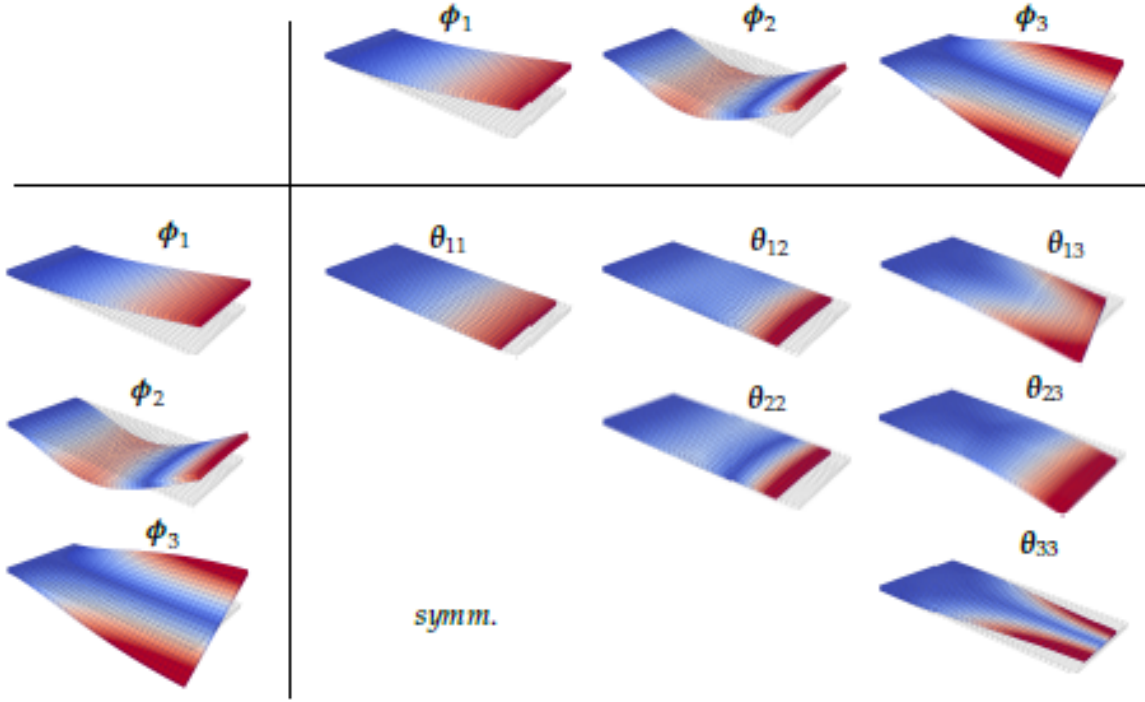


**Figure 7:** The amount  $o$  of SMDs (denoted by  $\theta$ ) associated with a certain reduction basis scales quadratically with the number of vibration modes (denoted by  $\phi$ ). Reproduced from Rutzmoser (2018) [75].

### 1.4.3 Selection of Modal Derivatives

As discussed previously in subsection 1.4.2, the number of "normal" modal derivatives  $o$  that is associated with  $m$  vibration modes scales quadratically:

$$o = m^2 \quad (22)$$

However, as static modal derivatives are symmetric, we can disregard the lower portion of the triangle (Figure 7), which almost halves the amount of static modal derivatives to consider:

$$o = \frac{m(m+1)}{2} \quad (23)$$

Nonetheless, even after disregarding the lower diagonal of symmetric modes, the amount of static modal derivatives scales quadratically with the number of vibration modes. This can cause the total number of DoFs  $n = m + o$  to balloon quickly. For example, using 10 vibration modes and their associated SMD will result in a base consisting of 65 reduced degrees of freedom, which can result in an increase in the required computational effort during later solution procedures. To curb this quadratic growth, a selection can be made of the modal derivatives. This can be done at two stages:

- a priori selection: before computing any SMDs, a guess is made as to which will be relevant, and only these are computed. Usually, modal derivatives associated with the lowest frequency vibration modes are significant and should be included in an a priori selection of static modal derivatives.

- a posteriori selection: after computing all SMDs associated with a set of vibration modes, a variety of selection methods can be applied to select the static modal derivatives that are expected to be most influential on the dynamic response.

Both types of methods can be used to make a selection of modal derivatives by completely disregarding those scoring badly on the selection criterion. Alternatively, the selection methods can be used to build a weighing matrix  $\mathbf{W}$  which, instead of completely disregarding unimportant DoFs, simply places more weight on the modal derivatives considered important. As a priori methods have the advantage of not having to compute all static modal derivatives before selecting them, this type of selection criterion has received the most attention in literature and previous work and will therefore be described here in more detail:

**Frequency Weighting (FW):** First proposed by Barbic and James in 2005 [52], the frequency weighting selection criterion is based on the assumption that the low-frequency modes and their associated modal derivatives dominate the dynamic response of the structure under consideration:

$$W_i^\phi = \frac{\omega_1}{\omega_i}, W_{ij}^\theta = \frac{\omega_1^2}{\omega_i \omega_j} \quad (24)$$

Where  $\omega_i$  is the eigenfrequency associated with vibration mode  $\phi_i$ . These weights  $W_{ij}$  are then applied to respectively the vibration modes  $\phi_i$  and the mass-normalized modal derivatives  $\bar{\theta}^{ij}$ :

$$\mathbf{R} = \left\{ W_i^\phi \phi_i \mid i = 1, \dots, k \right\} \cup \left\{ W_{ij}^\theta \bar{\theta}^{ij} \mid i \leq j; i, j = 1, \dots, k \right\} \quad (25)$$

The reasoning behind this scaling is simple - as low-frequency modes are generally more important, the frequency weighting criterion prioritizes these modes and prevents them from being masked by higher frequency modes and their derivatives.

**Maximum Modal Interaction (MMI):** Tiso proposed an a priori selection criterion in 2011 based on the convergence of the underlying (linear) modal truncation approximation [59]. This convergence is split into a spatial part which depends on the shape of the vibration modes  $\phi_i$  and the applied load  $\mathbf{f}$ , and a spectral part which depends on the eigenfrequencies of the vibration modes and that same load. The spatial weighing criterion will prioritize selecting modes that have large deflections in the directions of the load; in other words, vibration modes that are orthogonal to the loading direction will be disregarded sooner. The spectral weighing criterion will prioritize vibration modes that have eigenfrequencies close to that of an applied harmonic load.

Both the spatial and the spectral components of the MMI selection criterion have solid "common sense" foundations in that they would select vibration modes that move in the direction of and have approximately the same frequency as the applied load, which are likely to be large part of the solution of the dynamic problem. Tiso shows that these selection criteria outperform random selection of modal derivatives (or "second-order modes" as he calls them) for certain numerical examples [59].

**(Symmetric) Modal Virtual Work (SMVW):** Jain proposed a selection criterion in 2017 in which the weighing coefficient for a certain modal derivative is equal to the virtual work

done by the nonlinear elastic forces that arise when the first underlying vibration mode acts upon the second underlying mode [69]. In this sense, this selection criterion also quantifies a priori the interaction between two modes and then ranks the resulting modal derivatives accordingly. However, as the weighing matrix  $\mathbf{W}$  in this case is not symmetric (as is the case for the Maximum Modal Interaction proposed by Tiso), this weighing matrix is also suited for selecting normal "non-static" modal derivatives and in this sense a more flexible approach to a weighing matrix for modal derivatives.

In all the above cases, the a-priori selection criteria are based on information that is solely obtained from the linear vibration modes and their interaction with the applied loading and other modes in linear analysis. While they intuitively give some information about the importance of the selected modes, the assumption is then made that modal derivatives derived from these vibration modes will also be significant for the nonlinear dynamic problem at hand. This assumption does not always hold, and these a-priori criteria thus cannot be used to make statements with 100% certainty regarding the use of these degrees of freedom in subsequent nonlinear analysis. Therefore, the weighing matrix resulting from an a priori selection method should ideally be used to rank the degrees of freedom and weigh their contribution, instead of disregarding completely those DoFs scoring badly.

#### 1.4.4 Quadratic manifold

In recent years, another approach has been proposed by Jain & Tiso to counteract the quadratic growth issue apparent in Figure 7 [69, 72]. This method, dubbed "quadratic manifold", adds the information normally contained in the additional modal derivative basis vectors to the linear basis vectors instead. In this way, it constructs a "quadratically curved" manifold on which the true solution can be projected.

Vizzacarro (2020) has recently identified additional constraints on this method, however: for structures with strong quadratic coupling, such as arches and shells, quadratic manifolds might not produce accurate results [83]. Furthermore, it was shown by Haller and Ponsioen (2017) and Vizzacarro that this QM is accurate only when a slow/fast assumption holds: namely, when the ratio

$$\rho = \frac{\omega_{\text{slave}}}{\omega_{\text{master}}} \quad (26)$$

of the eigenfrequencies of the slave coordinates to those of the master DoFs is larger than 4 [67, 83]. This is illustrated in Figure 8.

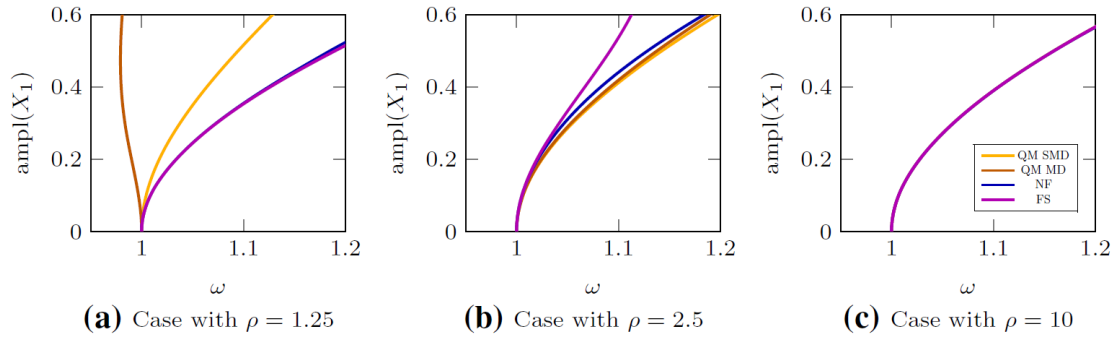


**Figure 8:** A full solution (purple) compared to two forms of the quadratic manifold theory (yellow/orange) and an approximation based on normal form theory. As shown, the quadratic manifold predictions converge to the full solution for high values of  $\rho$ . Reproduced from Vizzacarro (2020) [83].

### 1.4.5 Nonlinear normal modes

The theory of nonlinear normal modes (NNMs) was first proposed in the 60s by Rosenberg [5, 10], and was developed further in the 90s by Shaw & Pierre [22, 28, 32] and Vakakis [35, 41, 57]. They are an extension of the linear normal modes (LNMs) discussed in subsection 1.3.3. Shaw and Pierre define NNMs as a "two-dimensional invariant manifold in phase space": the manifold is invariant in the sense that nonlinear orbits starting out in the manifold will remain in it indefinitely. The invariance-property of the LNMs is therefore extended to nonlinear analysis. Kerschen [57] states that

"Geometrically, LNMs are represented by planes in phase space, and NNMs are two-dimensional surfaces that are tangent to them at the equilibrium point."

A visualization of this statement can be seen in Figure 9.

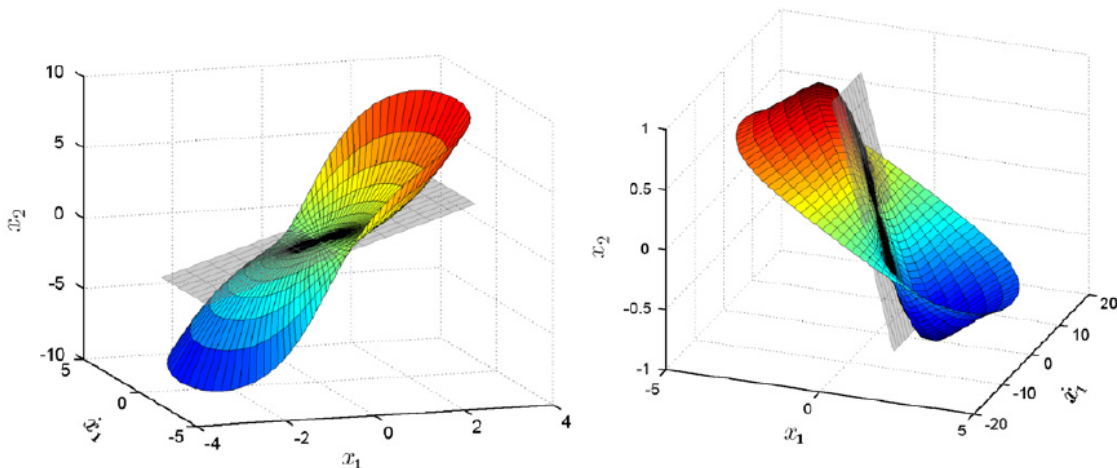


**Figure 9:** Linear normal modes (grey) and nonlinear normal modes (colored) of a 2-DoF example system. Reproduced from Kerschen et al. (2009) [57].

Nonlinear normal modes differ from their linear counterparts in that the vibrations they describe have a frequency-energy dependence. This is shown in frequency response functions (FRFs)

of nonlinear systems as peaks change shape and can "tip over" when the forcing amplitude is increased (Figure 10). The FRFs of nonlinear systems are thus no longer invariant and can show behaviour such as jumps, bifurcations, internal resonances and limit cycle oscillations.

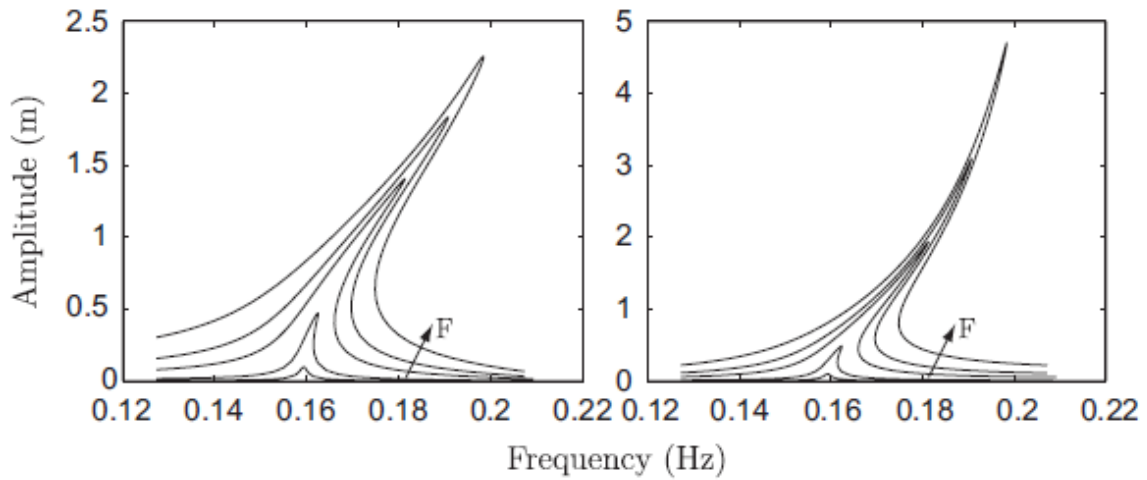


**Figure 10:** As the forcing amplitude increases, the shape of the frequency response function changes, showing a clear frequency-energy dependence. Reproduced from Kerschen et al. (2009) [57].

#### 1.4.6 Spectral submanifolds

In recent years, Haller, Ponsioen and others have developed the theory of spectral submanifolds (SSMs) as a generalization of the theory of nonlinear normal modes [64, 71, 74, 82]. More specifically, they define a spectral submanifold as an

"invariant manifold asymptotic to a NNM, serving as the smoothest nonlinear continuation of a spectral subspace of the linearized system along the NNM."

While the math used to compute these SSMs seems very involved, the method promises to produce robust results, which can be done in a non-intrusive manner for up to third-order approximations [82]. Recent comparisons by other authors [83, 88] seem to agree that the method has merit, but more investigation is required to assess how easy it is to implement this method.

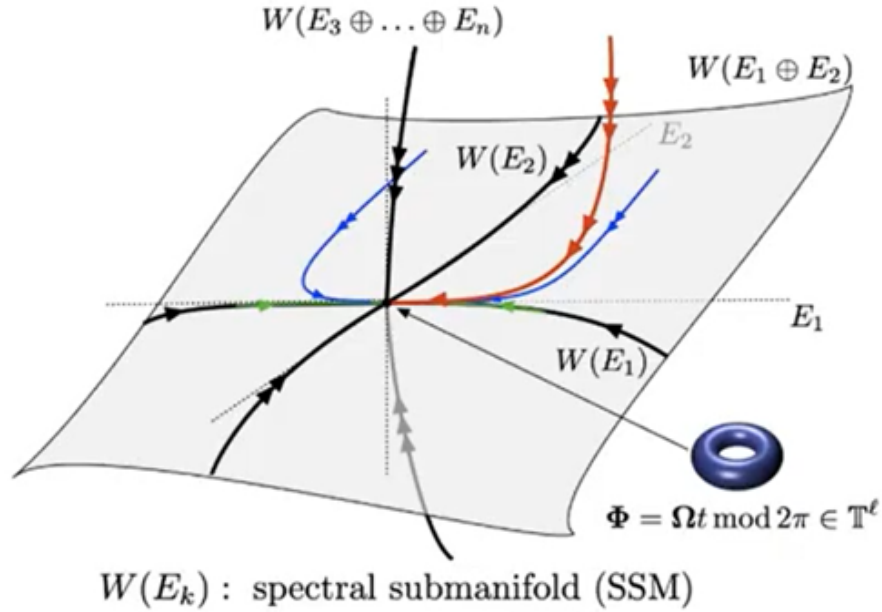


**Figure 11:** The theory of spectral submanifolds (SSMs) looks for nonlinear continuations of the eigenmodes ( $E_k$ ) around the point of origin. Reproduced from Haller (2021) [85].

## 1.5 Data-driven model order reduction methods

Data-driven model order reduction methods use snapshots or full-system simulation runs to retroactively find a reduced-order model approximating the full system. In this sense, they differ from model-based reduction methods in that they always require some amount of solving of the full (nonlinear) system. A multitude of data-driven reduction methods exist, such as the proper orthogonal decomposition (POD) method [54], dynamic mode decomposition (DMD) [65], the sparse identification of nonlinear dynamics (SINDy) method [63], and many more. Proper orthogonal decomposition, for example, uses the results from a full system solve to find a projection matrix which minimizes the average squared distance between the original solution and its reduced representation - in this sense it is comparable to principle component analysis, which is well-known in the field of statistics [75].

For this thesis, data-driven methods were briefly considered as a means to construct reduced order models. For most structural dynamics problems, however, a time integration to acquire the full system solves and/or snapshots isn't feasible, and this thesis therefore focuses on model-based reduction methods. For more information on data-driven model order reduction methods, I refer to Kerschen et al. [54], Sampaio et al. [55], and Brunton & Kutz [81].

## 1.6 Research goals

Based on the research presented above the following research objectives were identified:

- Construct a method to automatically analyze nonlinear vibrations of thin-walled structures from the starting point of a FE discretization;
- Verification of the work previously done, regarding the integration of geometrically nonlinear shell elements, by other members of the Hybrida research group [73];
- Verification of the work previously done on nonlinear model order reduction by other members of the Hybrida research group [87];
- Validation of all these methods by comparison to numerical experiments of nonlinearly forced vibrating structures.
- Application of the Modal Derivative model order reduction method to flat, single-curved, and double-curved shell structures.

## 2 Modal Derivatives-based Model Order Reduction for Non-linear Structural Analysis

### 2.1 Verification of triangular shell finite element

#### Method

As this thesis considers solely thin-walled structures, the shell element described by Van Keulen in 1993 was used to discretize all structures under consideration [26]. To verify that the Hybrida implementation of Van Keulen's triangular shell element is valid for large rotations and displacements, it was first compared to three static problems often used to benchmark nonlinear finite element analysis of shells [50]. To show that large rotations could be captured by the element kinematics alone, coarse meshes made up out of triangular shell elements were generated in GMSH v4.8.4. Details of the meshes and other parameters used in the experimental setups can be found in Appendix B.

The meshes were discretized using the Van Keulen s3f element as described in subsection A.1. The incremental-iterative solver for nonlinear statics as described in subsection A.5 was then used to find static displacements of three cantilever structures undergoing large rotations [68]. In their 2004 paper, Sze, Liu & Lo report the deflection values they calculated in datasets of  $n$  points per benchmarking problem [50]. As the incremental-iterative solver with arc-length control (described in Appendix A.5) used for these static problems does not find balanced solutions at steady forcing intervals, the mean average percentage error (MAPE), being the difference between the Hybrida deflection values  $h_i$  and the reported values  $x_i$  from literature:

$$\text{MAPE} = \frac{1}{n} \sum_{i=1}^n \left| \frac{h_i - x_i}{x_i} \right|, \quad (27)$$

was calculated from these datasets for all benchmark problems by fitting a cubic spline to the deflections calculated in Hybrida and then sampling that interpolation at the benchmark forcing intervals from literature.

#### Cantilever subjected to end shear force

The first benchmarking problem is shown in Figure 12; this problem considers a flat, rectangular cantilever being subjected to an end shear force. The benchmark deflections can be found in Table 1; the experimental parameters used to perform nonlinear analysis in Hybrida are found in Table 2. The material constants and geometric parameters are scaled such that

$$\frac{EI}{L^2} = 1 \quad (28)$$

which is equal to the load parameter  $P_0$ . The maximum load applied is equal to  $4P_0$ .

The final deflection of the structure as computed in Hybrida using a mesh of 67 Van Keulen elements is shown in Figure 12d. A comparison of the deflection of the tip in x- and z-direction ( $U_{\text{tip}}$  and  $W_{\text{tip}}$ , respectively) given by Sze, Liu & Lo to the results from Hybrida is shown in Figure 13. As can be seen, the results from Hybrida match those from the literature very well; the MAPE within the nonlinear regime for this problem was 0.17% for the displacement in x-direction ( $U_{\text{tip}}$ ) and 0.27% for the displacement in z-direction ( $W_{\text{tip}}$ ), respectively.

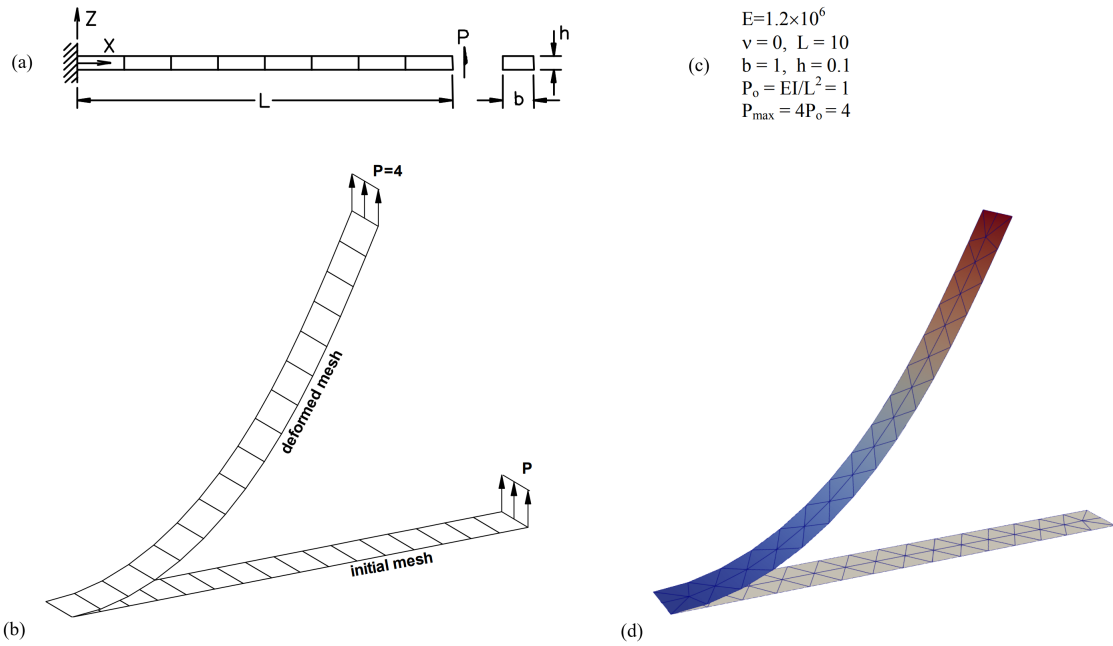


**Figure 12:** (a) Constant cross-section cantilever loaded with an end shear force. (b) Deformed benchmark mesh under maximum load. (c) Material constants and geometric parameters used in benchmark. (d) Final displacement of the cantilever subjected to an end shear force from Hybrida, using 67 triangular van Keulen elements. This final configuration was reached in 31 force increments. Adapted from Sze, Liu & Lo (2004) [50].

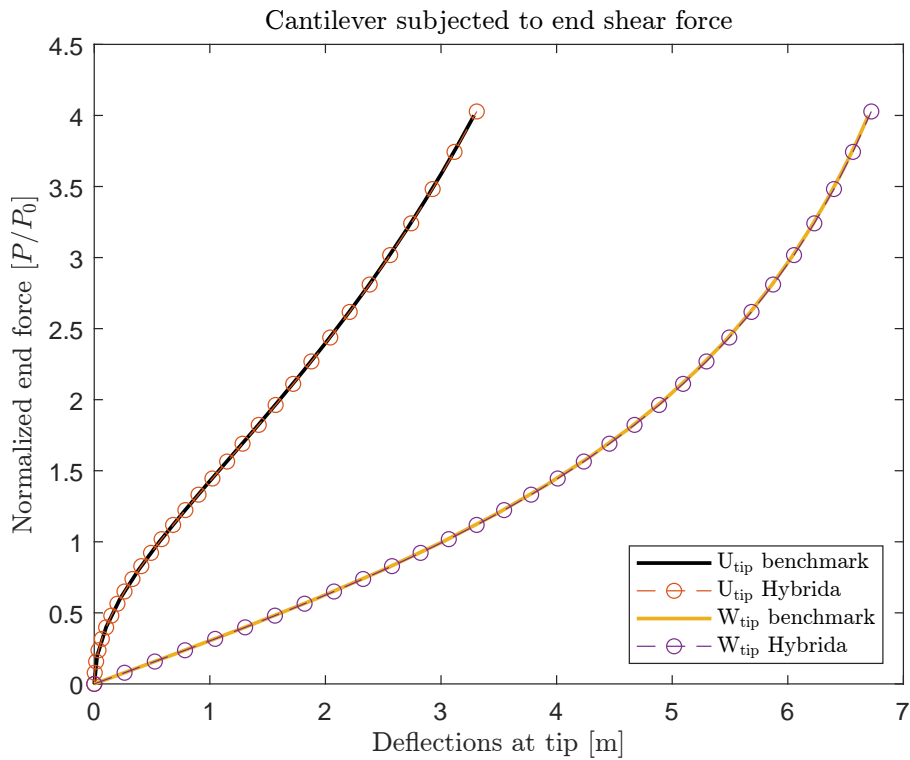


**Figure 13:** Incremental static displacements of a cantilever subjected to a shear force at its free end. Comparison of results from literature (Sze, Liu & Lo [50]) to results from Hybrida nonlinear finite element analysis.

### Cantilever subjected to end moment

The second benchmarking problem is shown in Figure 14; it describes a rectangular flat cantilever subjected to an end moment around the y-axis. The benchmark deflections can be found in Table 3; the experimental parameters used to perform nonlinear analysis in Hybrida are found in Table 4. The final deflection of the structure as computed in Hybrida, achieved using a mesh of 341 Van Keulen elements, is shown in Figure 14d. A comparison of the results from Sze, Liu & Lo to the results from Hybrida is shown in Figure 15. The MAPE within the nonlinear regime for this problem was 0.026% for the displacement in x-direction ( $U_{tip}$ ) and 0.058% for the displacement in z-direction ( $W_{tip}$ ), respectively.

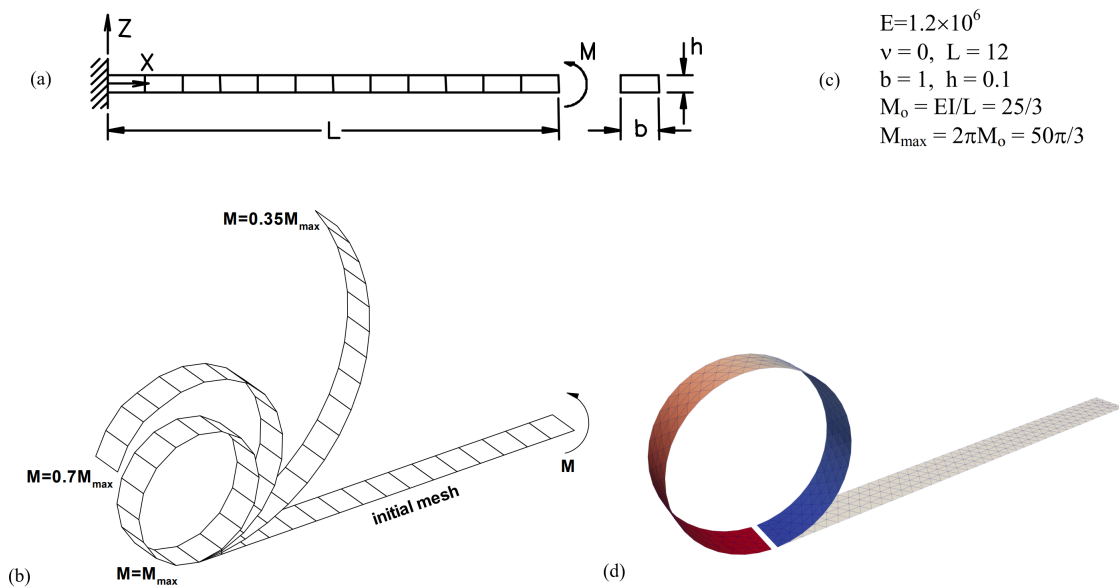


**Figure 14:** (a) Constant cross-section cantilever loaded with an end moment. (b) Deformed benchmark mesh under maximum load. (c) Material constants and geometric parameters used in benchmark. (d) Final displacement of the cantilever subjected to an end moment from Hybrida, using 341 triangular van Keulen elements. This final configuration was reached in 396 moment increments. Adapted from Sze, Liu & Lo (2004) [50].

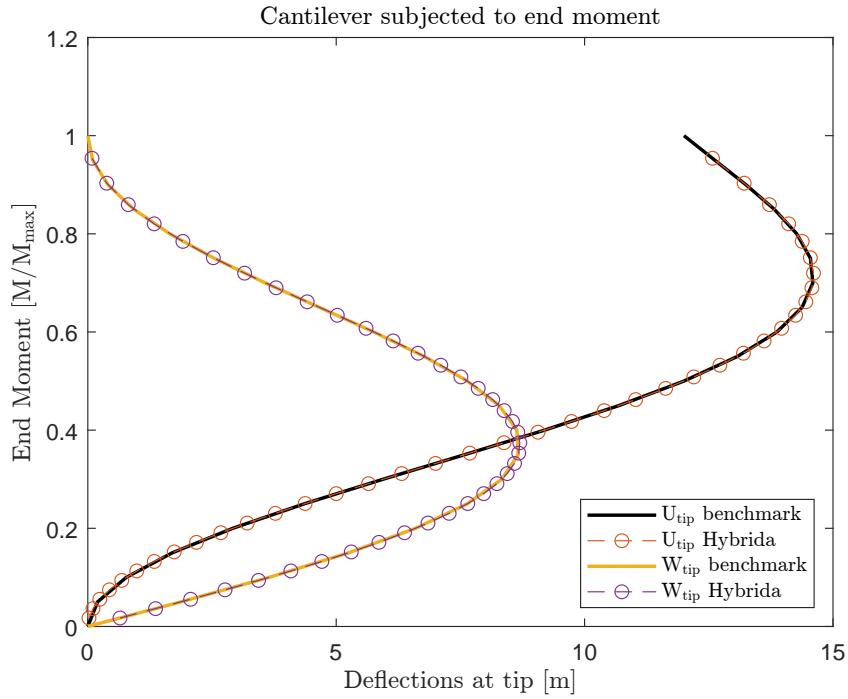


**Figure 15:** Comparison of incremental static displacements from literature (Sze, Liu & Lo [50]) to results from Hybrida finite element analysis.

### Slit annular plate subjected to shear force

The third benchmarking problem is shown in Figure 16; it describes a flat annular plate subjected to a shear force. The final deflection of the structure as computed in Hybrida is shown in Figure 17. A comparison of the results from Sze, Liu & Lo to the results from Hybrida is shown in Figure 18. The average errors throughout the nonlinear regime for the displacements at points A and B are about 3.2% and 2.5% for this experiment, respectively.

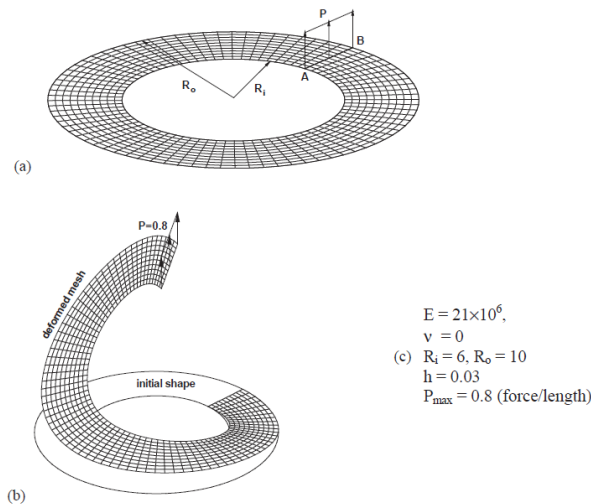


**Figure 16:** (a) Slit annular plate loaded with a line shear force  $P$ . (b) Deformed mesh under maximum load. (c) Material constants and geometric parameters used in this experiment. Adapted from Sze, Liu & Lo (2004) [50].

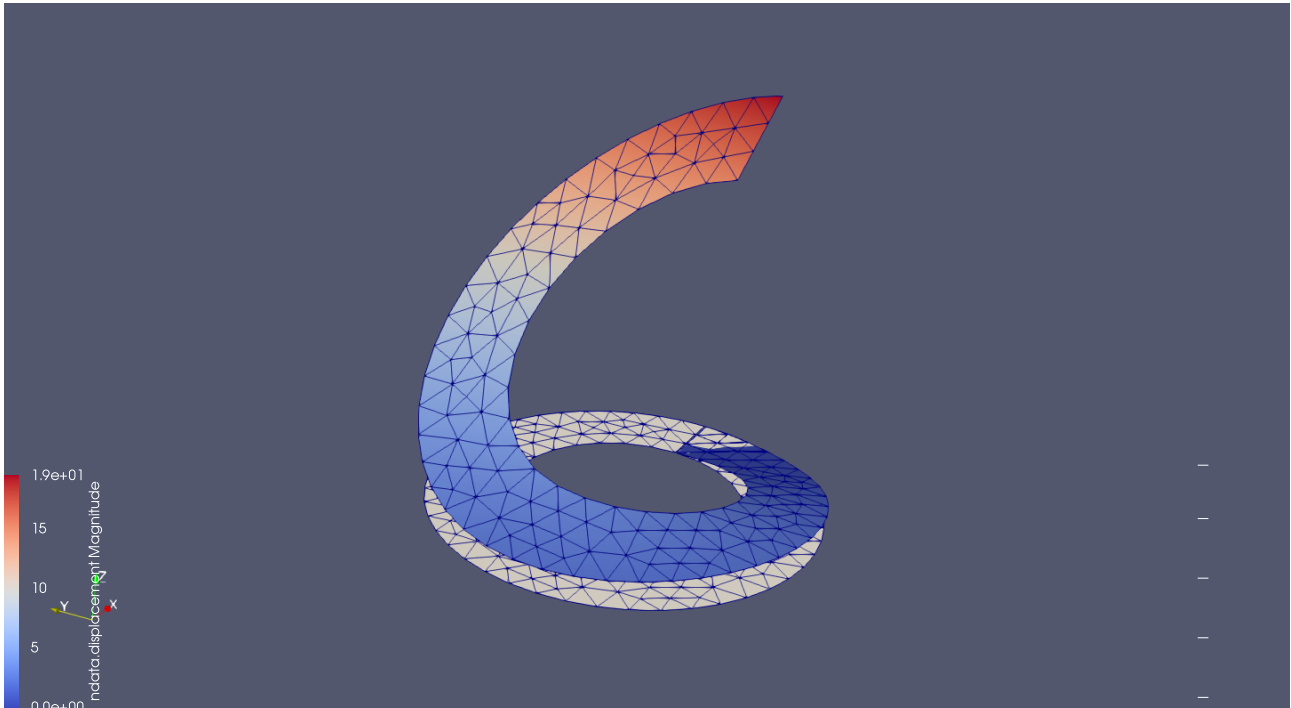


**Figure 17:** Final displacement of the slit annular plate subjected to an line shear force from *Hybrida*, using 266 triangular van Keulen elements. This final configuration was reached in 215 force increments.

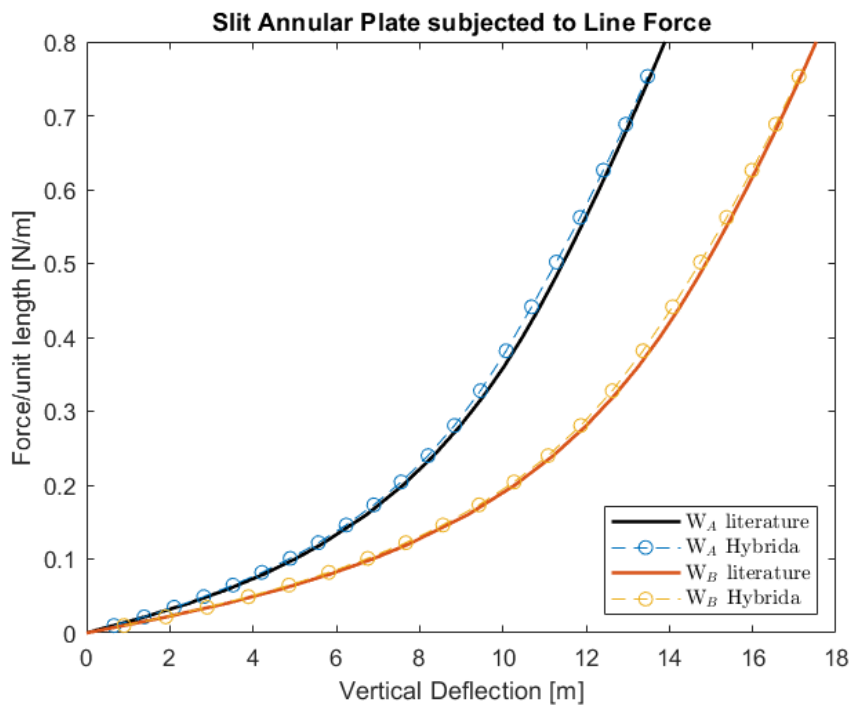


**Figure 18:** Comparison of incremental static displacements from literature (Sze, Liu & Lo [50]) to results from *Hybrida* finite element analysis.

## 2.2 Verification of static modal derivatives

After verifying the implementation of the Van Keulen in Hybrida by Markestein [73], verification of the computation method for static modal derivatives, given by

$$\theta_{ij}^{ST} = \frac{\partial \phi_i}{\partial q_j} = - \mathbf{K}_{eq}^{-1} \frac{\partial \mathbf{K}^{NL}}{\partial q_j} \Bigg|_{q=0} \phi_i \quad (29)$$

was necessary to be sure that our reduction basis is set up correctly. Verification was done in two ways:

1. Comparison of the static modal derivatives computed by intrusive and non-intrusive methods, respectively, to see whether they give the same results;
2. Comparison of the static modal derivatives computed in Hybrida to those from literature, to see whether these results line up with those from earlier work.

### Intrusive vs. Non-intrusive Static Modal Derivatives

The intrusive method of computing SMDs was developed by Pilania in 2021 and is described in more detail in Appendix A.2.2 [87]. It computes the critical term of the SMDs by taking the derivatives of the components  $\mathbf{D}_a$  and  $\mathbf{G}$  of the nonlinear stiffness matrix  $\mathbf{K}^{NL}$  with respect to the modal amplitudes  $q_j$ :

$$\frac{\partial \mathbf{K}^{NL,e}}{\partial q_j} \Bigg|_{q=0} = \frac{\partial \mathbf{D}_a^T}{\partial q_j} \cdot \mathbf{S} \cdot \mathbf{D}_a + \mathbf{D}_a^T \cdot \mathbf{S} \cdot \frac{\partial \mathbf{D}_a}{\partial q_j} + \frac{\partial \mathbf{G}}{\partial q_j} \quad (30)$$

In contrast, the non-intrusive method uses a central difference scheme, in which the structure is excited in the direction of vibration mode (VM)  $\phi_i$  with amplitude  $h$  to approximate the critical derivative:

$$\begin{aligned} \mathbf{K}_+^{NL} &= \mathbf{K}(\mathbf{u}|_{+h \cdot \phi_i}) \\ \mathbf{K}_-^{NL} &= \mathbf{K}(\mathbf{u}|_{-h \cdot \phi_i}) \end{aligned} \quad (31)$$

$$\frac{\partial \mathbf{K}^{NL}}{\partial q_j} \Bigg|_{q=0} \approx \frac{(\mathbf{K}_+^{NL} - \mathbf{K}_-^{NL})}{2h} \quad (32)$$

In order to compare the two methods, the finite difference scheme was used to compute static modal derivatives using varying step size  $h$ , which were compared to intrusively computed SMDs. The relative percentage error of the displacements fields found with the central difference scheme with regards to those found by the intrusive scheme is shown in Figure 19. The convergence shown here is similar to those found by other researchers. However, the "flatlining" on the lower end of the step size was probably due to numerical errors during computation.

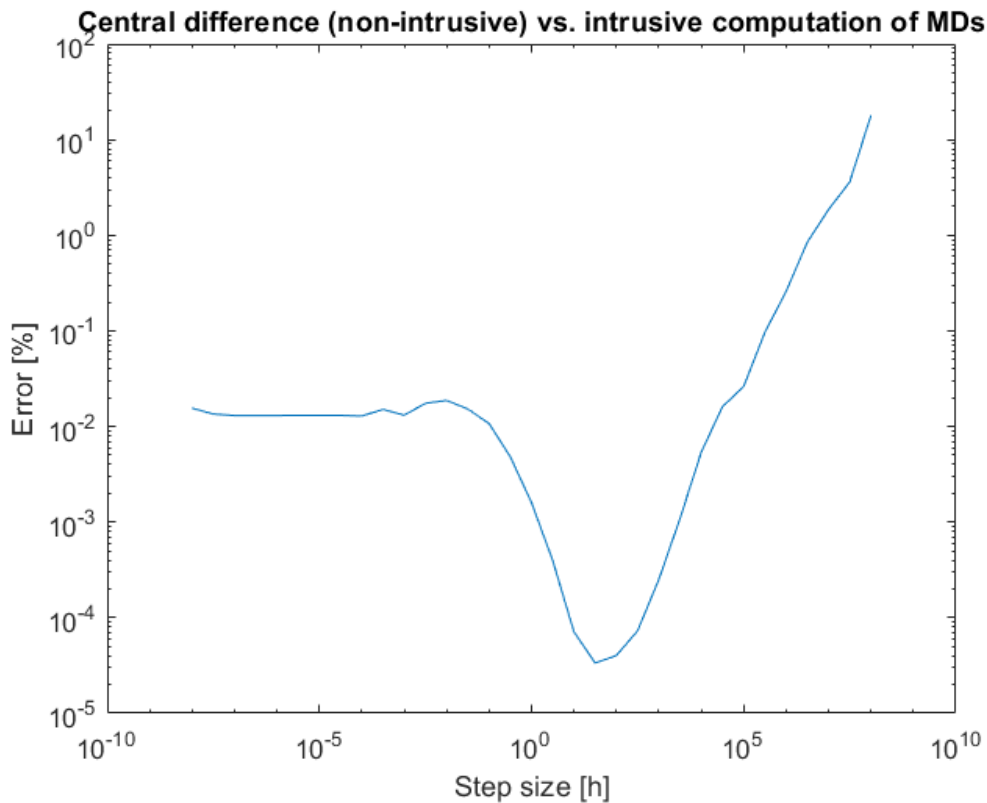


**Figure 19:** Relative difference between results computed with non-intrusive methods to reference results computed intrusively. As also found by Rutzmoser (2018), the optimal step size  $h$  for the central difference scheme usually falls around  $h = 10^0$  to  $h = 10^1$  [75].

### Comparison of Static Modal Derivatives to literature

In order to verify that the Static Modal Derivatives computed in Hybrida were comparable to methods from literature, they were visually compared to SMDs as found by Tiso in 2011 [60]. For this purpose, the cantilever investigated by Tiso was re-created in GMSH and an identical mesh was generated, as shown in Figure 20; the other parameters used in this numerical experiment can be found in Table 7. The Static Modal Derivatives  $\theta_{11}$ ,  $\theta_{13}$ , and  $\theta_{22}$  computed in Hybrida, overlaid in red on top of Tiso's Modal Derivatives in green in Figure 21, are found to have an identical shape. The differences in the Static Modal Derivatives  $\theta_{12}$ ,  $\theta_{23}$ , and  $\theta_{33}$  could be explained by differences between the finite element and orthogonalization methods used in Hybrida and the corresponding methods used by Tiso, which was confirmed by Tiso in an online meeting in 2021 [89].

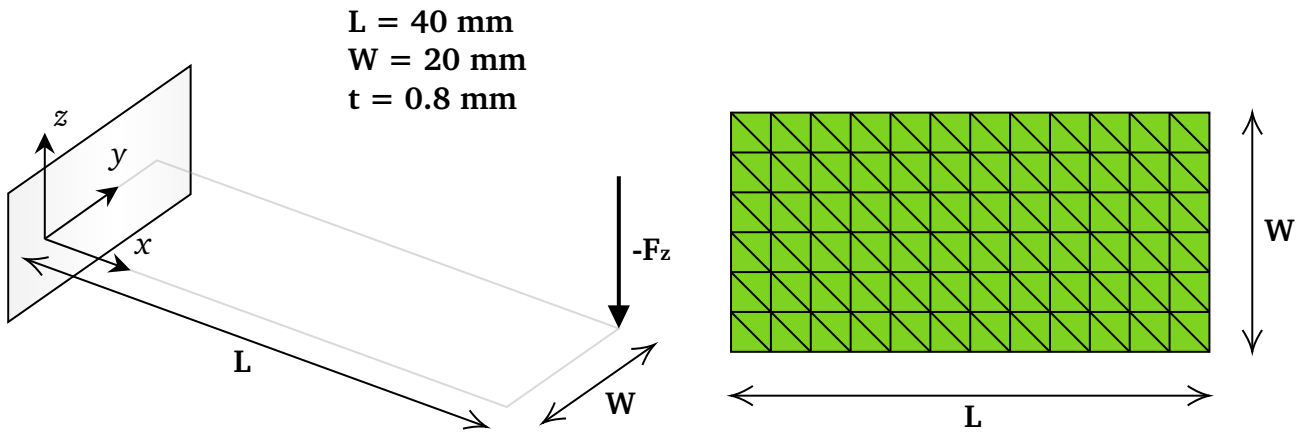


**Figure 20:** Short cantilever plate subjected to a corner force used as verification experiment to compare computed static modal derivatives. Adapted from Tiso (2011) [59].

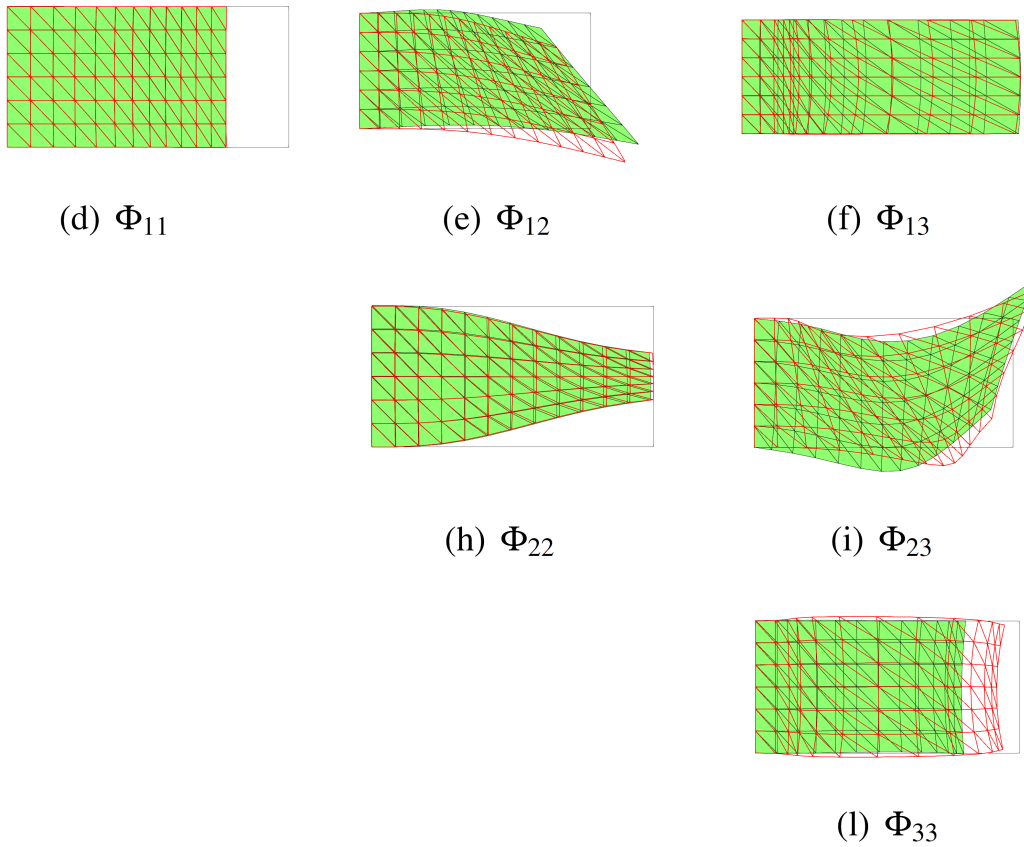


**Figure 21:** Comparison of Static Modal Derivatives from literature in green (Tiso, [60]) to those computed in Hybrida (red).

## 2.3 SMD-based Model Order Reduction in Non-linear Dynamics

### 2.3.1 Simply supported square plate, immovable edges

In this experiment, a simply supported rectangular plate with immovable edges is considered, as discussed by Ribeiro (2002) and Amabili (2004) [43, 47]. As shown in Figure 22, the plate has width  $a$  and height  $b$ , with simply supported immovable boundary conditions at all edges:

$$u = v = w = w_0 = M_x = \partial^2 w_0 / \partial x^2 = 0 \quad \text{at } x = 0, a, \quad (33)$$

$$u = v = w = w_0 = M_y = \partial^2 w_0 / \partial y^2 = 0 \quad \text{at } y = 0, b. \quad (34)$$

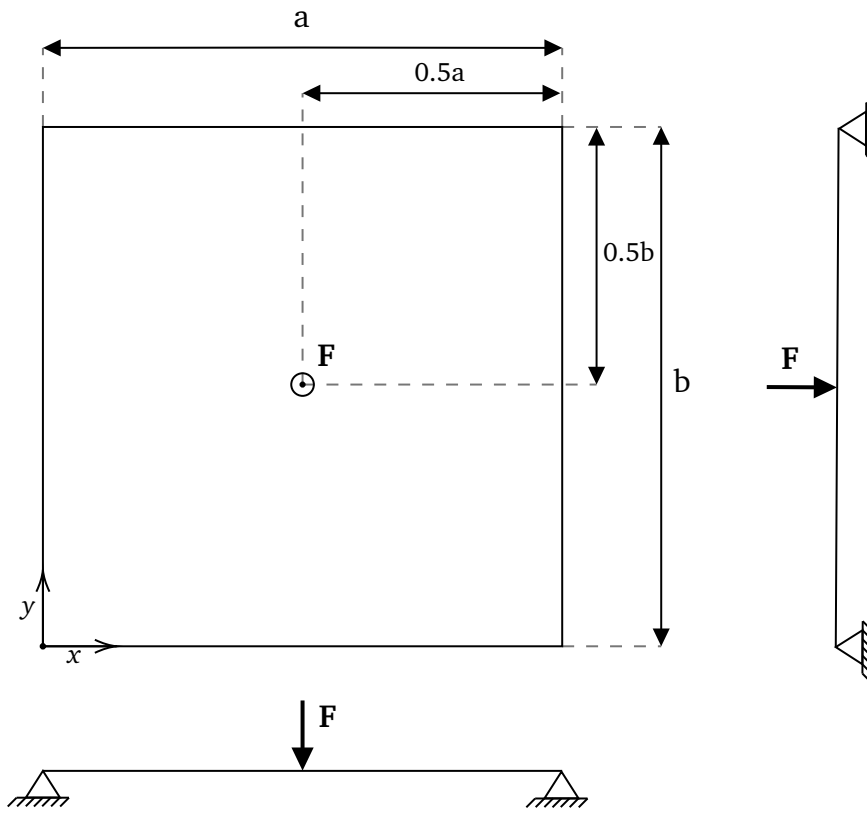


**Figure 22:** Rectangular plate with simply supported immovable edges. Adapted from Amabili (2004) and Pilia (2021) [47, 87].

The harmonic point load  $\mathbf{F} = \bar{f} \sin(\Omega t)$  is located at the center of the plate, with the read-out point placed at the same location. Amabili, in his research, used von Karman kinematics to set up an analytical model of linear combinations of panel displacements. In the case of the plate with simply supported immovable edges, he used a linear combination of 16 DoFs to compute its nonlinear frequency response around the first resonance frequency  $\Omega_0$  [47].

In Hybridra, a mesh consisting of 2021 elements was used to construct reduction bases containing linear vibration modes and modal derivatives, as described in Appendices A.2.1 and A.2.2. These reduction bases were then used to reduce the EoMs, as described in Appendix A.3.1, after which the AUTO nonlinear continuation software package was used to perform a

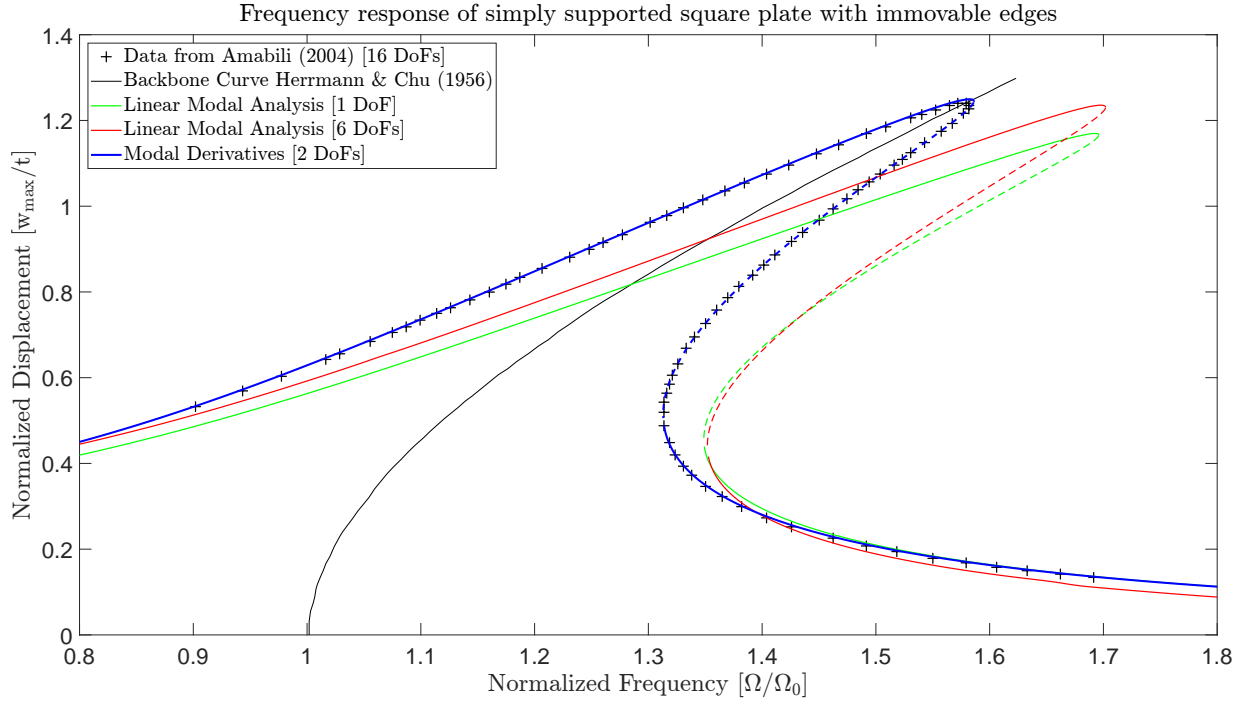


**Figure 23:** Comparison of linear modal analysis (green / red) and modal derivatives-based analysis (blue) of the simply supported plate with immovable edges in Figure 22 to results from Herrmann & Chu (1956) and Amabili (2004, fig. 2) [4, 47].

frequency sweep with normalized frequency  $\Omega/\Omega_0$  as continuation parameter. The parameters used to set up these numerical simulations can be found in Table 8.

The results are shown in Figure 23. As can be seen, the reduced-order model consisting of only vibration modes over-estimates the stiffness of the plate, even when adding additional degrees of freedom to the reduction basis. This behaviour remains when in-plane modes are added to the basis, which are hard to find: the first mode with primarily in-plane displacements,  $\phi_{321}$ , has a resonance frequency of 9933 Hz, which is roughly 180 times higher than the resonance frequency of the first mode (52.97 Hz).

When static modal derivatives are added to the reduction basis, however, the frequency response curve produced by only 2 DoFs, VM  $\phi_1$  and SMD  $\theta_{11}^{ST}$ , is nearly identical to the one computed by Amabili using 16 DoFs and matches the backbone curve predicted by Herrmann & Chu [4, 47]. This shows that the static modal derivatives inherently contain the geometrically nonlinear in-plane effects, while only needing to compute two degrees of freedom. As the in-plane displacement components are purely due to membrane stretching, i.e. the displacements of the sides of the plate are fully constrained, the modal derivatives-based analysis seems especially well suited to this problem.

### 2.3.2 Simply supported square plate, movable edges

In this section, a simply supported plate with movable edges subjected to boundary conditions

$$v = w = w_0 = N_x = M_x = \partial^2 w_0 / \partial x^2 = 0 \quad \text{at } x = 0, a, \quad (35)$$

$$u = w = w_0 = N_y = M_y = \partial^2 w_0 / \partial y^2 = 0 \quad \text{at } y = 0, b, \quad (36)$$

is analyzed by the same method as above. The results from the Hybrid finite element (FE)-based analysis using several combinations of vibration modes and modal derivatives are compared to an analytical model comprising 27 DoFs as described by Amabili [47]. The slightly changed boundary conditions are indicated in Figure 24, while the parameters used in this numerical experiment can be found in Table 9.

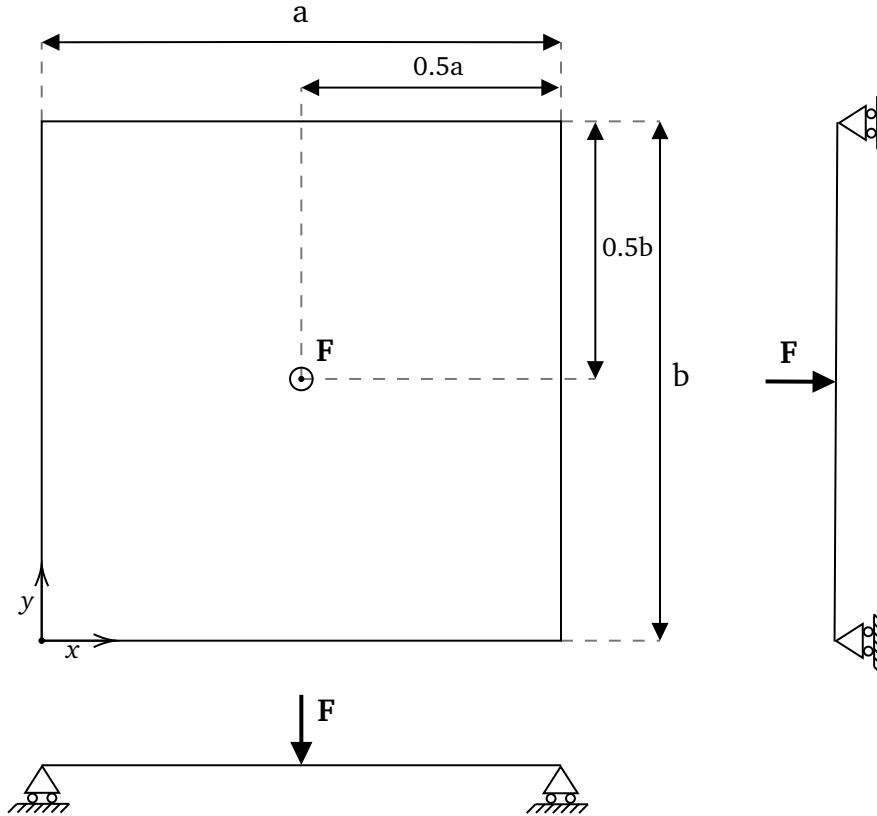


**Figure 24:** Rectangular plate with simply supported movable edges. Adapted from Amabili (2004) and Pilia (2021) [47, 87].

As shown in Figure 25, in this case the reduction basis using only linear vibration modes over-estimates the stiffness of the structure even more than for the plate with immovable edges in subsection 2.3.1. The reduced model including SMDs is much more in agreement with the results from Amabili (2004), but still slightly over-estimates the stiffness of the structure in comparison with his predicted frequency response curve [47]. This could be due to the edges of the plate not being fully constrained in this problem, which will lead to in-plane displacement components that are not only caused by membrane stretching but also by warping of the edges.

When additional DoFs are added to the reduction basis an effect is observed wherein for purely vibration-modes based analysis, the amplitude of the dynamics increases, but for modal derivatives-based analysis, the amplitude of the dynamics decreases. In this latter case, the vibration modes  $\phi_1, \phi_5, \phi_{11}$  and the static modal derivatives  $\theta_{11}^{ST}, \theta_{15}^{ST}, \theta_{1-11}^{ST}, \theta_{55}^{ST}, \theta_{5-11}^{ST}, \theta_{11-11}^{ST}$  seem to have a dampening effect on the frequency response of the plate. This could be due to energy being absorbed by vibrations that do not contribute to the vertical deflection of the read-out point, which is the coordinate plotted in Figure 25.

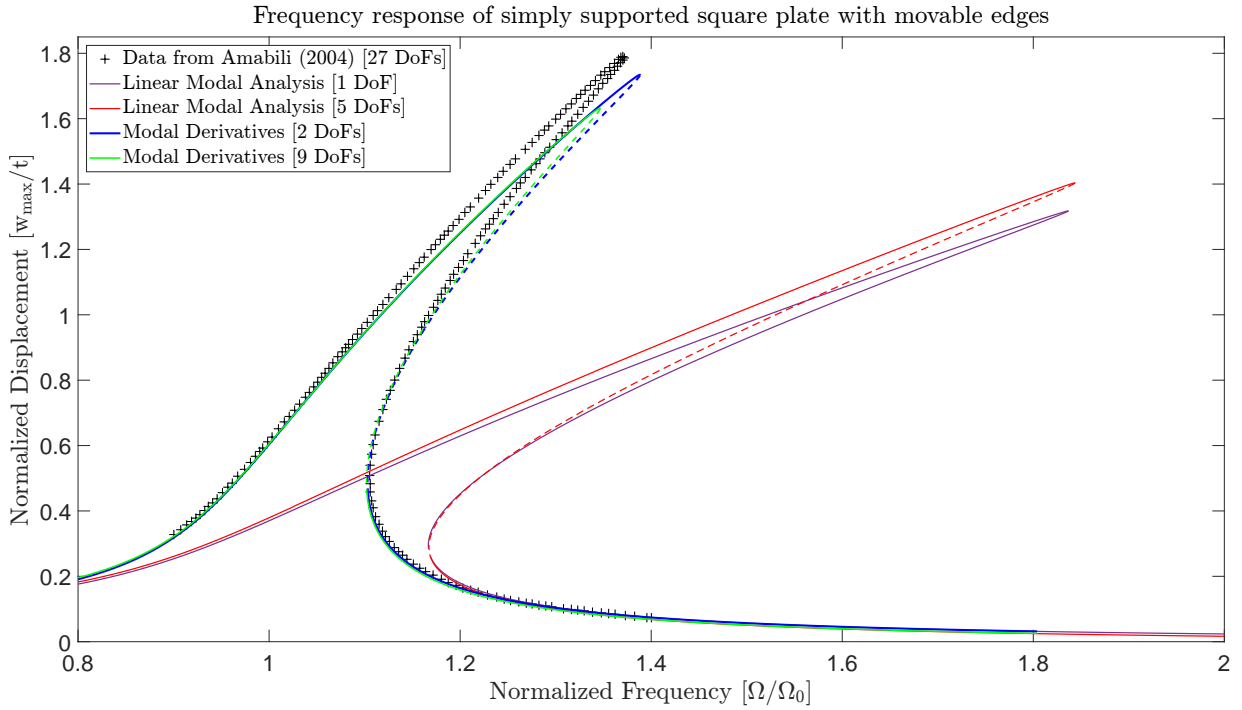


**Figure 25:** Comparison of linear modal analysis (purple / red) and modal derivatives-based analysis (blue / green) of the simply supported plate with movable edges in Figure 24 to results from Amabili (2004, fig. 4) [47].

### 2.3.3 Vertical Cantilever

The third numerical experiment considers the vertical cantilever shown in Figure 26 as described by Malatkar in 2003 [44]. The cantilever discussed in his paper constitutes a lightly damped, weakly nonlinear system without internal resonances. Malatkar both numerically derived equations of motion and performed physical experiments on a steel beam to estimate the parameters describing the nonlinear behaviour of the cantilever. Malatkar specifically investigated the third and fourth modes of the vertical cantilever in more detail.

In HybridA, reduced-order modelling was performed using both linear in-plane vibration modes and modal derivatives as a reduction basis. The parameters used in these experiments can be found in Table 10. In Figure 28, the results of the reduced-order modelling using in-plane vibration modes are shown. As can be seen, the linear modal analysis once again grossly over-estimates the stiffness of the structure. By adding in-plane modes, we can reduce the stiffness estimate, but even by using all in-plane modes  $\phi_n$  with  $n < 200$ , the weak softening response as found by Malatkar cannot be reproduced.

When the static modal derivative  $\theta_{33}$  is added to the basis, however, the softening non-linearity of the third mode is captured by the reduced-order model Figure 29, showing unstable regions (dotted lines) for the two highest forcing values  $F = 0.00165$  and  $F = 0.0022$ . While the static modal derivative  $\theta_{33}$  shown in Figure 27i looks similar to the first in-plane vibration mode  $\phi_{29}$  (Figure 27b), the in-plane strain is distributed evenly along cantilever for the in-plane vibration mode whereas it is distributed non-linearly for the modal derivative. This difference in the distribution of the in-plane strains ensures that the basis containing static modal derivatives captures the geometric non-linearity much more accurately than the basis containing the in-plane vibration mode.

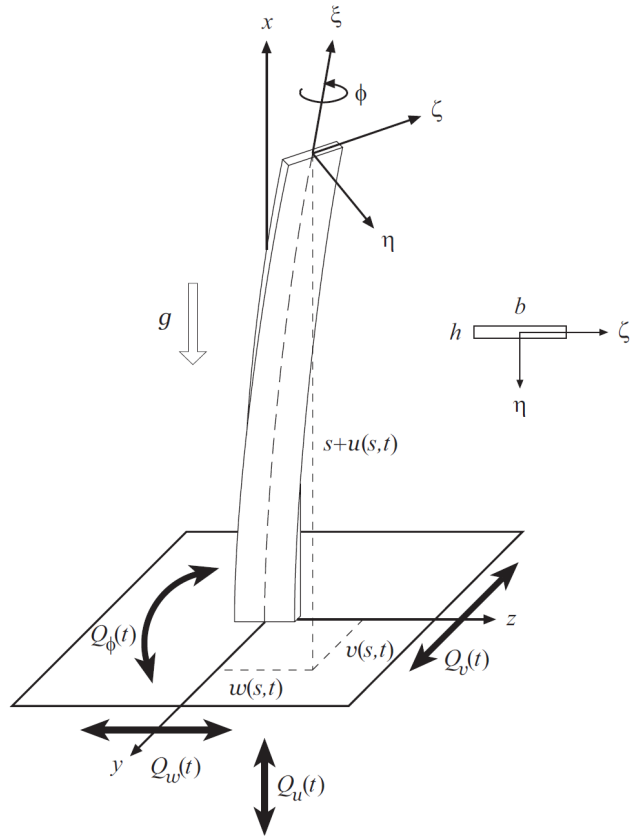


**Figure 26:** Vertical cantilever. Reprinted from Malatkar (2003) [44].

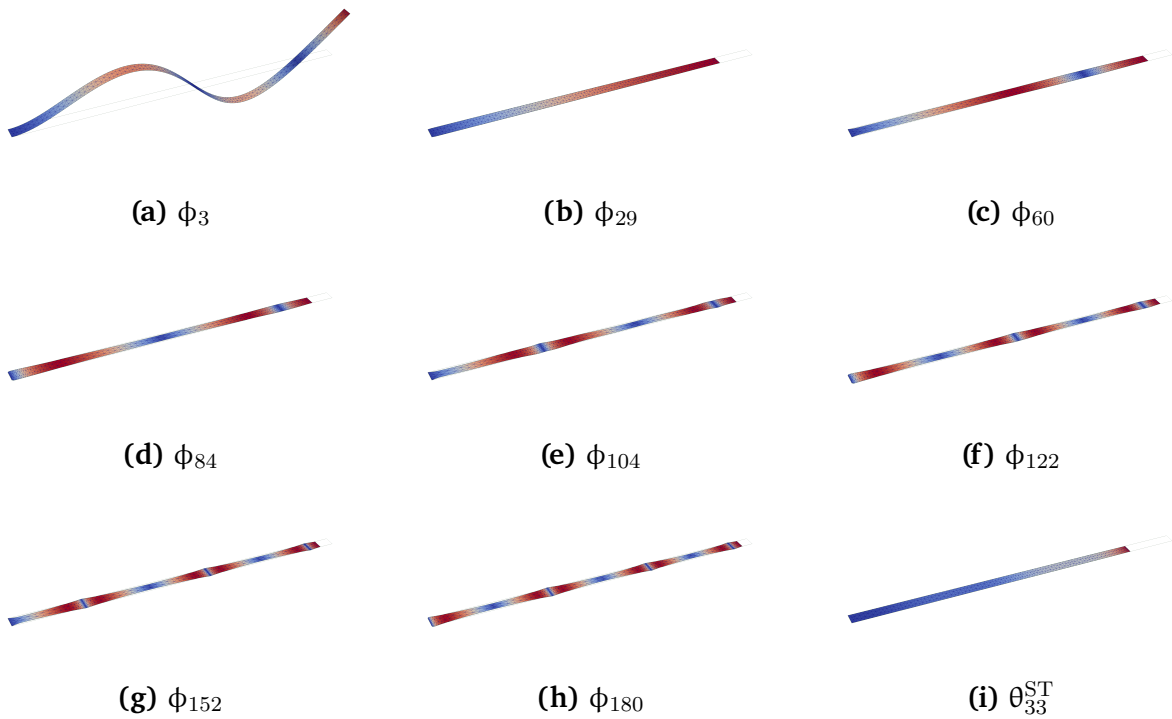


**Figure 27:** Third mode, in-plane modes  $\phi_n$  with  $n < 200$ , and the Static Modal Derivative  $\theta_{33}^{ST}$  associated with the third mode of the vertical cantilever shown in Figure 26. The results of the model reduction using these DoFs is shown in Figures 28 and 29.

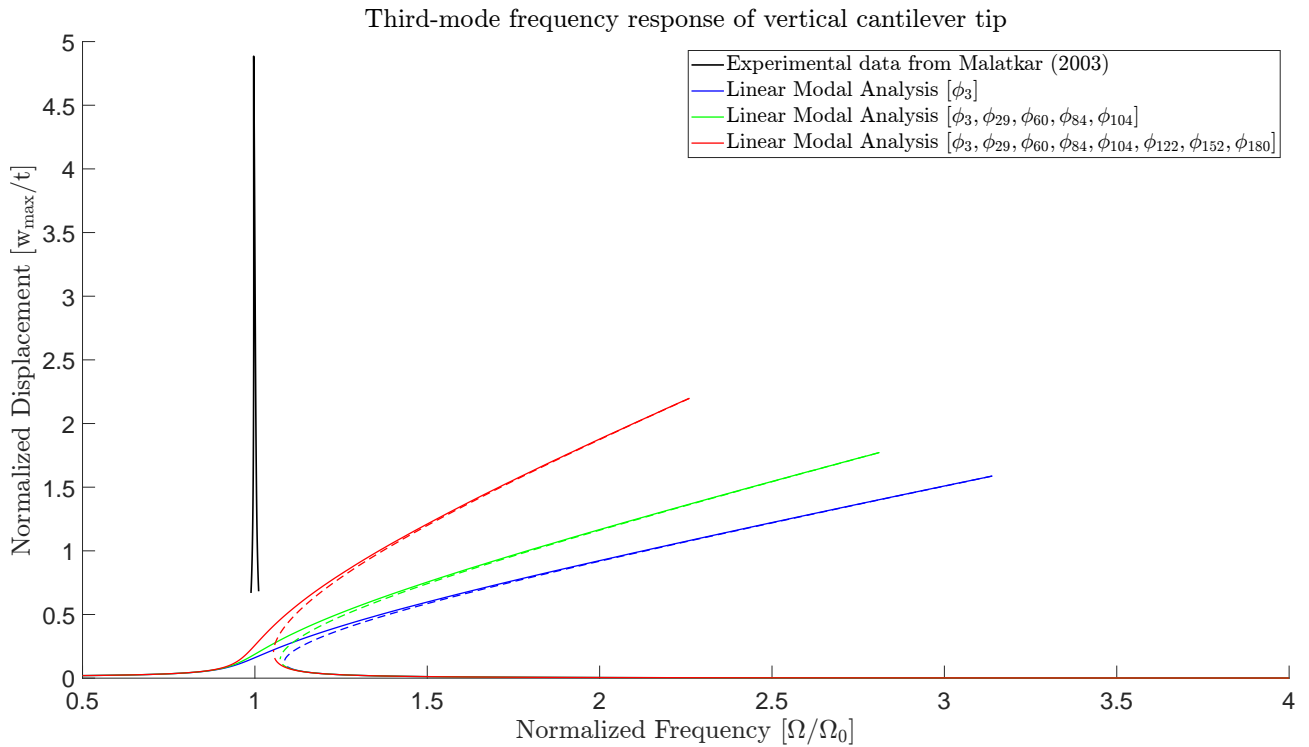


**Figure 28:** Comparison of linear modal analysis (blue / green / red) of the vertical cantilever in Figure 26 to experimental results from Malatkar (2003, fig. 3.4) [44].

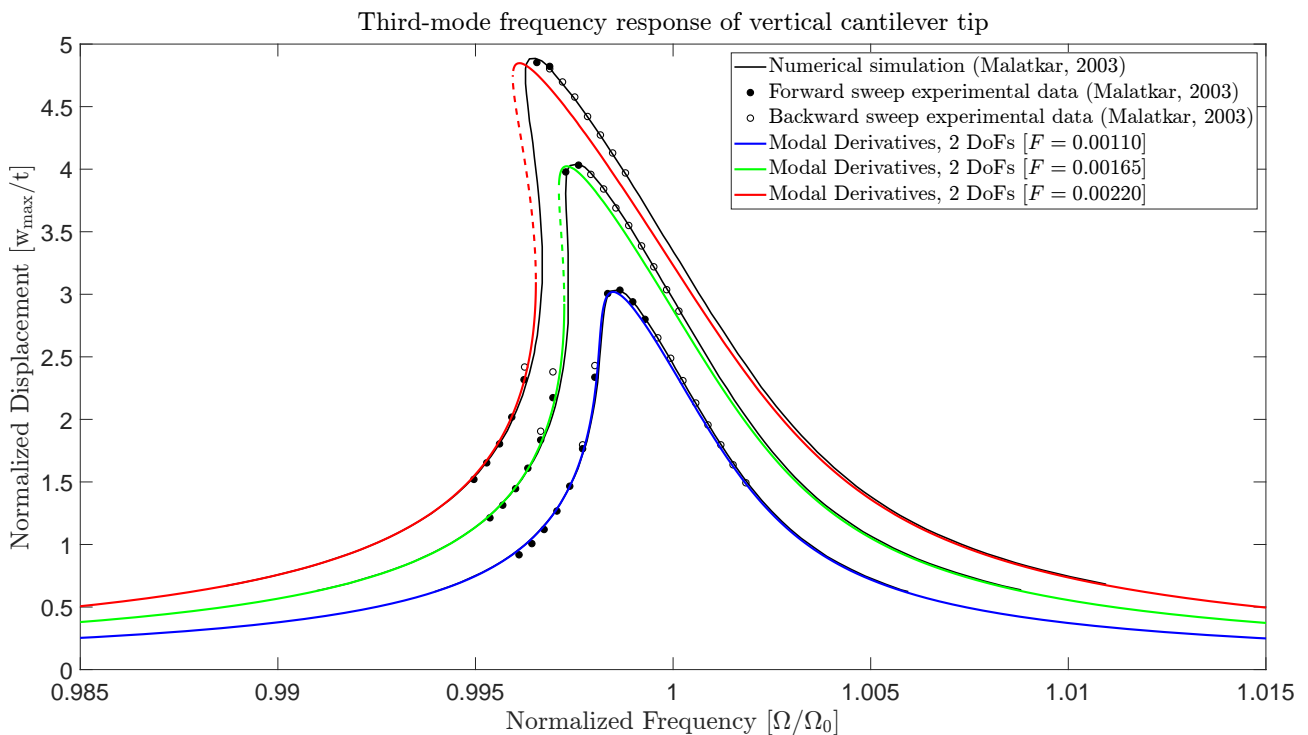


**Figure 29:** The same graph as in Figure 28, but zoomed in on the x-axis, using static modal derivatives-based analysis (blue / green / red) of the vertical cantilever in Figure 26 for increasing forcing values. Comparison to experimental results from Malatkar (2003, fig. 3.4) [44].

### 2.3.4 MEMS Double Clamped Beam

This numerical experiment considers a double-clamped beam as investigated by Vizzacarro, which features an internal 3:1 resonance between the first and fourth modes [83]. Vizzacarro compared a reduced-order model using the direct normal form (DNF) to a full solve of the systems' nonlinear dynamics using the harmonic balance finite element method (HBFEM). In Hybrida, the same structure was meshed using 96845 elements and a ROM was constructed using 10 DoFs in both cases. The parameters used to set up this experiment can be found in Table 11.

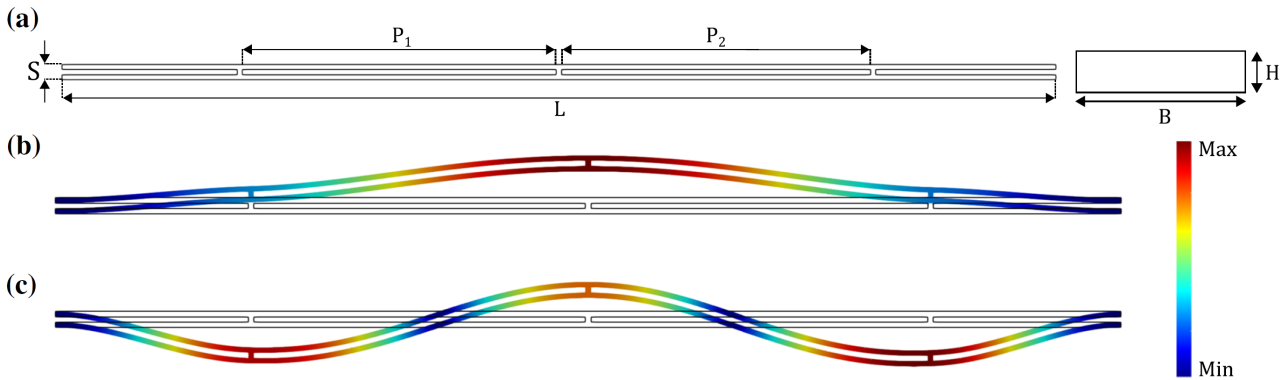


**Figure 30:** Double-clamped MEMS beam. Reproduced from Vizzacarro (2021) [83].

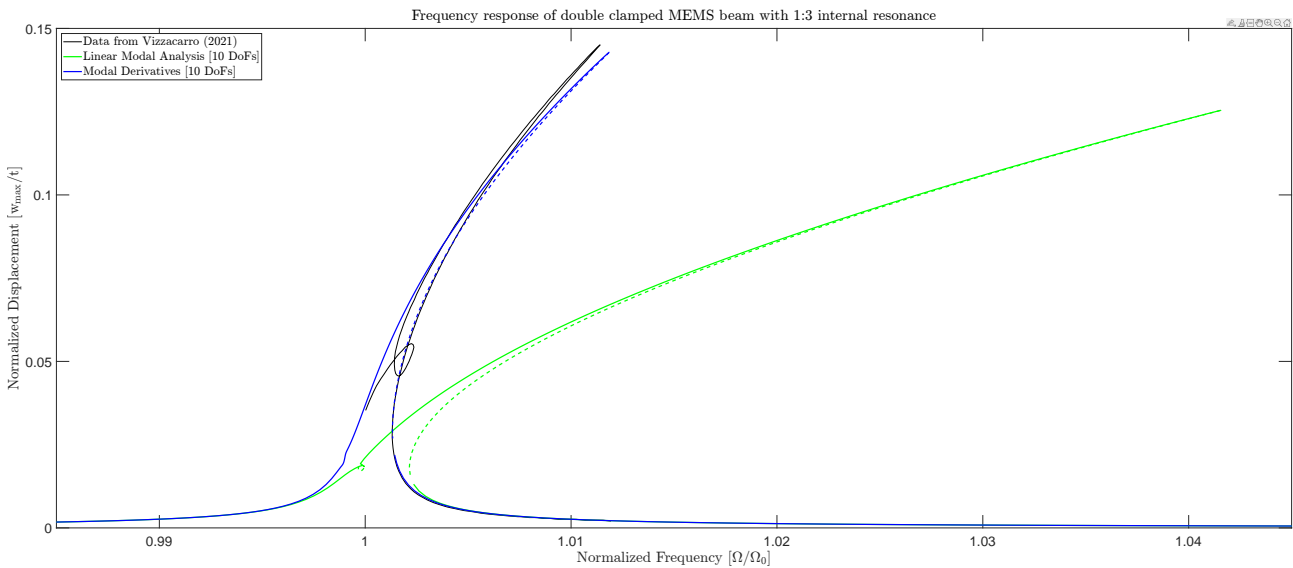


**Figure 31:** Comparison of frequency response functions of the double clamped beam shown in Figure 30. Responses were computed using reduced order models based on vibration modes (green), static modal derivatives (blue), and direct normal form (black) [83].

As can be seen, once again the vibration modes overestimate the stiffness of the structure, while the modal derivatives come very close to the data from Vizzacarro's full HBFEM solve in regards to amplitude and nonlinearity of the solution. The internal 1:3 resonances, however, are not fully reproduced by either the vibration-modes or modal-derivatives based ROM. Great effort was undertaken to make sure the internal resonance was as close as possible to an exact 1:3 ratio, by slightly increasing the length of the beam and decreasing the mesh size until a ratio of  $3.000 \pm 0.001$  between the resonance frequencies of modes  $\phi_4$  and  $\phi_1$  was achieved.

### 2.3.5 Single-curved circular cylindrical shell

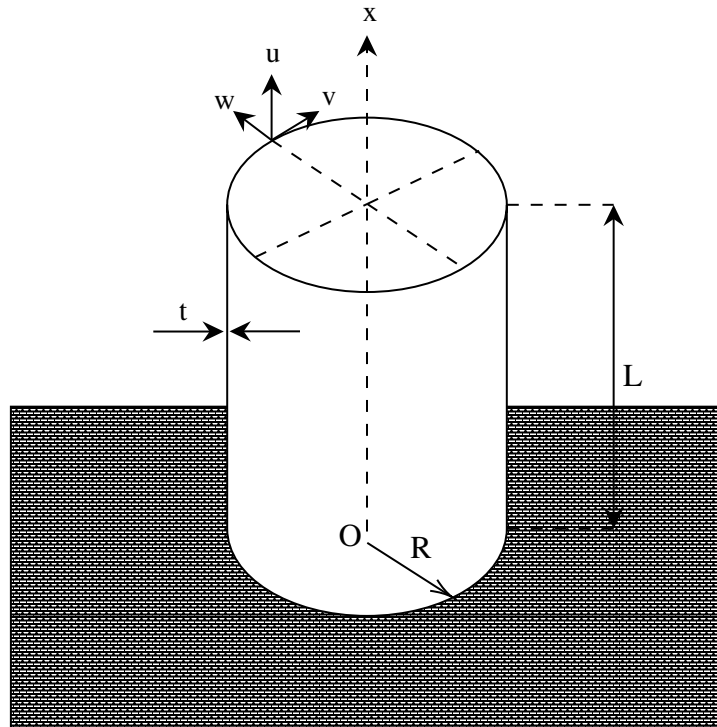


**Figure 32:** *Circular cylindrical shell with clamped bottom edge. Adapted from Kurylov (2011) [58].*

After looking at various flat structures, the next step is to look at shells in 3D. The first 3D experiment is the circular polyester shell as described numerically by Kurylov and Amabili (2011) [58], which was also tested experimentally by Chiba in 1993 [25]. Kurylov & Amabili used harmonic functions to describe the vibrations of the structure in radial direction and Chebyshev polynomials to describe the displacements in axial direction. The bottom edge of the cylinder is completely clamped. A harmonic concentrated force in radial direction at  $x = L/2$  acts on the shell. Kurylov & Amabili tried to remove the over-stiffening by adding DoFs until the frequency response function converged, as shown in Figure 33:

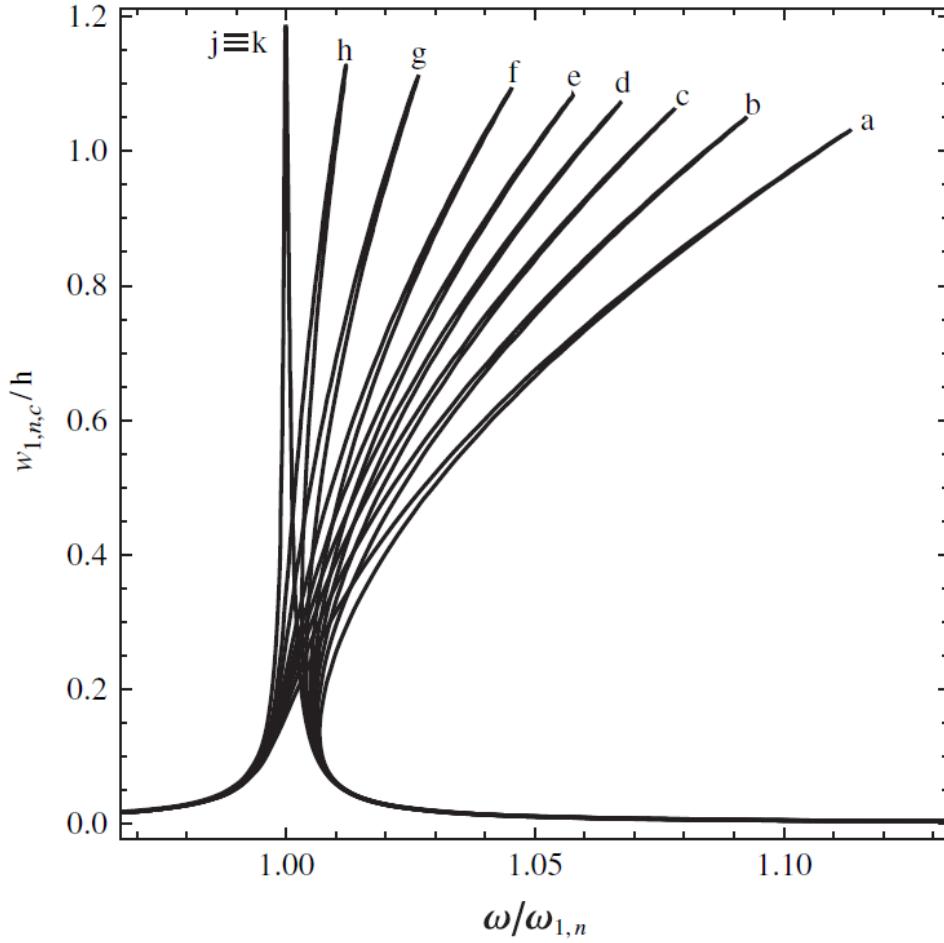


**Figure 33:** The frequency response function due to forcing  $f_1 = 0.0012$  of the cylindrical shell, shown in Figure 32, converges to a steady solution when adding enough DoFs: (a) 18 DoFs; (b) 20 DoFs; (c) 22 DoFs; (d) 24 DoFs; (e) 26 DoFs; (f) 28 DoFs; (g) 30 DoFs; (h) 40 DoFs; (j) 43 DoFs; and (k) 47 DoFs. Reprinted from Kurylov (2011) [58].

In Hybrida, the numerical experiment in Figure 33 was repeated, using a mesh of 98416 triangular shell elements to set up the equations of motion. The reduction bases used to reduce these EoMs consisted of either 1 DoFs, vibration mode  $\phi_1$ , or 2 DoFs, vibration mode  $\phi_1$  + static modal derivative  $\theta_{11}^{ST}$ . The results of this experiment are shown in Figure 34. As can be seen, the numerical analysis using vibration modes grossly overestimates the stiffness of the structure, whereas the modal derivatives-based analysis converges to the same response as Kurylov's 47 DoFs using only two degrees of freedom.

### 2.3.6 Double curved shallow shell

The last example is the double curved shallow (i.e. relatively large radius of curvature) shell shown in Figure 35 investigated by Amabili in 2005 [51]. The boundary conditions are the same simply supported with movable edges as in subsection 2.3.2:

$$v = w = w_0 = M_x = \partial^2 w_0 / \partial x^2 = 0 \quad \text{at } x = 0, a, \quad (37)$$

$$u = w = w_0 = M_y = \partial^2 w_0 / \partial y^2 = 0 \quad \text{at } y = 0, b. \quad (38)$$

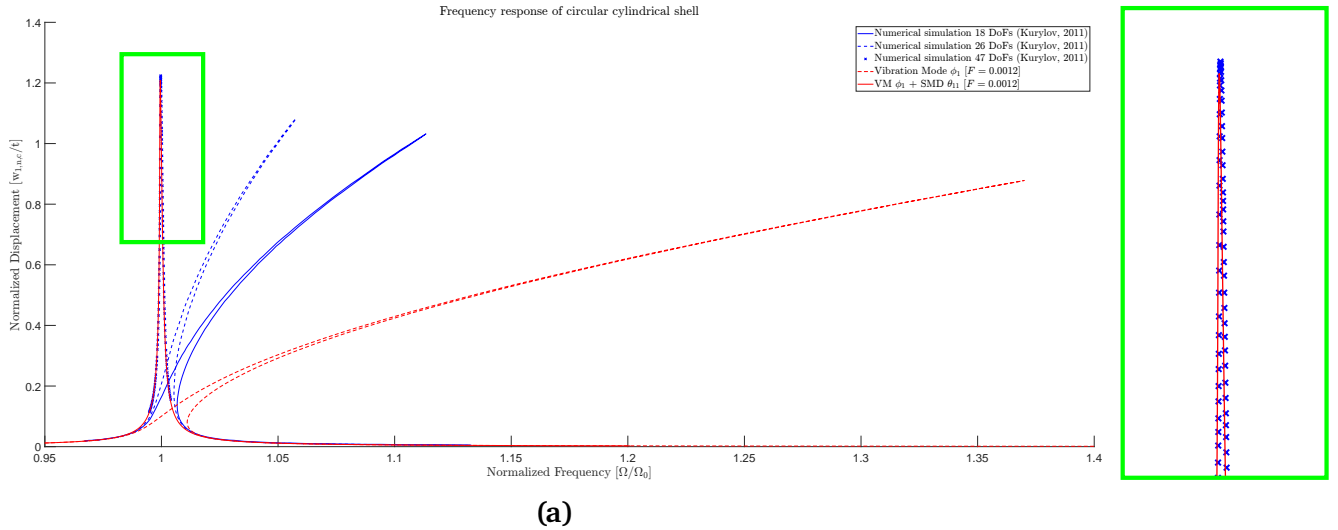


**Figure 34:** Comparison of frequency response functions of the circular cylindrical shell shown in Figure 32. Data from Kurylov Figure 2 is shown in blue, showing the convergence of the result using 47 DoFs in total [58]. The Hybrid MOR results were computed using VM  $\phi_1$  and VM  $\phi_1$  + SMD  $\theta_{11}$ , respectively.

Amabili reported resonance frequencies for the out-of-plane modes  $w_{1,1}$ ,  $w_{1,3} = w_{3,1}$ , and  $w_{3,3}$  of 952.31, 2575.9, and 4472.3 Hz, respectively. In Hybrid, the frequencies of the same modes were found to be  $\omega_0 = 953.2$  Hz,  $\omega_4 = \omega_5 = 2569$  Hz, and  $\omega_{10} = 4461$  Hz, respectively, for a maximum relative percentage error of 0.25%.

Amabili used Donnell's shell theory and a basis of 9 degrees of freedom (being the out-of-plane mode  $w_{1,1}$  and the in-plane modes  $u_{1,1}$ ,  $v_{1,1}$ ,  $u_{1,3}$ ,  $v_{1,3}$ ,  $u_{3,1}$ ,  $v_{3,1}$ ,  $u_{3,3}$ , and  $v_{3,3}$ ) to find the minimum and maximum amplitude of the frequency response of a shell with  $R_x = R_y = 10a$ , which is a relatively small curvature with respect to the principal dimensions of the shell. The other parameters of this experiment can be found in Table 12. Amabili splits the results into two, giving separate frequency response curves for both the maximum positive and maximum negative excitation of the generalized coordinate  $w_{1,1}$  at the center of the shell.

In Hybrid, I tried to repeat these results by mimicking the basis created by Amabili, using the out-of-plane mode  $\phi_0$  and in-plane modes  $\phi_{117}$ ,  $\phi_{148}$ ,  $\phi_{149}$ , and  $\phi_{162}$ . The results of this vibration-mode based analysis are shown in Figure 36. As shown, even when adding the in-plane modes to the reduction basis, the softening-hardening response shown by Amabili could not be reproduced. However, by adding the SMD  $\theta_{11}$  (shown in Figure 37) the response predicted by Amabili using 9 degrees of freedom is followed up to amplitudes approximately equal to the thickness of the shell. Afterwards, a large deviation can be seen including higher order dynamics caused by internal resonances. These are unphysical, as internal resonances should not be caused by the static modal derivatives.

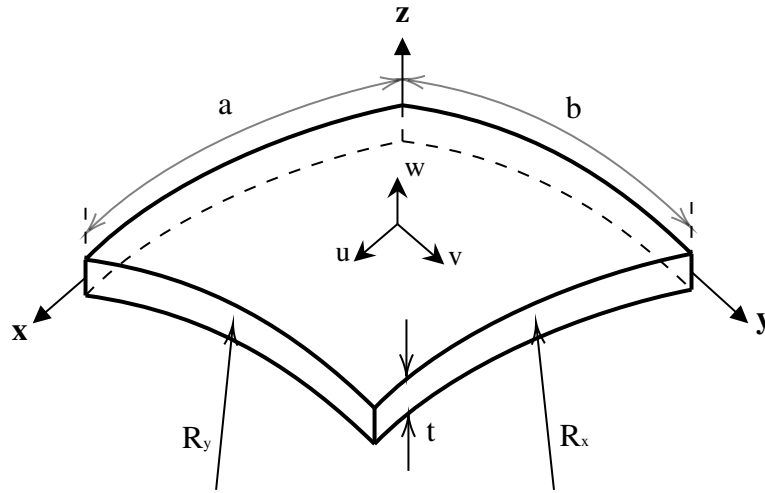


**Figure 35:** Double curved shallow shell with simply supported immovable edges. Adapted from Amabili (2005) [51].

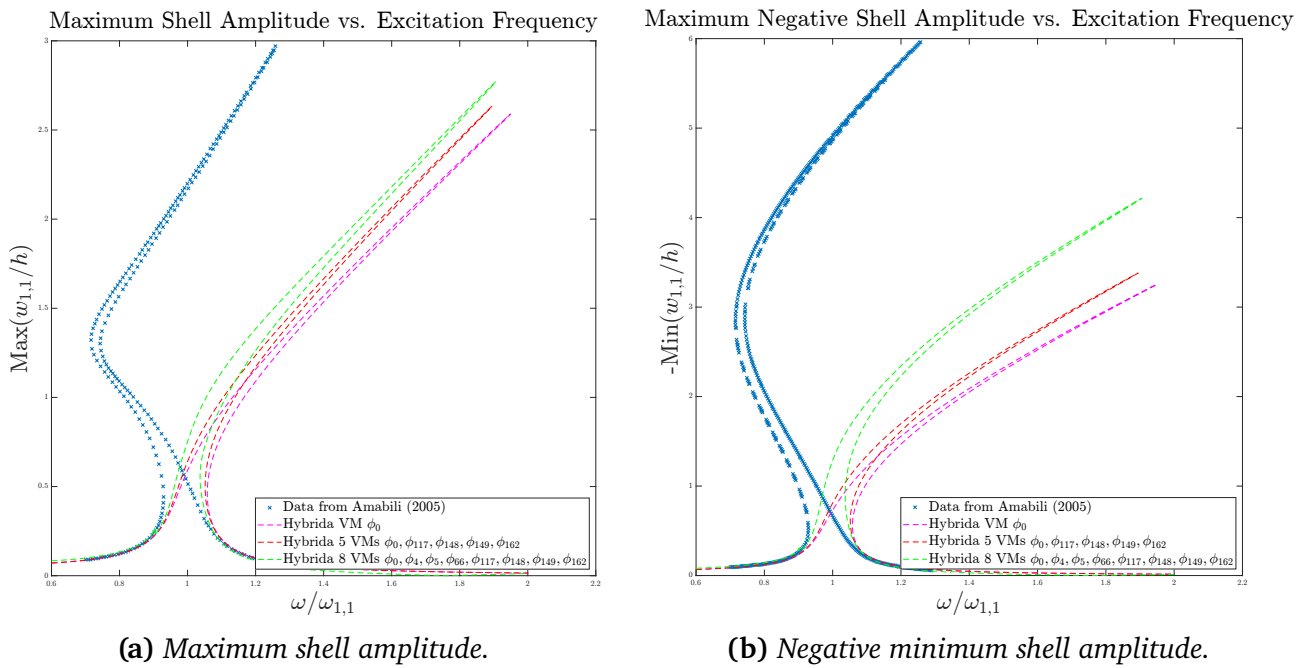


**Figure 36:** Comparison of linear vibration modes-based reduced order modelling to results from Amabili (Figure 3, 2005) based on out-of-plane and in-plane vibration modes. Results on the left are the maximum out-of-plane coordinate of the first mode  $w_{1,1}$ , while results on the right represent the negative minimum coordinate  $-w_{1,1}$  [51].

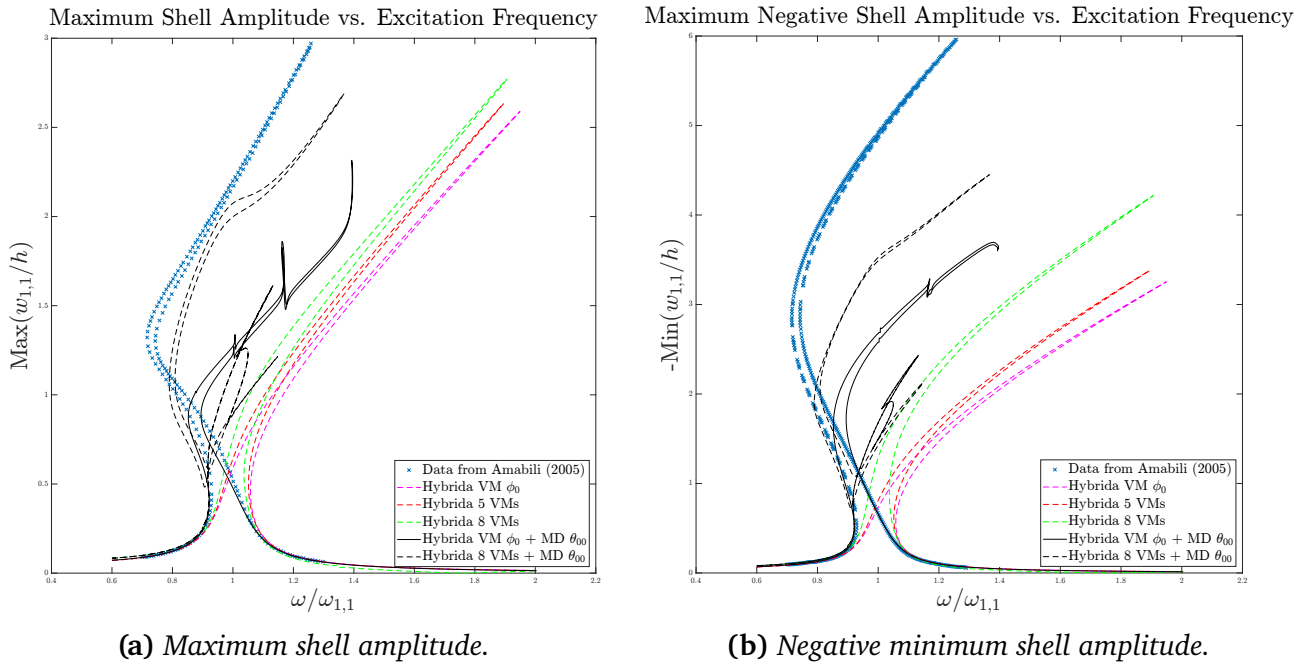


**Figure 37:** Comparison of static modal derivatives-based reduced order modelling to results from Amabili (Figure 3, 2005) based on out-of-plane and in-plane vibration modes. Results on the left are the maximum out-of-plane coordinate of the first mode  $w_{1,1}$ , while results on the right represent the negative minimum coordinate  $-w_{1,1}$  [51].

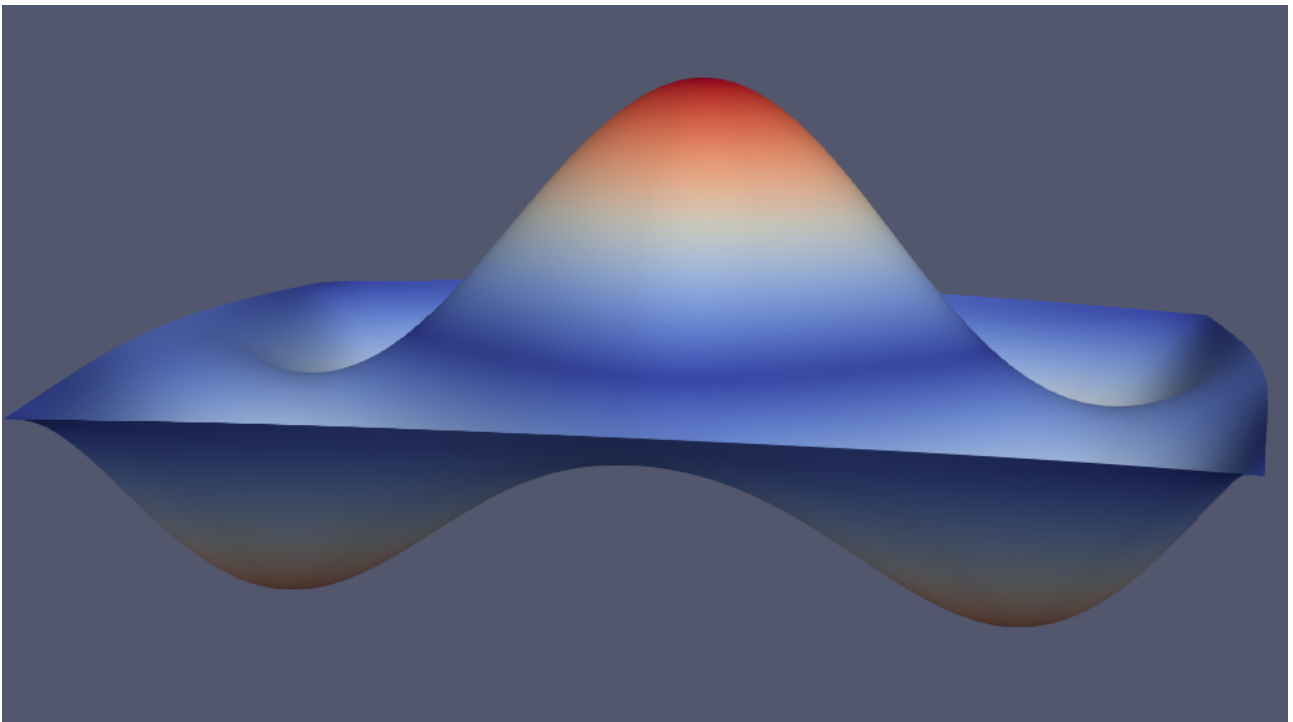


**Figure 38:** The first static modal derivative  $\theta_{11}$  associated with the double curved shallow shell shown in Figure 35. As shown, the static modal derivative for this structure shows almost purely out-of-plane behaviour, differing from the flat structures in Subsections 2.3.a - 2.3.d.

## 2.4 Conclusions

### 2.4.1 Verification of finite element implementation

In all three benchmarking problems shown in subsection 2.1, errors are in the order of 1% throughout the nonlinear regime, even while using relatively course meshes. The final displacements are also very similar to the final reported displacements by Sze, Liu and Lo [50]. I therefore conclude that the van Keulen triangular shell elements are verifiably accurate for static geometrically nonlinear displacements of shell structures.

### 2.4.2 Verification of static modal derivative implementation

Based on the verification results presented in subsection 2.2, I conclude that the Hybrida-based code to compute static modal derivatives of shell structures, as initially written by Pilaiania [87] and thereafter slightly tweaked by the author, produces repeatable results that are in agreement with existing literature [59, 75]. This conclusion was confirmed by the author of one of the references papers in a separate interview in 2021 [89]. The correct implementation of the static modal derivatives is further proven in subsection 2.3, as the SMDs are used to great effect in computing reduction bases used to reduce equations of motion in analysis of nonlinear dynamics.

### 2.4.3 SMD-based model order reduction for nonlinear dynamics

In all 6 numerical experiments discussed in subsection 2.3, it can clearly be seen that model order reduction bases using only vibration modes overestimate the stiffness and hardening of nonlinearly vibrating structures, usually to a large extent. This can be duly explained by the lack of terms in the reduced EoMs which account for geometrically nonlinear effects. However, when enhancing these VM-based modal reduction bases with static modal derivatives, the frequency response curves are found to match the results expected from literature to a far greater extent. This is true even for reduction bases using only two degrees of freedom (usually  $\phi_1 + \theta_{11}$ ), of which the computed frequency response curves agree with results from literature using far greater amounts of DoFs (see, for example, subsection 2.3.5).

The Hybrida-based nonlinear analysis performed in subsection 2.3 takes only minutes to complete, with  $\pm 30\%$  of the time spent on computations related to the finite element discretization (which only have to be done once if the structure, loading, and readout point do not change between experiments). The time spent online, that is, computing a reduction basis, reducing the equations of motion, and performing time integration usually accounts for  $\pm 70\%$  of the total analysis time. This could be shortened further when computer with additional cores are used, as piece-wise reduction of the equations of motions on the element level, detailed in subsection A.3.1, can be performed in parallel on separate cores. In this case, the main limiting factor is the amount of DoFs passed to the AUTO nonlinear continuation software. For a number of DoFs  $m$  surpassing 15, slower results were observed, taking more than an hour to produce results, if any were produced at all.

The projective model order reduction method as implemented in Hybrida, using vibration modes and static modal derivatives to perform piece-wise reduction of the higher order tensors in the equations of motion, shows great promise when used for analysis of nonlinear dynamics with amplitudes of up to 5 times the shell thickness. However, when used for curved structures, this static modal derivative-based method only holds up to amplitudes of roughly 1 - 1.5 times

the thickness of the underlying structure, after which large deviations from results found in literature were observed.

Therefore, based on the method implemented in the Hybrida codebase, I conclude that while static modal derivatives are a great tool for enhancing vibration mode-based reduction bases when amplitudes are limited and no higher order dynamics are present, they fall short when those features are present and/or of interest to the observer.

## 2.5 Discussion

The results shown in subsection 2.3 show that non-intrusively computed static modal derivatives can be a quick and easy way to increase the accuracy of model-based model order reduction for nonlinearly vibrating structures. While a massive decrease in computation time can be achieved by using only a handful of degrees of freedom in a nonlinear continuation, the method has limitations in accurately describing nonlinear dynamic effects such as bifurcations and limit cycles, as vibration modes causing these effects are usually excluded from the reduction basis. Furthermore, static modal derivatives do not have a "resonance frequency" in the traditional sense of the word and therefore do not trigger these types of chaotic behaviours themselves.

Taking all this into account, it seems that the method presented in this thesis using (static) modal derivatives is a compelling "quick and dirty" method of enhancing reduction bases in nonlinear dynamic analysis for shells with constant wall thickness, as the presented method produces results that are largely in agreement with results presented in literature while only taking minutes to compute said results. However, no quantitative comparison to results or computation times of other model order reduction methods was done, as no such methods were implemented in the Hybrida library at the time of writing of this report. To really judge the performance of the presented static modal derivative-based reduction method, such a comparison would be necessary.

## 2.6 Recommendations

- Other methods for computing reduced-order models should be implemented in Hybrida, to quantitatively compare the accuracy and computation time gain of each method;
- While the workflow in Hybrida has been expanded to automatically call the Intel oneAPI Fortran compiler and the AUTO nonlinear continuation software, this has not yet been used to perform iterative nonlinear dynamic analysis and/or parameter sweeps;
- The incremental-iterative solution method for reduced-order models in statics should be further expanded in Hybrida. This will allow for using reduced-order models in statics, and comparing them to full static solutions.

### 3 Process Reflection

At the end of November 2020, I started my thesis project under professors Aragon and Alijani. Because of the Covid pandemic, which was still raging at the time, I had been looking for a thesis project which I could mostly do from home (due to closing of schools and universities during lockdown). Therefore, I looked for a project which would let me pursue my interest in various applications of the Finite Element method, without requiring me to be present at the (at that time often closed) faculty for experiments or lab work. A research project into the use of Model Order Reduction in Non-linear Dynamics, which was originally started in 2018 by Koen Markestein, was available at that time and piqued my interest.

The work in 2018 done by Markestein focused on the inclusion of the triangular "Van Keulen" shell element into the Hybrid finite element library, and then using this element in reduced-order modelling. To this end, he pioneered the still in use tensor decomposition and piecewise (elemental) reduction of the elements as described in Appendix A.3.1. The method for projective model order reduction that he used, however, was only based on (linear) vibration modes, with its associated limitations in describing nonlinearly vibrating systems [73]. His method was extended, therefore, by Yogesh Pilia in 2020/2021 by including Modal Derivatives. Pilia showed promising results for some structures, but was not able to fully validate the method he built for a wider range of structures [87]. My goal was therefore to supply a well-founded substantiation of the complete method as built by my predecessors and, where necessary, change the method if it was found to include any errors or oversights.

Work started in December of 2020 by reading literature and having multiple talks with my predecessor, Yogesh Pilia. In a short series of meetings he explained the workings of the method within Hybrid, and how to use the reduced-order model output by Hybrid in combination with the AUTO97 nonlinear continuation software. The working method at that time still relied on the Digital Visual Fortran 6.0 software package, released in April of 1997, to compile the FORTRAN test.f files output by Hybrid into files executable by AUTO97. Due to the age of this program it had some limitations, such as a maximum allowable random access memory (RAM) allocation of 4 MB which prevented it from compiling larger Hybrid output files. I therefore decided to start work on this immediately, while still in the process of literature review, to see if it was possible to remove this limitation.

After some attempts to alter or fix the DVF 6.0 software, I asked for help on the Intel community forums, whose users pointed me to the Intel oneAPI toolkit as a potentially useful replacement. A feature of this software especially useful to me was the inclusion within the Intel oneAPI HPC toolkit of a classic FORTRAN compiler which is compatible with old FORTRAN files. A first attempt to implement this new compiler into the existing model order reduction method was made in January 2021, and quickly afterwards the first results were obtained by running test programs from my predecessors. I saw this as a first big step, as it continually took me a lot of effort and time to read through and understand the codebase left behind by my predecessors. At that time, only the top-level programs specifically aimed at model order reduction consisted of 2500+ lines of code, which of course does not account for the thousands of lines of code of the mid-and bottom level functions that these programs were depending on.

With the main method operational on my machine, I started work on verifying and validating the results it was obtaining. While originally intended as only the first research goal of many,

this proved far harder than I had anticipated at the start of the project. This was partly due to me not understanding the way certain methods worked in Hybrida, and partly due to what I now consider to be wrong strategic choices in how to verify and validate the code: instead of trying to troubleshoot parts of the code piece by piece, I focused on the end results (nonlinear static deflections or frequency response curves) in order to assert that everything worked correctly. This works, of course, when everything does, and you can conclude from 1 complete result that all the parts do their job correctly. However, when unexpected results are obtained, it proved difficult for me to ascertain where the root cause lay inside the multiple nested Python classes and code bases.

After some months of work, however, I slowly realized that partial results were required in order to systematically, step by step, verify the complete analysis methodology, and I got to work on finding ways to first verify the Hybrida finite element implementation of the Van Keulen shell element. In this matter, the benchmarking problems from Sze, Liu & Lo proved very helpful as they included completely tabled results [50]. Of course, this also included use of the nonlinear static analysis class, but as this class was already sufficiently proven to work correctly in the work of Holtzer, I could assume that the only parameter of interest was the FE implementation of the shell element [68].

After this, it was time to verify the implementation of the intrusive computation of static modal derivatives as originally created by Pilania [87]. This once again proved to be a lot more difficult than anticipated, as I wrongfully concluded that when partial results did not align with those from literature, this could only be due to errors in the code implementation. However, as the constitutive methods from literature (kinematics, finite element description, etc.) differ from the Hybrida method, the SMD code implementation could well be correct while still giving different results than those from literature. In the end, an online meeting with Paolo Tiso was held to discuss the results I was getting with him. He gave context on the results he got in 2011 and confirmed that the difference in the computed static modal derivatives that I was seeing could well be due to different underlying methods. In the end, the partial verification of the static modal derivatives by comparing two computation methods (intrusive vs. non-intrusive) was the only way I could think of to isolate the SMD computation step itself from other potentially influential computation characteristics.

Luckily, the slow partial verification process I had went through had an additional benefit in that I now understood the code structure and inner workings of the "black box" much better, and it proved far easier to continue with dynamic analysis of shell structures afterwards. By the end of 2021, I managed to reproduce results from Amabili (2004) for flat structures, which at least proved that the reduction of EoMs using a basis of vibration modes and static modal derivatives was working well for flat structures:

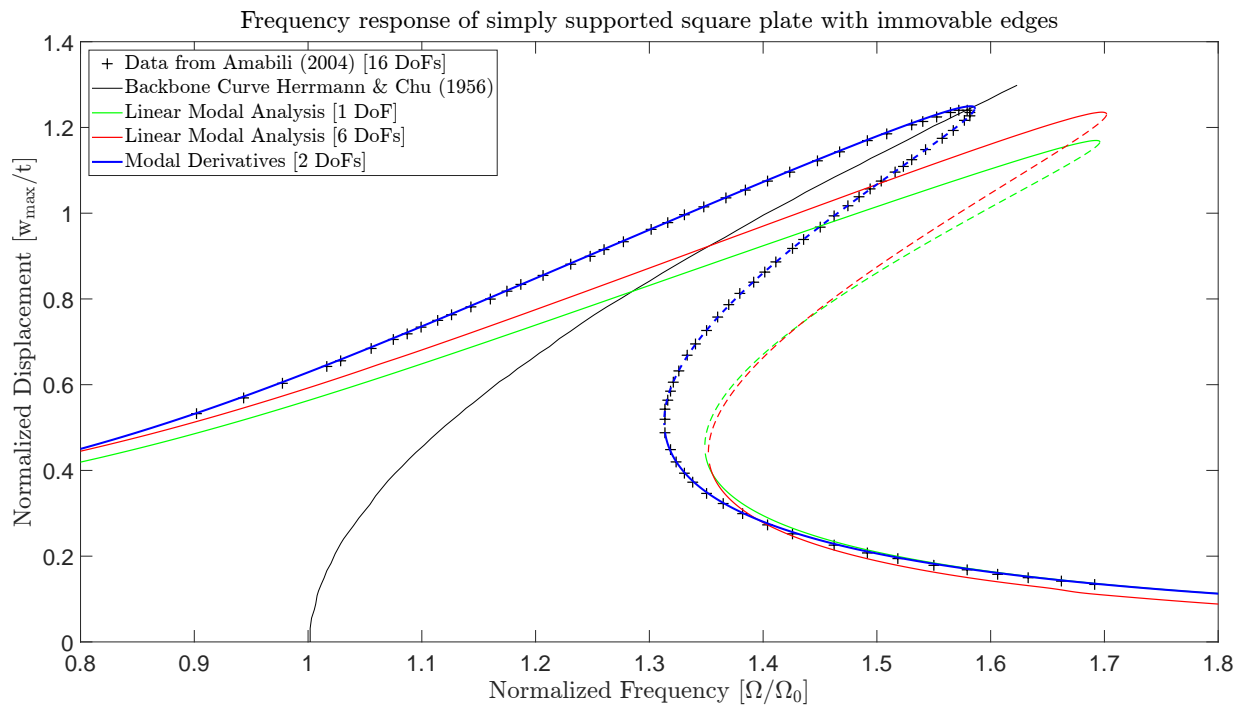


**Figure 39:** Some first positive results when using the static modal derivative method to compare to results from literature [4, 47].

However, now that I finally understood the code well and started getting interesting results, I got notified that my student loans would end in less than a month, while still roughly half a month away from graduating. In order to keep being able to afford rent, I accepted a part-time job, which of course frustrated my graduation efforts. In the end, I decided to put my thesis on hold while I pursued my career for 2.5 years. This was definitely not the road that I had planned for myself, and I would not recommend this to anyone else, as I found that working part-time on a thesis is like not working on a thesis at all: I missed the focus, time and energy to pursue my research in the same way as before, and therefore progress slowed down to a crawl.

I am very glad that I decided to quit my job and take time to finish my thesis before pursuing my career further. Taking stock now, at the end of the project, I conclude that the main things which cost me too much time were:

- Trying to verify and/or validate single analysis steps by looking at results of all steps combined;
- Jumping into analysis too quickly without a proper basis of research, which led me to not know about certain conclusions already reached in literature;
- Not asking for help quickly enough, but spending a lot of time figuring out things that could easily have been answered by colleagues and/or my supervisors;
- Misunderstanding of predecessors' implementation methods in Hybrida, which led me to draw wrong conclusions from results especially during the first half year of my graduation project.

In spite of all these things, I believe that during my thesis project I did make improvements on the existing reduced-order modelling analysis methodology and did achieve some interesting results and conclusions, especially when looking at using modal derivatives for curved shell structures. These conclusions seem to agree with those recently reached by other researchers

in the field when looking at curved arches [83]. While I would definitely approach the project completely differently now, for example by implementing more of my own code instead of often taking legacy code from my predecessors, I feel that I have also learned a lot from the mistakes I made during it, especially regarding troubleshooting and strategic choices in larger projects.

## A Model Order Reduction implementation in Hybrida

All numerical analysis performed for this thesis was done using the Hybrida finite element library, which is run and maintained by a research group at the Technical University of Delft under the supervision of prof. Alejandro Aragón. This Python-based library houses a large collection of code relating to finite element analysis, written by master students, PhD students, and professors. In this section, I will describe the analysis methodology for nonlinear statics, dynamics, and model order reduction as was used to carry out the numerical experiments in this thesis.

### A.1 Finite Element implementation

The element that I used for all analysis of thin-walled structures is a geometrically nonlinear triangular shallow shell element devised by van Keulen in 1993 [26], shown in Figure 40. This element is based on Kirchhoff-Love plate theory and has 12 associated DoFs: 9 translational DoFs at the corner nodes, and 3 rotational DoFs at the edges.

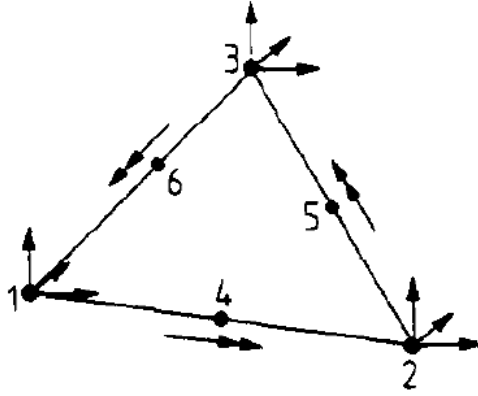


**Figure 40:** Degrees of freedom of the nonlinear shell element used in Hybrida for nonlinear dynamic analysis of thin-walled structures. Reprinted from F. van Keulen (1993) [26].

A detailed description of the derivation of the mass and stiffness matrices associated with this shell element from the elemental kinematic relations and the discrete constitutive equations, based on the assumption of linear elastic material behaviour

$$\sigma = \mathbf{S}\epsilon, \quad (39)$$

can be found in the works of van Keulen, Bout, Markestijn and Pilania [26, 30, 73, 87]. I will not copy these derivations here; rather, I start at the resulting tangent stiffness and mass matrices from van Keulen and Bout, respectively [26, 30]:

$$\mathbf{K}(\mathbf{u}) = \mathbf{D}^T \cdot \mathbf{S} \cdot \mathbf{D} + \mathbf{G} \quad (40)$$

$$\mathbf{M}_{uu} = \mathbf{M}_{vv} = \mathbf{M}_{ww} = \frac{\rho h A}{12} \begin{bmatrix} 2 & 1 & 1 \\ 1 & 2 & 1 \\ 1 & 1 & 2 \end{bmatrix} \quad (41)$$

Here  $\mathbf{G}$  is the geometric stiffness matrix,  $\mathbf{D}$  is the matrix containing the discrete strain-displacement relations, and  $\mathbf{S}$  contains the constitutive (material) relations. Van Keulen gives two options for  $\mathbf{D}$  as it depends on the displacement  $\mathbf{u}$ : a variant  $\mathbf{D}$  which is valid only for small rotations, and a matrix  $\mathbf{D}_a$  which is valid for large rotations, as long as the size of the elements is defined to be small enough compared to the local deformation pattern and minimum radius of curvature of the meshed surface [26]. Care should be taken to use the right variant for the problem at hand. In this thesis, the element description containing the large-rotation strain-displacement relations  $\mathbf{D}_a$  was used in all cases.

For the damping matrix  $\mathbf{C}$ , Hybridra incorporates either a linear combination of the mass and stiffness matrices known as Rayleigh damping:

$$\mathbf{C}\dot{\mathbf{u}} = (\mu\mathbf{M} + \lambda\mathbf{K})\dot{\mathbf{u}}, \quad (42)$$

or a matrix with constant coefficients which are applied to the reduced degrees of freedom, which is known as modal damping:

$$\hat{\mathbf{C}}\dot{\mathbf{q}} = \xi\mathbf{I}\dot{\mathbf{q}}. \quad (43)$$

In all cases, the damping constants  $\mu$ ,  $\lambda$ , and  $\xi$  and the forcing vector  $\mathbf{F}$  are used as input variables for the dynamic problem under consideration and are therefore based on estimates, not on numerical or physical analysis of the structure.

## A.2 Construction of the reduction basis $\mathbf{R}$

### A.2.1 Vibration modes

The method implemented in Hybridra for finding the vibration modes of a structure generally matches the method described in subsection 1.3.3. The vibration modes or "eigenmodes" of a structure are found by solving the eigenvalue problem of the structure at equilibrium, as described in subsection 1.4.2:

$$(\mathbf{K}_{ij}^{\text{LIN}} - \omega_i^2\mathbf{M}_{ij})\phi_i = 0, \quad (44)$$

This eigenvalue problem is solved in Python by either the numpy linalg.eig function, the ARPACK package which specializes in large sparse matrices, or the locally optimal block preconditioned conjugate gradient (scipy.sparse.linalg.lobpcg) eigensolver [37, 40]. All solvers solve the eigenvalue problem with the  $\mathbf{K}$  and  $\mathbf{M}$  matrices in sparse format, to save on computation time.

### Selection of Vibration Modes

The method used to compute vibration modes from a FE mesh containing  $N$  degrees of freedom as described above, will also result in  $N$  eigenmodes. As we want to reduce the size of our model and thus the number of DoFs in our model as much as possible, Hybridra uses various methods to select only those vibration modes of interest:

- Firstly, a user-defined number of low frequency modes is pre-selected from the total number  $N$  of vibration modes. The goal of this "truncation" is to reduce computation time further on in the process.
- Secondly, rigid body modes can be deleted by deleting the first six modes with zero (or close to zero) modal frequencies.
- Thirdly, redundant modes can be deleted. Redundant modes in this context are for example mirrored or other symmetrical copies of modes already in the basis. As redundant modes often have very similar, if not exactly the same eigenfrequencies, this is usually done by specifying a percentage window around the eigenfrequencies of already selected modes. If a mode that is about to be added to the reduction basis has a frequency that falls into one of these windows, it is automatically disregarded.
- Lastly, from these non-redundant low frequency deformation modes, the most significant can be selected using a number of selection criteria implemented in Hybridra. The most often used criteria are either the norm of a vibration mode, or the maximum modal amplitude at a specified node or "readout point", for example the tip of a cantilever [73, 75].

After this selection process, we are left with  $m$  vibration modes in our reduction basis which approximate the displacement of the structure by linear superposition:

$$\Delta \mathbf{u} = \sum_{i=1}^N \phi_i \mathbf{q}_i \approx \sum_{i=1}^m \phi_i \mathbf{q}_i, \quad \text{with } m \ll N \quad (45)$$

While the low-frequency vibration modes usually dominate the dynamic response of a thin-walled structure, they are also mostly out-of-plane vibration modes. This means that a reduction basis  $\mathbf{R}$  comprising solely out of the low-frequency vibration modes

$$\mathbf{R} = [\phi_1 \ \phi_2 \ \dots \ \phi_m]. \quad (46)$$

will most of the time only contain information about out-of-plane motion of thin-walled structures. This leads to a mechanism called "locking", where the stiffness of a structure undergoing large displacements is hugely overestimated as the out-of-plane degrees of freedom in the reduction basis cannot describe the in-plane movement caused by the present geometric nonlinearities [75]. Axial or in-plane vibration modes could be used to add this information to the reduction basis: however, they are usually found at relatively high frequencies:



**Figure 41:** The first three vibration modes  $\phi_1$ ,  $\phi_2$ , and  $\phi_3$ , and the first in-plane axial vibration mode  $\phi_{29}$  of a cantilever with aspect ratio of 13, as described by Malatkar (2003) [44].

As shown in Figure 41, after deleting all rigid body and redundant modes, the 28 lowest frequency vibration modes of this cantilever are out-of-plane bending and torsional modes. The first vibration mode exhibiting mostly in-plane motion is the 29th mode, with a frequency 857

times as high as the first out-of-plane bending mode. Finding these high frequency in-plane modes is not trivial, and by simply truncating the base at a certain frequency they are almost certainly cut off, removing the in-plane displacement information from the reduction basis. Hybrida therefore uses static modal derivatives as described in subsection 1.4.2 to easily find information about the in-plane effects geometrically coupled to the out-of-plane motion of thin-walled structures.

## A.2.2 Static Modal Derivatives

Modal derivatives are the second-order Taylor expansion component of the displacements  $\mathbf{u}$  with regards to the modal coordinates  $q_j$ , and thus give information about how a vibration mode  $\phi_i$  will change when excited in the direction of this modal coordinate:

$$\theta_{ij}^{\text{ST}} = \frac{\partial \phi_i}{\partial q_j} = - \mathbf{K}_{\text{eq}}^{-1} \left. \frac{\partial \mathbf{K}^{\text{NL}}}{\partial q_j} \right|_{q=0} \phi_i \quad (47)$$

In this equation, the  $\left. \frac{\partial \mathbf{K}^{\text{NL}}}{\partial q_j} \right|_{q=0}$ -term is critical, as the other terms ( $\mathbf{K}_{\text{eq}}^{-1}$ ) and  $\phi_i$  are already available from previous calculations. Hybrida houses two methods for calculating this term: a non-intrusive method, implemented according to section 6.3 of Rutzmoser (2018), and an intrusive method, implemented as described by Pilaian (2021) [75, 87]. Both methods compute static modal derivatives, and will be described shortly here.

### Non-intrusive computation of Modal Derivatives

For the non-intrusive computation of static modal derivatives, Hybrida makes use of a central difference scheme: firstly, the structure is excited around the equilibrium position in the positive and negative direction of a mode shape  $\phi_i$  by a step size  $h$  of a chosen magnitude, and the nonlinear stiffness matrix is computed at each configuration:

$$\begin{aligned} \mathbf{K}_+^{\text{NL}} &= \mathbf{K}(\mathbf{u}|_{+h \cdot \phi_i}) \\ \mathbf{K}_-^{\text{NL}} &= \mathbf{K}(\mathbf{u}|_{-h \cdot \phi_i}) \end{aligned} \quad (48)$$

The central difference around the equilibrium  $q = 0$  can then be computed and filled in in Equation 47:

$$\theta_{ij}^{\text{ST}} = \frac{\partial \phi_i}{\partial q_j} = - \mathbf{K}_{\text{eq}}^{-1} \left. \frac{\partial \mathbf{K}^{\text{NL}}}{\partial q_j} \right|_{q=0} \phi_i \approx - \mathbf{K}_{\text{eq}}^{-1} \frac{(\mathbf{K}_+^{\text{NL}} - \mathbf{K}_-^{\text{NL}})}{2h} \phi_i \quad (49)$$

With regards to the step size  $h$ , Rutzmoser (2018, p. 58) found that an optimum is generally found for  $10^{-1} \leq h \leq 10^1$ . In Hybrida, a step size of  $h = 1$  is standard [75].

As static modal derivatives are symmetric, that is,

$$\theta_{ij}^{\text{ST}} = \theta_{ji}^{\text{ST}}, \quad (50)$$

only the upper triangle of the "matrix" of static modal derivatives needs to be computed. For  $m$  vibration modes, this results in  $\frac{m(m+1)}{2}$  static modal derivatives.

## Intrusive computation of Modal Derivatives

As the name suggests, for the intrusive computation of modal derivatives we dive into the FE model by Van Keulen (1993), described in subsection A.1, to derive the required matrices analytically. The method used for this derivation is described more broadly by Piliaia (2021, appendix B) [26, 87].

In order to derive the  $\left. \frac{\partial \mathbf{K}^{\text{NL}}}{\partial q_j} \right|_{q=0}$ -term from Equation 47, we remember that the nonlinear element stiffness matrix is formulated as follows from the nonlinear finite element (Equation 40):

$$\mathbf{K}^{\text{NL},e} = \mathbf{D}_a^T \cdot \mathbf{S} \cdot \mathbf{D}_a + \mathbf{G} \quad (51)$$

As we assume that our material is linear and isotropic, the constitutive (material) relations  $\mathbf{S}$  contain no dependencies on the displacements  $q_j$ . This term can thus be left out in the following differentiation of the nonlinear element stiffness matrix:

$$\left. \frac{\partial \mathbf{K}^{\text{NL},e}}{\partial q_j} \right|_{q=0} = \frac{\partial \mathbf{D}_a^T}{\partial q_j} \cdot \mathbf{S} \cdot \mathbf{D}_a + \mathbf{D}_a^T \cdot \mathbf{S} \cdot \frac{\partial \mathbf{D}_a}{\partial q_j} + \frac{\partial \mathbf{G}}{\partial q_j} \quad (52)$$

The strain-displacement relations matrix (for moderate rotations)  $\mathbf{D}_a$  and geometric stiffness matrix  $\mathbf{G}$  resulting from the nonlinear finite element are composed as follows:

$$\mathbf{D}_a = \left[ \begin{array}{c|c|c|c} \mathbf{d}_1^T + \mathbf{u}^{e,T} \mathbf{C}_1 & \mathbf{v}^{e,T} \mathbf{C}_1 & \mathbf{w}^{e,T} \mathbf{C}_1 & 0 \\ \mathbf{u}^{e,T} \mathbf{C}_2 & \mathbf{d}_2^T + \mathbf{v}^{e,T} \mathbf{C}_2 & \mathbf{w}^{e,T} \mathbf{C}_2 & 0 \\ \mathbf{d}_2^T + \mathbf{u}^{e,T} \mathbf{C}_3 & \mathbf{d}_1^T + \mathbf{v}^{e,T} \mathbf{C}_3 & \mathbf{w}^{e,T} \mathbf{C}_3 & 0 \\ \hline \hat{n}_1 D_{bw} & \hat{n}_2 D_{bw} & \hat{n}_3 D_{bw} & D_{b\phi} \end{array} \right] \quad (53)$$

$$\mathbf{G} = \left[ \begin{array}{c|c|c|c} \mathbf{G}_d & 0 & 0 & 0 \\ 0 & \mathbf{G}_d & 0 & 0 \\ 0 & 0 & \mathbf{G}_d & 0 \\ \hline 0 & 0 & 0 & 0 \end{array} \right] \quad \text{with} \quad \mathbf{G}_d = \sigma_{m_1} \mathbf{C}_1 + \sigma_{m_2} \mathbf{C}_2 + \sigma_{m_3} \mathbf{C}_3 \quad (54)$$

Here  $\mathbf{d}_i$ ,  $D_{bw}$ , and  $D_{b\phi}$  are vectors and matrices containing element side vector constants,  $\hat{n}_i$  denotes the velocity component perpendicular to the flat configuration of the element, and

$$\sigma_m = \mathbf{S} \boldsymbol{\epsilon}_m = \mathbf{S} \mathbf{D}(\mathbf{u}^e; \mathbf{v}^e; \mathbf{w}^e) \quad (55)$$

$$\mathbf{D}(\mathbf{u}^e; \mathbf{v}^e; \mathbf{w}^e) = \left[ \begin{array}{c} \mathbf{d}_1^T \mathbf{u}^e + \frac{1}{2} \{ \mathbf{u}^{e,T} \mathbf{C}_1 \mathbf{u}^e + \mathbf{v}^{e,T} \mathbf{C}_1 \mathbf{v}^e + \mathbf{w}^{e,T} \mathbf{C}_1 \mathbf{w}^e \} \\ \mathbf{d}_2^T \mathbf{v}^e + \frac{1}{2} \{ \mathbf{u}^{e,T} \mathbf{C}_2 \mathbf{u}^e + \mathbf{v}^{e,T} \mathbf{C}_2 \mathbf{v}^e + \mathbf{w}^{e,T} \mathbf{C}_2 \mathbf{w}^e \} \\ \mathbf{d}_2^T \mathbf{u}^e + \mathbf{d}_1^T \mathbf{v}^e + \frac{1}{2} \{ \mathbf{u}^{e,T} \mathbf{C}_3 \mathbf{u}^e + \mathbf{v}^{e,T} \mathbf{C}_3 \mathbf{v}^e + \mathbf{w}^{e,T} \mathbf{C}_3 \mathbf{w}^e \} \end{array} \right] \quad (56)$$

is the generalized membrane stress parameter [26].

At this point, however, we cannot yet take the derivative of  $\mathbf{D}_a$  and  $\mathbf{G}$  with regards to the modal coordinate  $q_j$ , as they are both still described in terms of the original coordinate system. We therefore first transform the  $\mathbf{D}_a$  and  $\mathbf{G}$  matrices to their reduced counterparts by substituting the

original element coordinate vectors  $\mathbf{u}^e$ ,  $\mathbf{v}^e$ ,  $\mathbf{w}^e$  and  $\theta^e$  for its associated eigenmode contribution  $\phi$  and modal coordinate  $q_j$ :

$$\mathbf{U}^{e,T} = \left[ \mathbf{u}^{e,T} \mid \mathbf{v}^{e,T} \mid \mathbf{w}^{e,T} \mid \theta^{e,T} \right] \quad (57)$$

$$\mathbf{U}^e = \phi_i^e q_i \quad (58)$$

Where  $\mathbf{u}^e$ ,  $\mathbf{v}^e$ , and  $\mathbf{w}^e$  represent the displacements of the three nodes of a triangular element in the cardinal directions, and  $\theta^e$  represents the rotation of the three element sides, giving us a total of 12 DoFs.  $C_1$ ,  $C_2$ , and  $C_3$  contain element side vector constants, which do not change, and therefore their derivatives are always 0.

After substitution of Equation 58 in Equations 53 and 56, for example:

$$\mathbf{d}_1^T + \mathbf{u}^{e,T} C_1 = \mathbf{d}_1^T + \phi_i^{u,T} q_j C_1 \quad (59)$$

and taking the derivative with regards to  $q_j$  at the equilibrium position ( $\mathbf{u}^e = \mathbf{v}^e = \mathbf{w}^e = \theta^e = 0$ ):

$$\left. \frac{\partial(\mathbf{d}_1^T + \phi_i^{u,T} q_j C_1)}{\partial q_j} \right|_{q=0} = \phi_i^{u,T} \cdot C_1 \quad (60)$$

Equation 30 becomes [26, 87]:

$$\begin{aligned} \frac{\partial \mathbf{K}^{NL,e}}{\partial q_j} \Big|_{q=0} &= \begin{bmatrix} \phi_i^{u,T} \cdot C_1 & \phi_i^{u,T} \cdot C_2 & \phi_i^{u,T} \cdot C_3 & 0 \\ \phi_i^{v,T} \cdot C_1 & \phi_i^{v,T} \cdot C_2 & \phi_i^{v,T} \cdot C_3 & 0 \\ \phi_i^{w,T} \cdot C_1 & \phi_i^{w,T} \cdot C_2 & \phi_i^{w,T} \cdot C_3 & 0 \\ 0 & 0 & 0 & 0 \end{bmatrix} \cdot \mathbf{S} \cdot \begin{bmatrix} \mathbf{d}_1^T & 0 & 0 & 0 \\ 0 & \mathbf{d}_2^T & 0 & 0 \\ \mathbf{d}_2^T & \mathbf{d}_1^T & 0 & 0 \\ D_{bw} & D_{bw} & D_{bw} & D_{b\phi} \end{bmatrix} \\ &+ \begin{bmatrix} \mathbf{d}_1^T & 0 & \mathbf{d}_2^T & D_{bw} \\ 0 & \mathbf{d}_2^T & \mathbf{d}_1^T & D_{bw} \\ 0 & 0 & 0 & D_{bw} \\ 0 & 0 & 0 & D_{b\phi} \end{bmatrix} \cdot \mathbf{S} \cdot \begin{bmatrix} \phi_i^{u,T} \cdot C_1 & \phi_i^{v,T} \cdot C_1 & \phi_i^{w,T} \cdot C_1 & 0 \\ \phi_i^{u,T} \cdot C_2 & \phi_i^{v,T} \cdot C_2 & \phi_i^{w,T} \cdot C_2 & 0 \\ \phi_i^{u,T} \cdot C_3 & \phi_i^{v,T} \cdot C_3 & \phi_i^{w,T} \cdot C_3 & 0 \\ 0 & 0 & 0 & 0 \end{bmatrix} \\ &+ \begin{bmatrix} \frac{\partial \mathbf{G}_d}{\partial q_j} & 0 & 0 & 0 \\ 0 & \frac{\partial \mathbf{G}_d}{\partial q_j} & 0 & 0 \\ 0 & 0 & \frac{\partial \mathbf{G}_d}{\partial q_j} & 0 \\ 0 & 0 & 0 & 0 \end{bmatrix} \end{aligned} \quad (61)$$

All these terms can be retrieved from the original Finite Element partitioning of the structure and the computation of the vibration modes described in subsection A.2.1. The result of Equation 61 can then be filled in in Equation 47 in order to (intrusively) compute the static modal derivatives  $\theta_{ij}^{ST}$ .

### Selection of Static Modal Derivatives

As discussed previously in subsection 1.4.3, the number of static modal derivatives  $o$  that is associated with  $m$  vibration modes scales quadratically:

$$\mathbf{o} = \frac{m(m+1)}{2} \quad (62)$$

A number of 'a posteriori' selection schemes to automatically select the most relevant SMDs have been described in literature (see subsection 1.4.3). In Hybrid, however, only optional a priori manual selection of static modal derivatives was implemented to save on computation time. This means, however, that the relevant SMDs should be selected beforehand by inspection of the vibration modes and their possible interactions. After selecting the appropriate degrees of freedom, the VMs and static modal derivatives can be concatenated together to form the reduction basis:

$$\mathbf{R} = \left[ \phi_{1|eq} \ \phi_{2|eq} \ \dots \ \phi_{i|eq} \ \theta_{11}^{ST} \ \theta_{12}^{ST} \ \dots \ \theta_{ij}^{ST} \right]. \quad (63)$$

### A.2.3 Post-processing the Reduction Basis

#### Orthonormalization

After all DoFs in the reduction basis have been computed, they first need to be post-processed before they can be used to reduce the equations of motion: for a reduced order basis to span the space in which it is defined, the vectors in the basis should all be orthogonal and thus linearly independent. While the eigenmodes  $\phi_i$  are orthogonal with respect to the mass and stiffness matrices in a generalized sense, and any SMD  $\theta_{ij}^{ST}$  is mass-orthogonal with respect to their constitutive vibration modes  $\phi_i$  and  $\phi_j$ , the static modal derivatives do not have this property with regards to each other or other vibration modes [16, 48, 75]. Secondly, the basis should be normalized to simplify the subsequent calculations in Equations 70 - 72 and make them more numerically stable. As the  $\mathbf{M}$ ,  $\mathbf{C}$ , and  $\mathbf{K}$  matrices are multiplied by the reduction basis  $\mathbf{R}$  twice, the condition number of  $\mathbf{R}$  will be squared. This can cause problems during time integration, such as poor convergence and instability, as small changes in the input can lead to large changes in the output.

In literature, a number of methods to tackle these issues are proposed. Tiso (2011) and Rutzmoser (2017) propose a Gram-Schmidt-like scheme to ortho-normalize the SMDs  $\theta$  with regards to the VMs  $\phi$  [70]:

$$\theta_{\perp\phi} = \left( \mathbf{I} - \sum_{i=1}^n \phi_i \phi_i^T \right) \theta, \quad \text{with} \quad \phi_i^T \phi_i = 1 \quad (64)$$

In 2019, Cruz Varona proposed using either a rank-revealing QR (RRQR) or a singular value decomposition (SVD) algorithm to deflate the raw basis, by first normalizing the vectors in the reduction basis [78]:

$$\mathbf{R}_{\text{norm}} = \left[ \frac{\phi_{1,eq}}{\|\phi_{1,eq}\|} \ \dots \ \frac{\phi_{i,eq}}{\|\phi_{i,eq}\|} \ \frac{\theta_{11}}{\|\theta_{11}\|} \ \dots \ \frac{\theta_{1j}}{\|\theta_{1j}\|} \ \dots \ \frac{\theta_{ij}}{\|\theta_{ij}\|} \right] \quad (65)$$

and then performing a singular value decomposition on this "raw" basis:

$$\mathbf{R}_{\text{norm}} = \text{SVD}^T \quad (66)$$

Where  $\mathbf{S}$  and  $\mathbf{D}^T$  are orthonormal matrices containing singular vectors, and  $\mathbf{V}$  is a diagonal matrix with the singular values arranged in descending order. The left singular vectors contained in  $\mathbf{S}$  can now be used as orthonormal basis vectors to span the reduction basis:

$$\mathbf{R}_{\text{defl}} = [\mathbf{s}_1, \dots, \mathbf{s}_{\text{defl}}] \quad (67)$$

Similarly, in this thesis, the `numpy.linalg.qr` factorization function, which is an interface to the Fortran-based LAPACK routines `dgeqrf` and `dorgqr`, is used to deflate the basis and orthonormalize the vibration modes and modal derivatives in the reduction basis with regards to each other [34]. These LAPACK routines use Householder transformations to perform a QR-factorization, which generates a "thin" QR factorization of the original raw basis:

$$\mathbf{A} = \mathbf{Q}\mathbf{R} = \mathbf{Q} \begin{bmatrix} \mathbf{R}_1 \\ 0 \end{bmatrix} = \begin{bmatrix} \mathbf{Q}_1 & \mathbf{Q}_2 \end{bmatrix} \begin{bmatrix} \mathbf{R}_1 \\ 0 \end{bmatrix} = \mathbf{Q}_1\mathbf{R}_1, \quad (68)$$

Where  $\mathbf{Q}_1$ , similarly to the SVD method above, is a matrix containing orthonormal basis vectors which can now be used as our reduction basis:

$$\mathbf{R}_{\text{defl}} = \mathbf{Q}_1 = \left[ \phi_1 \dots \phi_i \theta_{11}^{\text{ST}} \dots \theta_{ij}^{\text{ST}} \right]_{\text{defl}} \quad (69)$$

## A.3 Reduction of Equations of Motion

### A.3.1 Reduction of linear System Matrices

The Hybrid model order reduction process uses pre- and post-multiplication of the system matrices with a reduced basis  $\mathbf{R}$ , construction of which is described in more detail in Appendix A.2, in order to dramatically reduce the number of DoFs. With linear system matrices, this is a fairly straight-forward process:

$$\hat{\mathbf{M}} = \mathbf{R}^T \mathbf{M} \mathbf{R} \quad (70)$$

$$\hat{\mathbf{C}} = \mathbf{R}^T \mathbf{C} \mathbf{R} \quad (71)$$

$$\hat{\mathbf{K}}^{\text{LIN}} = \mathbf{R}^T \mathbf{K}^{\text{LIN}} \mathbf{R} \quad (72)$$

$$\hat{\mathbf{F}} = \mathbf{R}^T \mathbf{F} \quad (73)$$

Similarly, the displacements  $\Delta \mathbf{u}$  are defined as the reduction basis multiplied by the modal coordinates  $\mathbf{q}$ :

$$\Delta \mathbf{u} = \mathbf{R}^T \mathbf{q} \quad (74)$$

However, the stiffness matrix  $\mathbf{K}(\mathbf{u})$  contains geometric nonlinearities, denoted by the dependency on  $\mathbf{u}$ , of a quadratic and cubic nature. Therefore, the reduction in Equation 72 cannot simply be performed, as the dependency of  $\mathbf{K}$  on  $\mathbf{q}$  in the reduced equations of motion will not be carried over correctly.

### A.3.2 Tensor Decomposition and Reduction of Nonlinear Stiffness Matrix

The observation above poses problems for the reduction process, as the nonlinear stiffness matrix cannot be reduced in the same way as the other system matrices. To solve this, the nonlinear stiffness matrix is redefined as a combination of third-order and fourth-order tensors with constant coefficients. This separates the displacement dependencies from the system tensors, as these tensors will only contain constant components:

$$\mathbf{K}_{ij}(\mathbf{u}) = \mathbf{K}_{ij}^{LIN} + \alpha_{ijk}\mathbf{u}_k + \beta_{ijkl}\mathbf{u}_k\mathbf{u}_l \quad (75)$$

These tensors are constructed by the method detailed in the following simplified example [73]:

- Separate the stiffness matrix into matrices corresponding to the polynomial order  $p$  of the displacement dependency of its components:

$$\mathbf{K}(\mathbf{u}) = \begin{bmatrix} u_1^2 & 1 & 1 \\ 1 & u_0 & 1 \\ 1 & 1 & 1 \end{bmatrix} = \begin{bmatrix} 0 & 1 & 1 \\ 1 & 0 & 1 \\ 1 & 1 & 1 \end{bmatrix} + \begin{bmatrix} 0 & 0 & 0 \\ 0 & u_0 & 0 \\ 0 & 0 & 0 \end{bmatrix} + \begin{bmatrix} u_1^2 & 0 & 0 \\ 0 & 0 & 0 \\ 0 & 0 & 0 \end{bmatrix} \quad (76)$$

- Write each matrix corresponding to order  $p$  as a tensor of order  $p + 2$  multiplied by  $p$  displacement vectors.

$$\begin{aligned} \mathbf{K}(\mathbf{u}) = & \begin{bmatrix} 0 & 1 & 1 \\ 1 & 0 & 1 \\ 1 & 1 & 1 \end{bmatrix} + \left[ \begin{bmatrix} 0 & 0 & 0 \\ 0 & 1 & 0 \\ 0 & 0 & 0 \end{bmatrix}, \begin{bmatrix} 0 & 0 & 0 \\ 0 & 0 & 0 \\ 0 & 0 & 0 \end{bmatrix} \begin{bmatrix} 0 & 0 & 0 \\ 0 & 0 & 0 \\ 0 & 0 & 0 \end{bmatrix} \right] \begin{bmatrix} u_0 \\ u_1 \\ u_2 \end{bmatrix} \\ & \left[ \begin{bmatrix} 0 & 0 & 0 \\ 0 & 0 & 0 \\ 0 & 0 & 0 \end{bmatrix}, \begin{bmatrix} 0 & 0 & 0 \\ 0 & 0 & 0 \\ 0 & 0 & 0 \end{bmatrix}, \begin{bmatrix} 0 & 0 & 0 \\ 0 & 0 & 0 \\ 0 & 0 & 0 \end{bmatrix} \right] \\ & + \left[ \begin{bmatrix} 0 & 0 & 0 \\ 0 & 0 & 0 \\ 0 & 0 & 0 \end{bmatrix}, \begin{bmatrix} 1 & 0 & 0 \\ 0 & 0 & 0 \\ 0 & 0 & 0 \end{bmatrix}, \begin{bmatrix} 0 & 0 & 0 \\ 0 & 0 & 0 \\ 0 & 0 & 0 \end{bmatrix} \right] \begin{bmatrix} u_0 \\ u_1 \\ u_2 \end{bmatrix} \begin{bmatrix} u_0 \\ u_1 \\ u_2 \end{bmatrix} \\ & \left[ \begin{bmatrix} 0 & 0 & 0 \\ 0 & 0 & 0 \\ 0 & 0 & 0 \end{bmatrix}, \begin{bmatrix} 0 & 0 & 0 \\ 0 & 0 & 0 \\ 0 & 0 & 0 \end{bmatrix}, \begin{bmatrix} 0 & 0 & 0 \\ 0 & 0 & 0 \\ 0 & 0 & 0 \end{bmatrix} \right] \end{aligned} \quad (77)$$

- Reduce the resulting tensors to sparse form:

$$\begin{aligned}
& \text{indices}([[0, 1], [0, 2], [1, 0], [1, 2], [2, 0], [2, 1], [2, 2]]) \\
\mathbf{K}_{ij}^{\text{LIN}} = & \text{values}([1, 1, 1, 1, 1, 1, 1]) \\
& \text{shape}([3, 3]) \\
& \text{indices}([0, 1, 1]) \\
\alpha_{ijk} = & \text{values}([1]) \\
& \text{shape}([3, 3, 3]) \\
& \text{indices}([1, 1, 0, 0]) \\
\beta_{ijkl} = & \text{values}([1]) \\
& \text{shape}([3, 3, 3, 3])
\end{aligned} \tag{78}$$

As shown, this does not do much to help reduce the size of the linear stiffness matrix - however, as the third- and fourth-order tensors contain a lot of zeroes, their size is massively reduced. The example shown above demonstrates how a 3-by-3 nonlinear stiffness matrix is decomposed into sparse tensors multiplied by vectors containing the displacement components. A fully assembled stiffness matrix of a complete structure could have a size of 1000x1000 or larger, however. This would mean that our  $\beta_{ijkl}$  tensor has  $10^{12}$  elements.

It is therefore not wise to decompose the fully assembled stiffness matrix of the whole structure into third- and fourth-order tensors. Either a) all analysis must be done in sparse form, or b) the stiffness matrix must be reduced at the element level, where the size of the matrix (12x12) is still manageable. In the Hybrid model order reduction implementation, the second option was chosen [73]. The element stiffness matrices are all separately decomposed into element stiffness tensors:

$$\mathbf{K}_{ij}^{[e]}(\mathbf{u}) = \mathbf{K}_{ij}^{[e]} + \alpha_{ijk}^{[e]} \mathbf{u}_k^{[e]} + \beta_{ijkl}^{[e]} \mathbf{u}_k^{[e]} \mathbf{u}_l^{[e]} \tag{79}$$

after which the tensors are reduced by multiplication with the components of the reduction basis  $R_{ij}^{[e]}$  corresponding to the elemental DoFs:

$$\hat{\alpha}_{ijk}^{[e]} = R_{ip}^{[e]} R_{jq}^{[e]} R_{kr}^{[e]} \alpha_{pqr}^{[e]} \tag{80}$$

$$\hat{\beta}_{ijkl}^{[e]} = R_{ip}^{[e]} R_{jq}^{[e]} R_{kr}^{[e]} R_{ls}^{[e]} \beta_{pqrs}^{[e]} \tag{81}$$

and only then assembled to form the reduced stiffness tensors  $\hat{\alpha}_{ijk}$  and  $\hat{\beta}_{ijkl}$  of the complete structure:

$$\hat{\alpha}_{ijk} = \sum_{n=1}^m \hat{\alpha}_{ijk}^{[e]} \tag{82}$$

$$\hat{\beta}_{ijkl} = \sum_{n=1}^m \hat{\beta}_{ijkl}^{[e]} \tag{83}$$

### A.3.3 Post-processing the Reduced Equations of Motion

After selection of the basis vectors and orthonormalizing them, the reduced basis can be used to reduce the system matrices as in Equations 70 - 73, 80, and 81. For the external force, we choose a harmonic excitation denoted by  $\hat{\mathbf{F}}_i \sin(\Omega t)$  with excitation frequency  $\Omega$ :

$$\hat{\mathbf{M}}_{ij} \ddot{\mathbf{q}}_j(t) + \hat{\mathbf{C}}_{ij} \dot{\mathbf{q}}_j(t) + \hat{\mathbf{K}}_{ij} \mathbf{q}_j(t) + \hat{\alpha}_{ijk} \mathbf{q}_j(t) \mathbf{q}_k(t) + \hat{\beta}_{ijkl} \mathbf{q}_j(t) \mathbf{q}_k(t) \mathbf{q}_l(t) = \hat{\mathbf{F}}_i \sin(\Omega t) \quad (84)$$

In order to prepare the reduced EoMs for use in AUTO, the continuation software for dynamic problems used in conjunction with Hybrida, they need to be non-dimensionalized. In order to simplify and parametrize the equations, all physical quantities (mass, shell thickness, and natural frequency) are removed from the equation. This is done by pre-multiplying with the inverse mass matrix  $\hat{\mathbf{M}}_{ij}^{-1}$ , dividing the reduced coordinates by the shell thickness of the structure at hand  $z = q/h$ , and substituting  $\tau = \omega_0 t$  so that the first resonance frequency is regarded as  $\omega_0 = 1$ . We then multiply the equation by  $1/h$  and  $1/\omega_0^2$  to compensate for the added factors:

$$\ddot{\mathbf{z}}_i(\tau) + \frac{1}{\omega_0} \hat{\mathbf{M}}_{ij}^{-1} \hat{\mathbf{C}}_{ij} \dot{\mathbf{z}}_j(\tau) + \frac{1}{\omega_0^2} \hat{\mathbf{M}}_{ij}^{-1} \hat{\mathbf{K}}_{ij} \mathbf{z}_j(\tau) + \frac{h}{2\omega_0^2} \hat{\mathbf{M}}_{ij}^{-1} \hat{\alpha}_{ijk} \mathbf{z}_j(\tau) \mathbf{z}_k(\tau) + \frac{h^2}{3\omega_0^2} \hat{\mathbf{M}}_{ij}^{-1} \hat{\beta}_{ijkl} \mathbf{z}_j(\tau) \mathbf{z}_k(\tau) \mathbf{z}_l(\tau) = \frac{1}{h\omega_0^2} \hat{\mathbf{M}}_{ij}^{-1} \hat{\mathbf{F}}_i \sin\left(\frac{\Omega}{\omega_0} \tau\right), \quad (85)$$

We can now write all the constants and matrix pre-multiplications into one notation for clarity:

$$\begin{aligned} \check{\mathbf{M}}_{ij} &= \hat{\mathbf{M}}_{ij}^{-1} \hat{\mathbf{M}}_{ij} = \mathbf{I} \\ \check{\mathbf{C}}_{ij} &= \frac{1}{\omega_0} \hat{\mathbf{M}}_{ij}^{-1} \hat{\mathbf{C}}_{ij} \\ \check{\mathbf{K}}_{ij} &= \frac{1}{\omega_0^2} \hat{\mathbf{M}}_{ij}^{-1} \hat{\mathbf{K}}_{ij} \quad \text{with } \check{k}_{11} = 1 \\ \check{\alpha}_{ijk} &= \frac{h}{2\omega_0^2} \hat{\mathbf{M}}_{ij}^{-1} \hat{\alpha}_{ijk} \\ \check{\beta}_{ijkl} &= \frac{h^2}{3\omega_0^2} \hat{\mathbf{M}}_{ij}^{-1} \hat{\beta}_{ijkl} \\ \check{\mathbf{F}}_i &= \frac{1}{h\omega_0^2} \hat{\mathbf{M}}_{ij}^{-1} \hat{\mathbf{F}}_i \\ \check{\Omega} &= \frac{\Omega}{\omega_0} \end{aligned} \quad (86)$$

to arrive at our final mass-normalized, non-dimensionalized, reduced equations of motion:

$$\ddot{\mathbf{z}}_i + \check{\mathbf{C}}_{ij} \dot{\mathbf{z}}_j + \check{\mathbf{K}}_{ij} \mathbf{z}_j + \check{\alpha}_{ijk} \mathbf{z}_j \mathbf{z}_k + \check{\beta}_{ijkl} \mathbf{z}_j \mathbf{z}_k \mathbf{z}_l = \check{\mathbf{F}}_i \sin(\check{\Omega} \tau) \quad (87)$$

## A.4 Dynamic nonlinear solution procedures

In order to solve the nonlinear differential equations of motion in Equation 87, they are first converted to state-space representation by defining a pair of state variables  $x_i^{[1]} = z_i$  and  $x_i^{[2]} = \dot{z}_i$ :

$$\begin{aligned} \dot{x}_i^{[1]} &= x_i^{[2]} \\ \dot{x}_i^{[2]} &= -\check{C}_{ij}x_j^{[2]} - \left( \check{K}_{ij} + \left( \check{\alpha}_{ijk} + \check{\beta}_{ijkl}x_l^{[1]} \right) x_k^{[1]} \right) x_j^{[1]} + \check{F}_i \sin(\check{\Omega}\tau). \end{aligned} \quad (88)$$

Hybrida houses two methods to solve this system of ordinary differential equations. Firstly, the `scipy.integrate.odeint` function, which uses the LSODA routine from the Fortran library `odepack` [53]. This time integration scheme is completely contained within the Hybrida library and can be used without having to compile Fortran code. The LSODA solver starts off using non-stiff methods, but dynamically monitors data in order to determine when to automatically switch to a stiff method. In this method, the continuation parameter can be set to be either force  $F_{\text{ext}}$  or excitation frequency  $\Omega$ . For a more detailed description of the use of the `ODEint` function within the Hybrida library I refer to Markestein (2018) [73].

The second method used to solve ordinary differential equations is the AUTO97 continuation and bifurcation software [14, 36]. This Fortran-based program uses a pseudo-arclength continuation method to follow solution branches. While Markestein (2018) and Paliana (2021) used the Digital Visual Fortran 6.0 compiler to compile and run Fortran code, this program had severe limitations with regards to admissible file size and random access memory (RAM) it could use, as it was written in 1997 [73, 87]. Therefore, in this thesis the Intel oneAPI toolkit was used, in order to compile Fortran code using the Intel Fortran Compiler Classic (`ifort`) and run the AUTO software all from one command window. For a detailed overview of AUTO parameters and their meanings, I refer to section C-3 of Markestein (2018) [73].

## A.5 Static nonlinear solution procedures

When displacements are large, the geometrically nonlinear regime is entered (see subsection 1.1.1). This means that the relation between the force on and the displacement of a structure (read: stiffness) becomes dependent on its previous state, or "configuration". Consequentially, explicit linear approximations, simple formulas relating forces and displacements, or purely incremental solution procedures will become increasingly inaccurate.

In order to find accurate displacements of a structure in the nonlinear regime, implicit incremental-iterative solver strategies can be used. The "incremental" here signifies that the force applied on the structure is increased incrementally, starting in the linear regime and slowly working towards the geometrically nonlinear. The "iterative" means that at each force increment, the displacement solution is reached through iteration until a certain error measure is reached, for example using a Newton-Raphson root finding algorithm. This is done to prevent the "drifting" of the solution from the true solution path that is usually present when purely incremental solution procedures are used (Figure 42a).

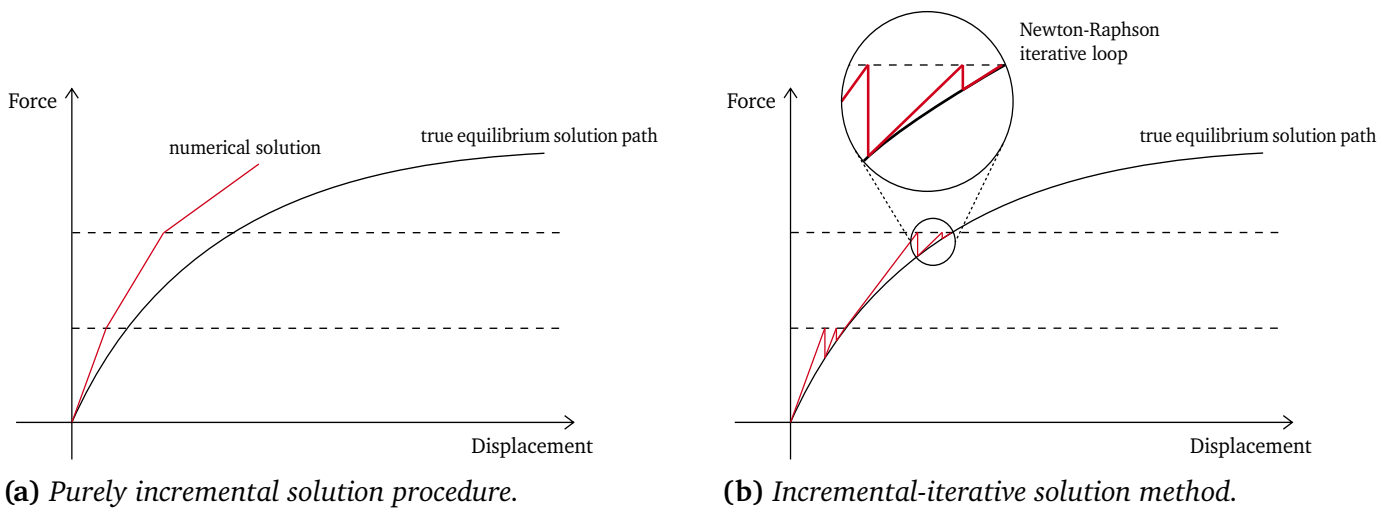


**Figure 42:** Incremental-iterative solution procedures follow the true solution path more closely when force-displacement relations become nonlinear [68].

### Incremental control strategies

When a force-deflection curve becomes highly nonlinear, care must be taken to control the incremental increase in the driving parameter or "step size". Not doing this may lead to inaccurate results, as the solution procedure "misses" the solution curve (Figure 43). Even when care is taken, the true solution might not be obtained if the structure undergoes snap-through or snap-back behaviour (Figure 44). Using either load or displacement control in these circumstances can lead to errors.

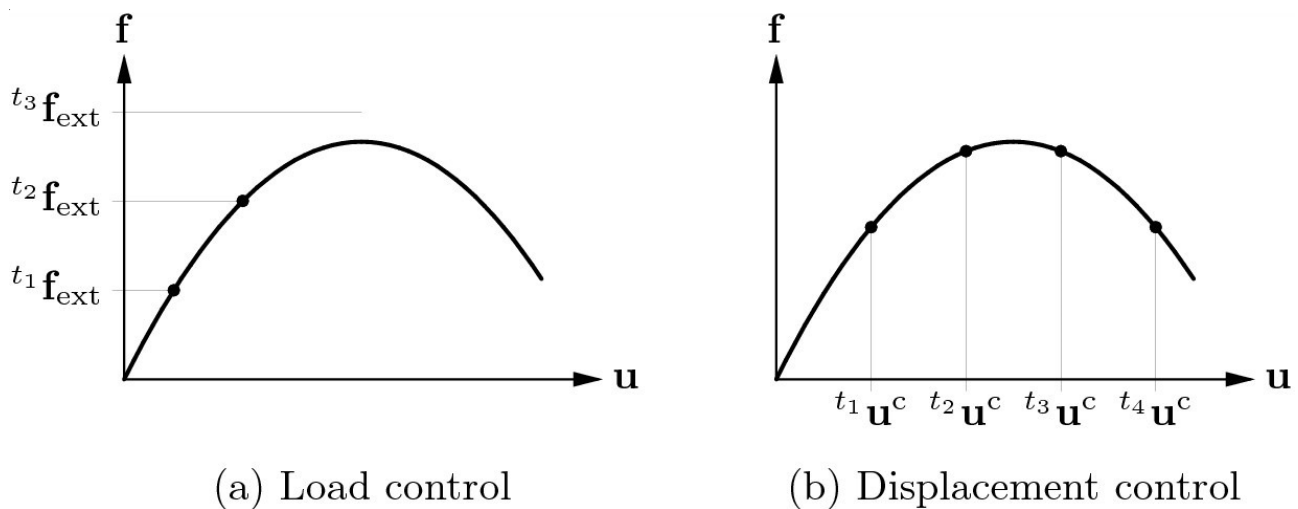


**Figure 43:** The most basic control strategies simply increment either the load or displacement as driving parameter. Reprinted from DIANA FEA User Manual v10.5, section 75.1 (2021) [84].

Using more advanced control procedures such as the arc-length method can mitigate these errors. In this control procedure, a combination of load and displacement control is used to constrain the norm of the incremental displacements to a prescribed value. In this sense the "length" of the incremental step along the solution curve is limited [84]. Our solution procedure thus cannot overshoot the true solution curve and go to infinity. The Hybrid incremental-iterative solver built by B.P.F. Holtzer in 2017 [68] uses a unified approach that works with a

variety of incremental control strategies. In this thesis the arc-length control strategy was used for all static analyses.

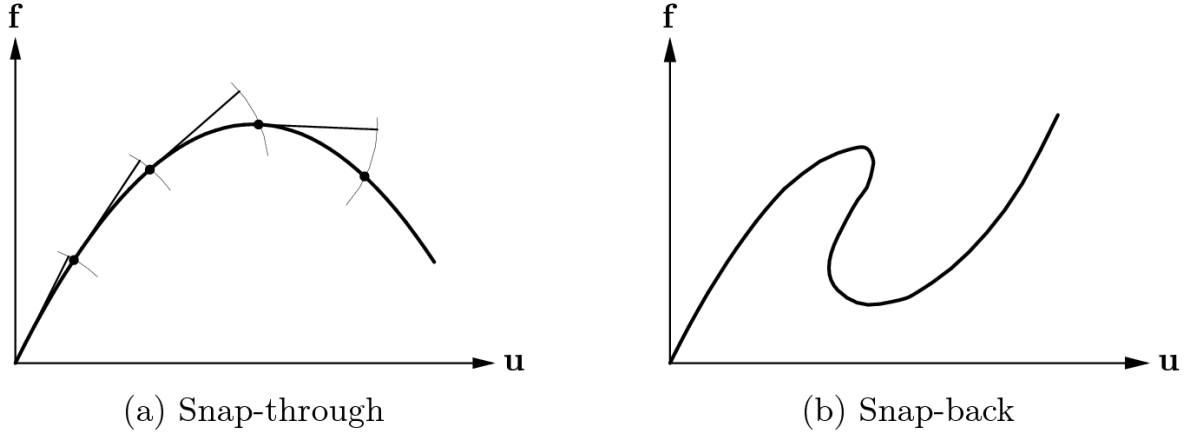


**Figure 44:** Force-deflection curves displaying snap-back or snap-through behaviour. An example of an arc-length control method is shown following the snap-through solution curve in figure (a). Reprinted from DIANA FEA User Manual v10.5, section 75.1 (2021) [84].

### A.5.1 Hybrid Incremental-iterative solver for nonlinear static analysis

The incremental-iterative solution procedure implemented in Hybrida was written by Holtzer (2017) - for a detailed description of his nonlinear finite element solution procedure I refer to his thesis [68]. A short overview of his method used to perform nonlinear static solutions of thin-walled structures is given here:

1. Load mesh and set boundary conditions.
2. Set material and shell thickness parameters.
3. Begin load increment by prescribing an external load  $\hat{\mathbf{f}}_{\text{ext}}$  and load scaling parameter  $\beta$ :
  - (a) Determine new load step size  $\delta l$
  - (b) Begin Newton-Raphson iteration:
    - i. Compute elemental tangent stiffness matrices and assemble into the nonlinear stiffness matrix corresponding to the latest calculated displacements.
    - ii. Apply an external force and solve the external and residual force-displacement equations:

$$\mathbf{K}\delta\mathbf{u}^{\text{ext}} = \mathbf{f}_{\text{ext}} \quad (89)$$

$$\mathbf{K}\delta\mathbf{u}^{\text{res}} = \mathbf{r} \quad (90)$$

- iii. Compute the iterative load parameter  $\delta\lambda$  via the arc-length constraint equation (Holtzer, 2017 [68]):

$$\delta\lambda_{j+1} = \begin{cases} \pm \frac{\delta l}{\sqrt{\delta\mathbf{u}_1^{\text{ext}} \cdot \delta\mathbf{u}_1^{\text{ext}} + \beta^2}} & \text{for } j = 0 \\ -\frac{\delta\mathbf{u}_1 \cdot \delta\mathbf{u}_{j+1}^{\text{res}}}{\delta\mathbf{u}_1 \cdot \delta\mathbf{u}_{j+1}^{\text{ext}} + \beta^2\delta\lambda_1} & \text{for } j \geq 1 \end{cases} \quad (91)$$

and add it to the load parameter  $\lambda$ .

- iv. Compute the new external force  $\mathbf{f}_{\text{ext}} = \lambda \hat{\mathbf{f}}_{\text{ext}}$ .
- v. Compute the new iterative displacement and add it to the total displacement:

$$\mathbf{u} = \mathbf{u} + \delta \mathbf{u}^{\text{res}} + \delta \lambda \delta \mathbf{u}^{\text{ext}} \quad (92)$$

- vi. Compute the new internal force  $\mathbf{f}_{\text{int}}$  caused by the latest total displacement.
- vii. Compute new residual force  $\mathbf{r} = \mathbf{f}_{\text{ext}} - \mathbf{f}_{\text{int}}$
- viii. Compute new error  $\frac{|\mathbf{r}|}{|\mathbf{r}_1|}$ .
- ix. If the error is larger than a previously specified tolerance, go through the Newton-Raphson iteration again.

This method was used to compute nonlinear static displacements for a number of benchmarking problems from Sze, Liu & Lo (2004) [50] as described in subsection 2.1.

## B Parameters and data used in numerical experiments

In this section, the parameters used to generate the data in the numerical experiments of subsection 2.1 are listed. Additionally, the data from literature that the Hybridra simulations are compared to is also listed for sake of reproduction.

### B.1 Parameters for statics benchmarking tests

#### Cantilever subjected to end shear force

The parameters and data listed here originate from section 3.1 of Popular Benchmark Problems for Geometric Nonlinear Analysis of Shells [50].

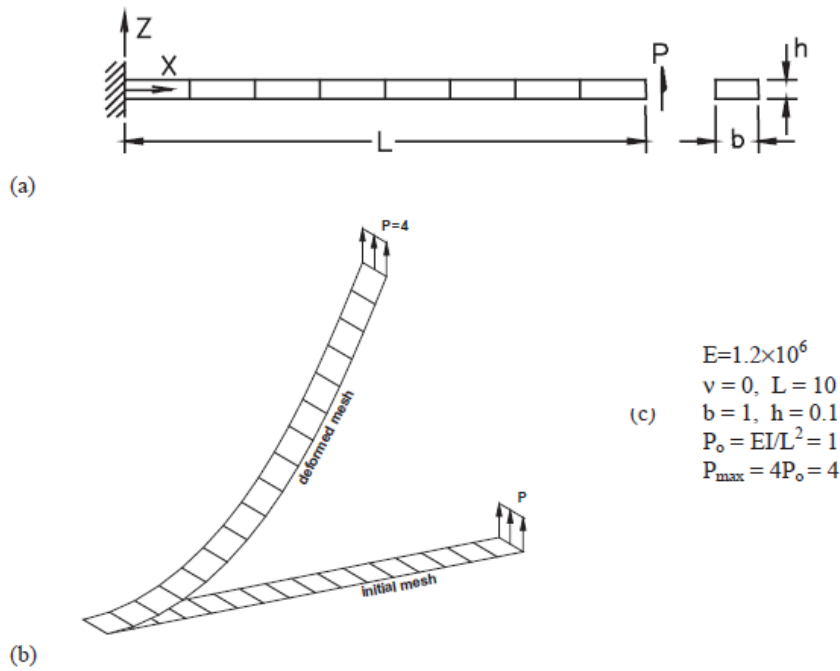


**Figure 45:** (a) Constant cross-section cantilever loaded with an end shear force. (b) Deformed mesh under maximum load. (c) Material constants and geometric parameters used in this experiment. Adapted from Sze, Liu & Lo (2004) [50].

$P/P_{\max}$	$-U_{\text{tip}}$	$W_{\text{tip}}$	$P/P_{\max}$	$-U_{\text{tip}}$	$W_{\text{tip}}$	$P/P_{\max}$	$-U_{\text{tip}}$	$W_{\text{tip}}$
0.05	0.026	0.663	0.40	1.184	4.292	0.75	2.541	6.031
0.10	0.103	1.309	0.45	1.396	4.631	0.80	2.705	6.190
0.15	0.224	1.922	0.50	1.604	4.933	0.85	2.861	6.335
0.20	0.381	2.493	0.55	1.807	5.202	0.90	3.010	6.467
0.25	0.563	3.015	0.60	2.002	5.444	0.95	3.151	6.588
0.30	0.763	3.488	0.65	2.190	5.660	1.00	3.286	6.698
0.35	0.971	3.912	0.70	2.370	5.855			

**Table 1:** Data used from Sze, Liu & Lo (2004) in the comparison with Hybridra shown in Figure 13 of a cantilever loaded by an end shear force [50].

Group	Parameter	Value
Mesh	Element Type	s3f
	Number of elements	67
	Boundary conditions	Dirichlet: $x, y, z, M_y = 0$ at $x = 0$ Neumann: $+F_z$ at $x = L$
Material	Young's Modulus	1.2 MPa
	Poisson Ratio	0
	Density	$2700 \text{ kg m}^{-3}$
	Shell Thickness	0.1 m
Incremental-iterative Solver	Control Strategy	Arc-length
	Convergence Norm	Force
	Iteration step size	0.95
	Max. iterations	20
	Number of increments	31

**Table 2:** Experimental parameters used in Hybrid nonlinear static analysis shown in Figure 13 of a cantilever subjected to an end shear force.

### Cantilever subjected to end moment

The parameters and data listed here originate from section 3.2 of Popular Benchmark Problems for Geometric Nonlinear Analysis of Shells [50].

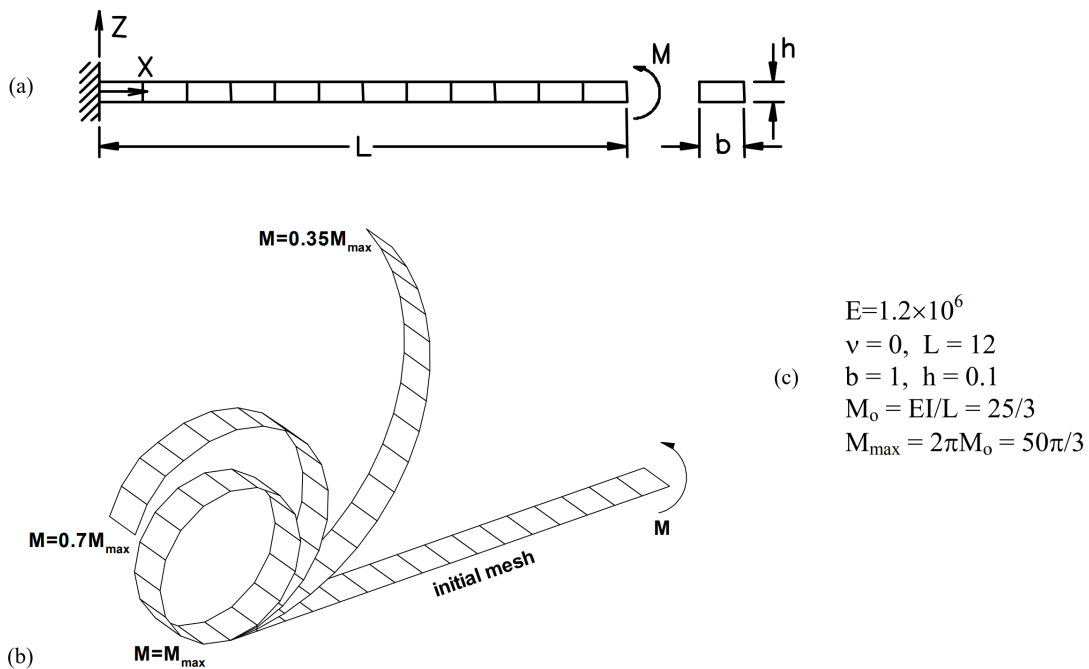


**Figure 46:** (a) Constant cross-section cantilever loaded with an end moment. (b) Deformed mesh under maximum load. (c) Material constants and geometric parameters used in this experiment. Adapted from Sze, Liu & Lo (2004) [50].

$M/M_{\max}$	$-U_{\text{tip}}$	$W_{\text{tip}}$	$M/M_{\max}$	$-U_{\text{tip}}$	$W_{\text{tip}}$
0.05	0.196	1.870	0.55	13.073	6.775
0.10	0.774	3.648	0.60	13.871	5.758
0.15	1.699	5.248	0.65	14.377	4.665
0.20	2.918	6.598	0.70	14.595	3.571
0.25	4.361	7.639	0.75	14.546	2.546
0.30	5.945	8.333	0.80	14.270	1.650
0.35	7.585	8.664	0.85	13.818	0.926
0.40	9.194	8.637	0.90	13.247	0.405
0.45	10.688	8.281	0.95	12.621	0.098
0.50	12.000	7.639	1.00	12.000	0.000

**Table 3:** Data used from Sze, Liu & Lo (2004) in the comparison with Hybrida shown in Figure 15 of a cantilever loaded by an end moment [50].

Group	Parameter	Value
Mesh	Element Type	s3f
	Number of elements	341
	Boundary conditions	Dirichlet: $x, y, z, M_y = 0$ at $x = 0$ Neumann: $+M_y$ at $x = L$
Material	Young's Modulus	1.2 MPa
	Poisson Ratio	0
	Density	$2700 \text{ kg m}^{-3}$
	Shell Thickness	0.1 m
Incremental-iterative Solver	Control Strategy	Arc-length
	Convergence Norm	Force
	Iteration step size	0.5
	Max. iterations	20
	Number of increments	395

**Table 4:** Experimental parameters used in Hybrida nonlinear static analysis shown in Figure 15 of a cantilever subjected to an end moment.

### Cantilever subjected to end moment

The parameters and data listed here originate from section 3.3 of Popular Benchmark Problems for Geometric Nonlinear Analysis of Shells [50].

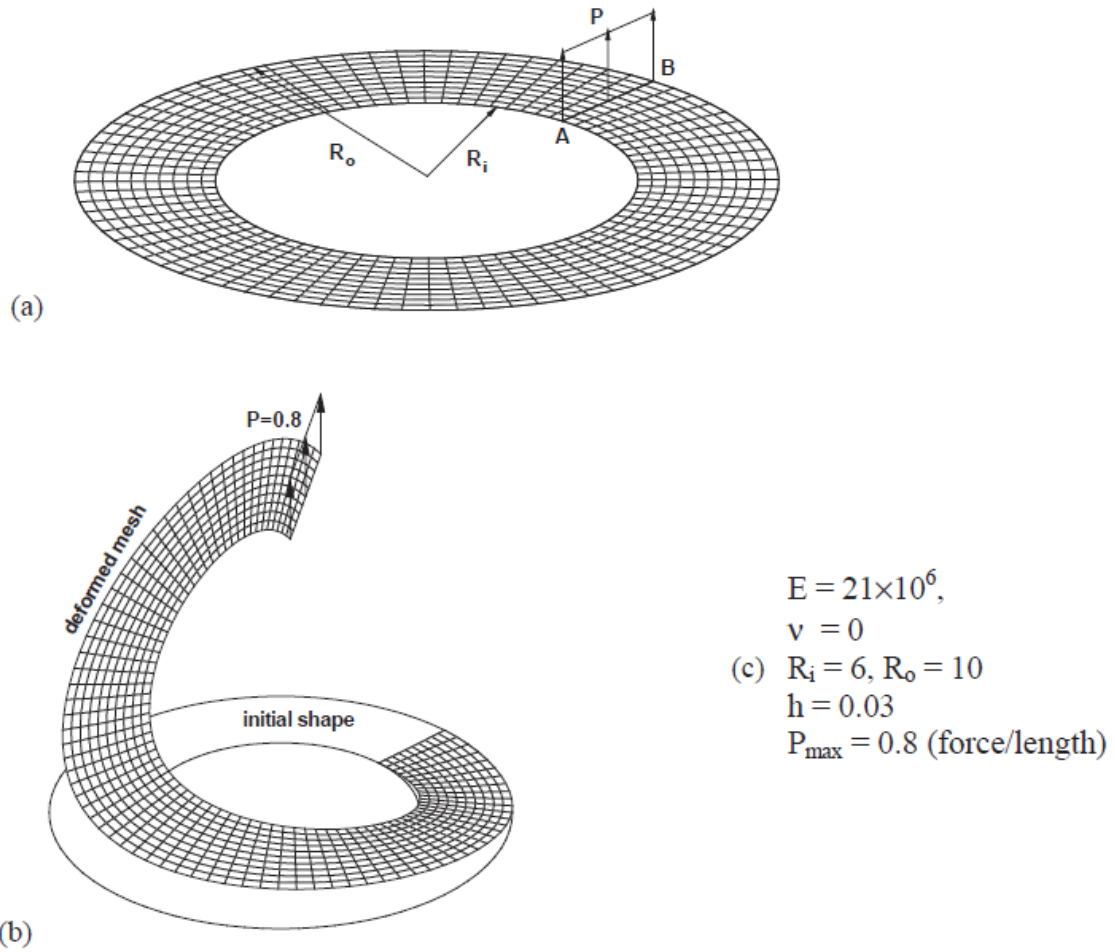


**Figure 47:** (a) Slit annular plate loaded with a line shear force  $P$ . (b) Deformed mesh under maximum load. (c) Material constants and geometric parameters used in this experiment. Adapted from Sze, Liu & Lo (2004) [50].

$P/P_{\max}$	$W_A$	$W_B$	$P/P_{\max}$	$W_A$	$W_B$
0.025	1.305	1.789	0.50	10.468	13.768
0.05	2.455	3.370	0.55	10.876	14.240
0.075	3.435	4.720	0.60	11.257	14.674
0.10	4.277	5.876	0.65	11.620	15.081
0.125	5.007	6.872	0.70	11.970	15.469
0.15	5.649	7.736	0.75	12.310	15.482
0.20	6.725	9.160	0.80	12.642	16.202
0.25	7.602	10.288	0.85	12.966	16.550
0.30	8.340	11.213	0.90	13.282	16.886
0.35	8.974	11.992	0.95	13.590	17.212
0.40	9.592	12.661	1.00	13.891	17.528
0.45	10.023	13.247			

**Table 5:** Data used from Sze, Liu & Lo (2004) in the comparison with HybridA shown in Figure 18 of a slit annular plate loaded with a line force [50].

Group	Parameter	Value
Mesh	Element Type	s3f
	Number of elements	266
	Boundary conditions	Dirichlet: $x, y, z, M_y = 0$ at $\theta = A+1^\circ$ Neumann: $+F_z$ at $\theta = A$
Material	Young's Modulus	21 MPa
	Poisson Ratio	0
	Density	$2700 \text{ kg m}^{-3}$
	Shell Thickness	0.03 m
Incremental-iterative Solver	Control Strategy	Arc-length
	Convergence Norm	Force
	Iteration step size	0.5
	Max. iterations	20
	Number of increments	215

**Table 6:** Experimental parameters used in Hybrid nonlinear static analysis shown in Figure 18 of a slit annular plate subjected to a line force.

## B.2 Parameters for verification of Modal Derivatives

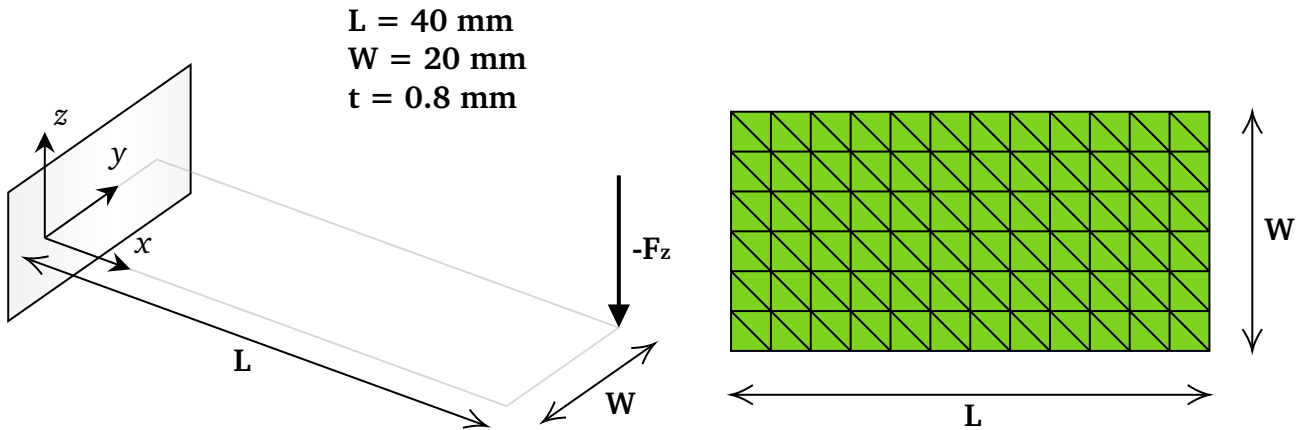


**Figure 48:** Short cantilever plate as discussed in subsection 2.2. Adapted from Tiso (2011) [59].

Group	Parameter	Value
Mesh	Element Type	s3f
	Number of elements	151
	Boundary conditions	Dirichlet: $x, y, z, M_y = 0$ at $x = 0$ Neumann: $-F_z$ at $x = L, y = W$
Material	Young's Modulus	70 GPa
	Poisson Ratio	0.3
	Density	$2700 \text{ kg m}^{-3}$
	Shell Thickness	0.0008 m

**Table 7:** Experimental parameters used in Hybrid to re-create the Static Modal Derivatives in Figure 21 as computed by Tiso in 2011 [59].

### B.3 Parameters for model order reduction for nonlinear dynamics

#### Simply supported plate with immovable edges (Amabili, 2004)

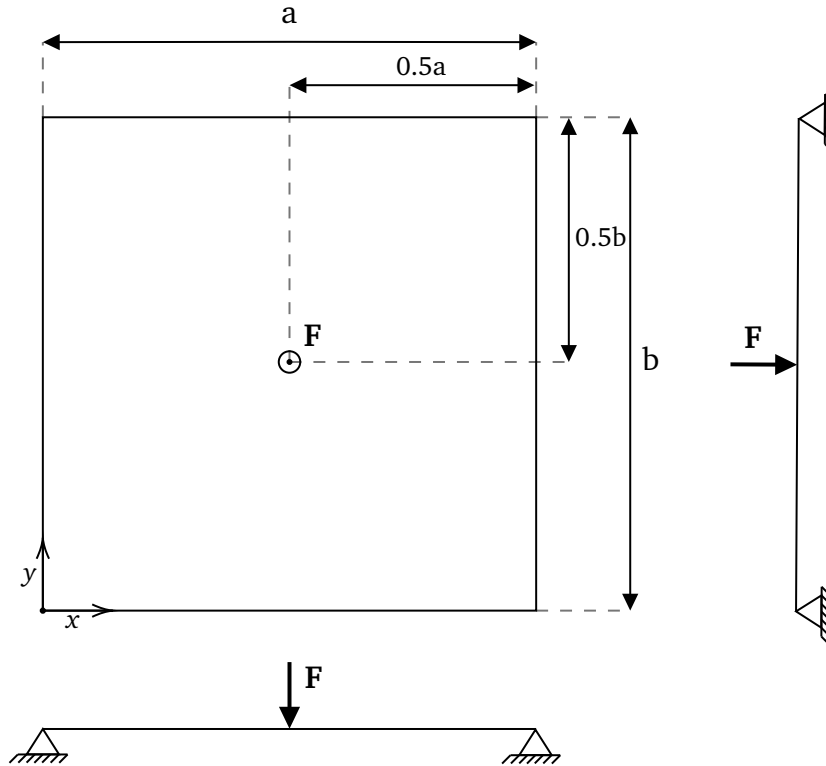


**Figure 49:** Rectangular plate with simply supported immovable edges as discussed in subsection 2.3.1. Adapted from Amabili (2004) and Pilania (2021) [47, 87].

Group	Parameter	Value
Mesh	Element Type	s3f
	Number of elements	2021
	Boundary conditions	Dirichlet: $x, y, z = 0$ at $x = 0, a$ and $y = 0, b$ Neumann: $-z$ at $x = 0.5a, y = 0.5b$
Material	Young's Modulus	70 GPa
	Poisson Ratio	0.3
	Density	$2778 \text{ kg m}^{-3}$
	Shell Thickness	0.001 m
ROM	Vibration Modes	$\phi_1$ (1 DoF), $\phi_1, \phi_5, \phi_{11}, \phi_{16}, \phi_{21}, \phi_{38}$ (6 DoF)
	Modal Derivatives	$\phi_1, \theta_{11}^{ST}$ (2 DoFs, Intrusive SMD)
	Modal Damping $\zeta_1$	0.065
AUTO	Forcing value	1.74
	Forcing step size	0.005
	Continuation parameter	Normalized frequency $\Omega/\Omega_0$
	Continuation range	[0.8, 1.8]
	Continuation step size	0.005

**Table 8:** Experimental parameters used in Hybrid nonlinear dynamic analysis shown in Figure 23 of a simply supported plate with immovable edges, shown in Figure 49 [47].

**Simply supported plate with movable edges (Amabili, 2004)**

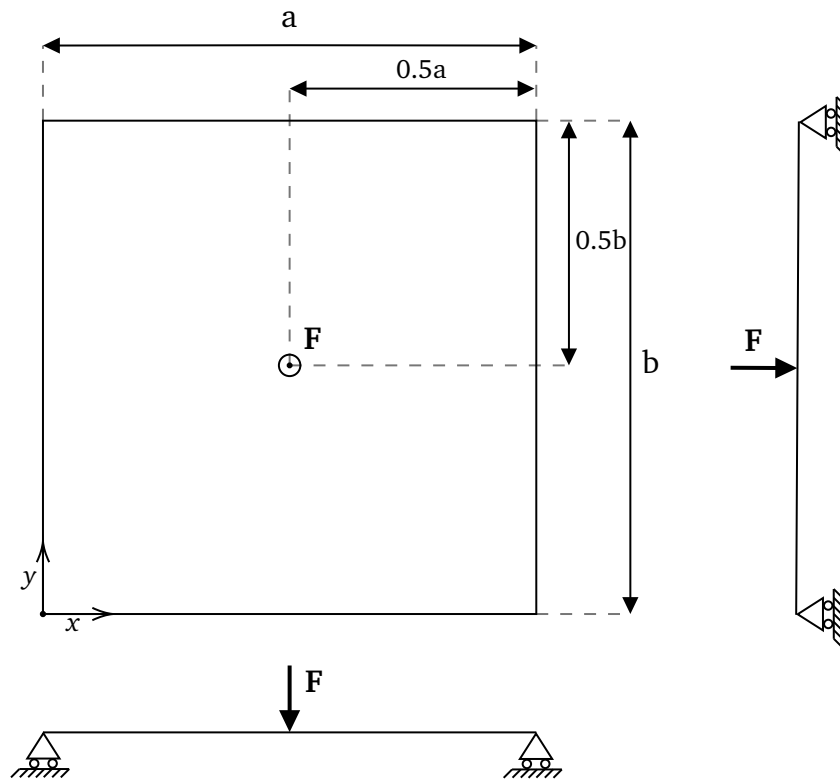


**Figure 50:** Rectangular plate with simply supported movable edges. Adapted from Amabili (2004) and Pilia (2021) [47, 87].

Group	Parameter	Value
Mesh	Element Type	s3f
	Number of elements	2021
	Boundary conditions	Dirichlet: $y, z = 0$ at $x = 0, a$ and Dirichlet: $x, z = 0$ at $y = 0, b$ Neumann: $-z$ at $x = 0.5a, y = 0.5b$
Material	Young's Modulus	70 GPa
	Poisson Ratio	0.3
	Density	$2778 \text{ kg m}^{-3}$
	Shell Thickness	0.001 m
ROM	Vibration Modes	$\phi_1$ (1 DoF) , $\phi_1, \phi_5, \phi_{11}, \phi_{16}, \phi_{17}$ (5 DoF)
	Modal Derivatives	$\phi_1, \theta_{11}^{ST}$ (2 DoFs, Intrusive SMD)
	Modal Damping $\zeta_1$	$\phi_1, \phi_5, \phi_{11}, \theta_{11}^{ST}, \theta_{15}^{ST}, \theta_{1-11}^{ST}, \theta_{55}^{ST}, \theta_{5-11}^{ST}, \theta_{11-11}^{ST}$ (9 DoFs)
AUTO	Forcing value	0.49
	Forcing step size	0.005
	Continuation parameter	Normalized frequency $\Omega/\Omega_0$
	Continuation range	[0.8, 2.0]
	Continuation step size	0.005

**Table 9:** Experimental parameters used in Hybrid nonlinear dynamic analysis shown in Figure 25 of a simply supported plate with movable edges, shown in Figure 50 [47].

## Vertical Cantilever (Malatkar, 2003)

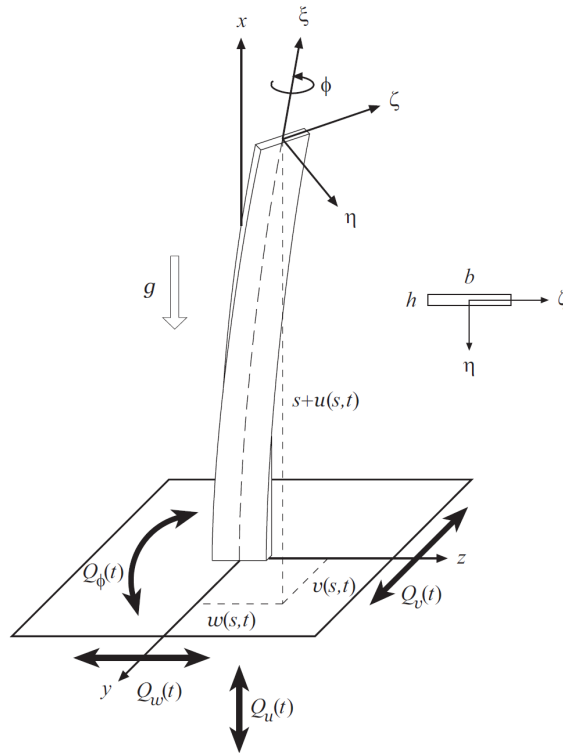


**Figure 51:** Vertical cantilever as discussed in subsection 2.3.3.

Group	Parameter	Value
Mesh	Element Type	s3f
	Number of elements	836
	Boundary conditions	Dirichlet: $x, y, z, M_y = 0$ at $x = 0$ Neumann: $+y$ at $x = L = 484.759\text{mm}$
Material	Young's Modulus	207 GPa
	Poisson Ratio	0.3
	Density	$7810 \text{ kg m}^{-3}$
	Shell Thickness	$0.00079375 \text{ m}$
ROM	Vibration Modes	$\phi_3$ (1 DoF), $\phi_3, \phi_{29}, \phi_{60}, \phi_{84}, \phi_{104}$ (5 DoF), $\phi_3, \phi_{29}, \phi_{60}, \phi_{84}, \phi_{104}, \phi_{122}, \phi_{152}, \phi_{180}$ (8 DoF)
	Modal Derivatives	$\phi_3, \theta_{33}^{\text{ST}}$ (2 DoFs, Intrusive SMD)
	Modal Damping $\zeta_3$	0.00252 for $F = 0.0011$ , 0.002814 for $F = 0.00165$ , 0.003114 for $F = 0.0022$ (Table 3.5, Malatkar)
AUTO	Forcing value	0.0011, 0.00165, 0.0022
	Forcing step size	$0.05 * \text{Forcing value}$
	Continuation parameter	Normalized frequency $\Omega/\Omega_0$
	Continuation range	[0.5, 4.0]
	Continuation step size	0.0025

**Table 10:** Experimental parameters used in Hybrid nonlinear dynamic analysis shown in Figures 28 and 29 of the third mode of a vertical cantilever, shown in Figure 51 [44].

### Double clamped MEMS beam (Vizzacarro, 2021)

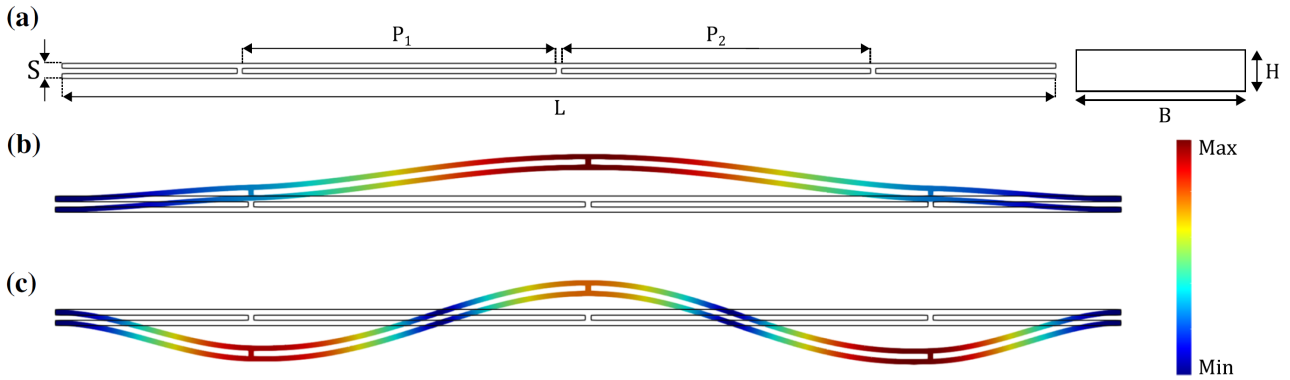


**Figure 52:** Double-clamped MEMS beam. Reproduced from Vizzacarro (2021) [83].

Group	Parameter	Value
Mesh	Element Type	s3f
	Number of elements	96845
	Length	0.00100565 m
	Boundary conditions	Dirichlet: $x, y, z, M_y = 0$ at $x = 0, L$ Neumann: $+y$ at $x = 0.5L$
Material	Young's Modulus	167 GPa
	Poisson Ratio	0.22
	Density	2350 kg m <sup>-3</sup>
	Shell Thickness	0.000012 m
ROM	Vibration Modes	$\phi_1, \phi_2, \phi_3, \phi_4, \phi_5, \phi_6, \phi_7, \phi_8, \phi_9, \phi_{10}$ (10 DoFs) $\phi_1, \phi_2, \phi_3, \phi_4, \theta_{11}^{ST}, \theta_{12}^{ST}, \theta_{22}^{ST}, \theta_{33}^{ST}, \theta_{14}^{ST}, \theta_{44}^{ST}$ (10 DoFs)
	Modal Damping $\zeta_1$	0.0003333
AUTO	Forcing value	$1.5 * 10^{-8}$ N
	Forcing step size	$0.05 * \text{Forcing value}$
	Continuation parameter	Normalized frequency $\Omega/\Omega_0$
	Continuation range	[0.8, 1.2]
	Continuation step size	0.0005

**Table 11:** Experimental parameters used in Hybrid nonlinear dynamic analysis shown in Figure 31 of a double clamped MEMS beam, shown- in Figure 52 [83].

### Double-curved shallow shell (Amabili, 2005)

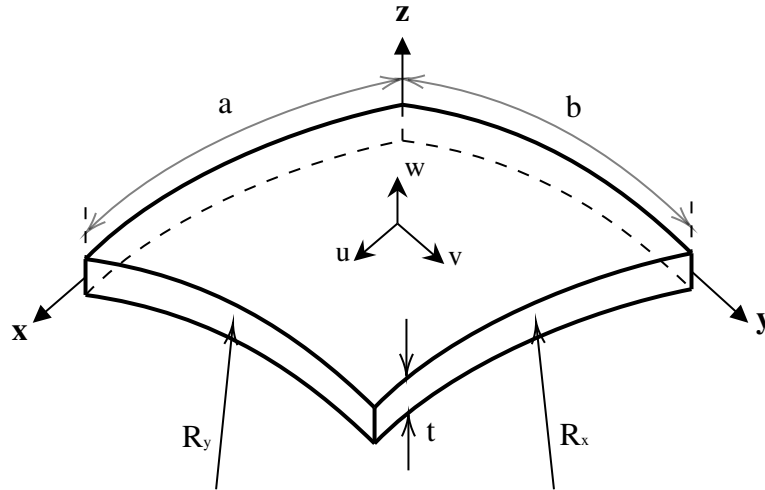


**Figure 53:** Double curved shallow shell with simply supported movable edges. Adapted from Amabili (2005)[51].

Group	Parameter	Value
Mesh	Element Type	s3f
	Number of elements	22992
	Lengths a, b	0.1 m
	Radius of Curvature $R_x, R_y$	1 m
	Boundary conditions	Dirichlet: $y, z = 0$ at $x = 0, a$ and Dirichlet: $x, z = 0$ at $y = 0, b$ Neumann: $-z$ at $x = 0.5a, y = 0.5b$
Material	Young's Modulus	206 GPa
	Poisson Ratio	0.3
	Density	$7800 \text{ kg m}^{-3}$
	Shell Thickness	0.001 m
ROM	Vibration Modes	$\phi_1$ (1 DoF)
	Modal Derivatives	$\phi_1, \theta_{11}^{ST}$ (2 DoFs)
	Modal Damping $\zeta_1$	0.004
AUTO	Forcing value	31.2 N
	Forcing step size	0.1
	Continuation parameter	Normalized frequency $\Omega/\Omega_0$
	Continuation range	[0.6, 2]
	Continuation step size	0.0025

**Table 12:** Experimental parameters used in Hybrid nonlinear dynamic analysis shown in Figure 31 of a double clamped MEMS beam, shown in Figure 52 [83].

**Circular cylindrical shell (Kurylov, 2011)**

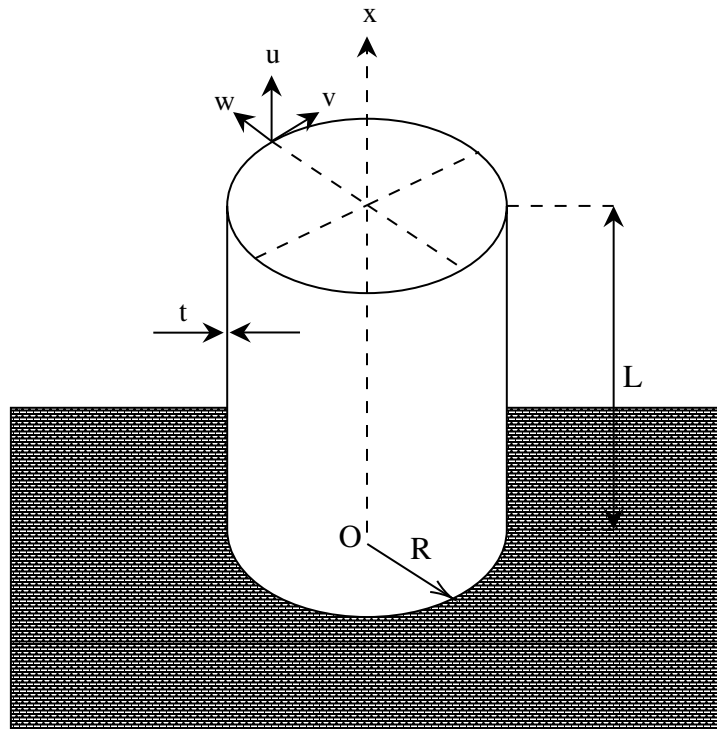


**Figure 54:** Circular cylindrical shell with clamped bottom edge. Adapted from Kurylov (2011) [58].

Group	Parameter	Value
Mesh	Element Type	s3f
	Number of elements	98416
	L	0.48 m
	R	0.24 m
	Boundary conditions	Dirichlet: $x, y, z = 0$ at $x = 0$ Neumann: $F_w$ at $x = 0.5L, \theta = 0$
Material	Young's Modulus	4.65 GPa
	Poisson Ratio	0.38
	Density	$1400 \text{ kg m}^{-3}$
	Shell Thickness	0.000254 m
ROM	Vibration Modes	$\phi_1$ (1 DoF)
	Modal Derivatives	$\phi_1, \theta_{11}^{ST}$ (2 DoFs)
	Modal Damping $\zeta_1$	0.0005
AUTO	Forcing value	0.0012 N
	Forcing step size	0.00005
	Continuation parameter	Normalized frequency $\Omega/\Omega_0$
	Continuation range	[0.8, 1.5]
	Continuation step size	0.005

**Table 13:** Experimental parameters used in Hybrid nonlinear dynamic analysis, results shown in Figure 34, of a clamped circular cylindrical shell clamped MEMS beam, shown in Figure 54 [58].

## References

- [1] Walter Ritz. “Über eine neue Methode zur Lösung gewisser Variationsprobleme der mathematischen Physik.” In: *Journal für die reine und angewandte Mathematik* 1909.135 (1909), pp. 1–61.
- [2] Raymond T Birge. “The calculation of errors by the method of least squares”. In: *Physical Review* 40.2 (1932), p. 207.
- [3] RICHARD BELLMAN and RAND CORP SANTA MONICA CA. “DYNAMIC PROGRAMMING”. In: (1956).
- [4] Hu-Nan Chu and George Herrmann. “Influence of large amplitudes on free flexural vibrations of rectangular elastic plates”. In: (1956).
- [5] Reinhardt Mathias Rosenberg. “Normal modes of nonlinear dual-mode systems”. In: (1960).
- [6] Robert J Guyan. “Reduction of stiffness and mass matrices”. In: *AIAA journal* 3.2 (1965), pp. 380–380.
- [7] Walter C Hurty. “Dynamic analysis of structural systems using component modes”. In: *AIAA journal* 3.4 (1965), pp. 678–685.
- [8] Bruce Irons. “Structural eigenvalue problems-elimination of unwanted variables”. In: *AIAA journal* 3.5 (1965), pp. 961–962.
- [9] DE Newland. “On the methods of Galerkin, Ritz and Krylov-Bogoliubov in the theory of non-linear vibrations”. In: *International Journal of Mechanical Sciences* 7.3 (1965), pp. 159–172.
- [10] RM Rosenberg. “On nonlinear vibrations of systems with many degrees of freedom”. In: *Advances in applied mechanics*. Vol. 9. Elsevier, 1966, pp. 155–242.
- [11] Robert L Goldman. “Vibration analysis by dynamic partitioning.” In: *AIAA journal* 7.6 (1969), pp. 1152–1154.
- [12] Richard H MacNeal. “A hybrid method of component mode synthesis”. In: *Computers & Structures* 1.4 (1971), pp. 581–601.
- [13] S Rubin. “An improved component-mode representation”. In: *15th Structural Dynamics and Materials Conference*. 1974, p. 386.
- [14] Eusebius J Doedel. “AUTO: A program for the automatic bifurcation analysis of autonomous systems”. In: *Congr. Numer* 30.265-284 (1981), pp. 25–93.
- [15] Edward L Wilson, Ming-Wu Yuan, and John M Dickens. “Dynamic analysis by direct superposition of Ritz vectors”. In: *Earthquake Engineering & Structural Dynamics* 10.6 (1982), pp. 813–821.
- [16] David J Ewins. “Modal testing: theory and practice, Vol. 15”. In: *Letchworth: Research studies press* (1984).
- [17] Bahram Nour-Omid and Ray W Clough. “Dynamic analysis of structures using Lanczos co-ordinates”. In: *Earthquake engineering & structural dynamics* 12.4 (1984), pp. 565–577.
- [18] Sergio R Idelsohn and Alberto Cardona. “A reduction method for nonlinear structural dynamic analysis”. In: *Computer Methods in Applied Mechanics and Engineering* 49.3 (1985), pp. 253–279.

- [19] Pierre Léger, Edward L Wilson, and Ray W Clough. *The use of load dependent vectors for dynamic and earthquake analyses*. Earthquake Engineering Research Center, College of Engineering, University . . ., 1986.
- [20] PTLM Van Woerkom et al. “Mathematical models of flexible spacecraft dynamics: a survey of order reduction approaches”. In: *Control-Theory and Advanced Technology* 6.4 (1990), pp. 609–632.
- [21] CK Chiang, C Mei, and CE Gray Jr. “Finite element large-amplitude free and forced vibrations of rectangular thin composite plates”. In: (1991).
- [22] Steven Shaw and Christophe Pierre. “Non-linear normal modes and invariant manifolds”. In: *Journal of sound and Vibration* 150.1 (1991), pp. 170–173.
- [23] Barna Szabó and Ivo Babuška. *Finite element analysis*. John Wiley & Sons, 1991.
- [24] N Bouhaddi and R Fillod. “A method for selecting master DOF in dynamic substructuring using the Guyan condensation method”. In: *Computers & Structures* 45.5-6 (1992), pp. 941–946.
- [25] M Chiba. “Non-linear hydroelastic vibration of a cantilever cylindrical tank—I. Experiment (empty case)”. In: *International journal of non-linear mechanics* 28.5 (1993), pp. 591–599.
- [26] Fred van Keulen, Adrie Bout, and Leo J Ernst. “Nonlinear thin shell analysis using a curved triangular element”. In: *Computer methods in applied mechanics and engineering* 103.1-2 (1993), pp. 315–343.
- [27] Alexander P Seyranian. “Sensitivity analysis of multiple eigenvalues”. In: *Journal of Structural Mechanics* 21.2 (1993), pp. 261–284.
- [28] Steven W Shaw and Christophe Pierre. “Normal modes for non-linear vibratory systems”. In: *Journal of sound and vibration* 164.1 (1993), pp. 85–124.
- [29] Mehmet A Akgun. “New family of modal methods for calculating eigenvector derivatives”. In: *AIAA journal* 32.2 (1994), pp. 379–386.
- [30] Adriaan Bout. “A finite element approach to nonlinear thin shell analysis.” In: (1994).
- [31] Ahmed K Noor. “Recent advances and applications of reduction methods”. In: (1994).
- [32] Steven W Shaw and Christophe Pierre. “Normal modes of vibration for non-linear continuous systems”. In: *Journal of sound and vibration* 169.3 (1994), pp. 319–347.
- [33] PMA Slaats, J De Jongh, and AAHJ Sauren. “Model reduction tools for nonlinear structural dynamics”. In: *Computers & structures* 54.6 (1995), pp. 1155–1171.
- [34] GH Golub, CF Van Loan, and Matrix Computations. “Johns Hopkins Univ”. In: *Press, Baltimore, Maryland, 3rd ed. edition* (1996).
- [35] Alexander Vakakis. “Non-linear normal modes (NNMs) and their applications in vibration theory: an overview”. In: *Mechanical systems and signal processing* 11.1 (1997), pp. 3–22.
- [36] Eusebius J Doedel et al. “Auto97”. In: *Continuation and bifurcation software for ordinary differential equations* (1998).
- [37] Richard B Lehoucq, Danny C Sorensen, and Chao Yang. *ARPACK users’ guide: solution of large-scale eigenvalue problems with implicitly restarted Arnoldi methods*. SIAM, 1998.
- [38] Jianmin Gu, Zheng-Dong Ma, and Gregory M Hulbert. “A new load-dependent Ritz vector method for structural dynamics analyses: quasi-static Ritz vectors”. In: *Finite Elements in Analysis and Design* 36.3-4 (2000), pp. 261–278.

- [39] Kazuteru Garatani et al. “Three-dimensional elasto-static analysis of 100 million degrees of freedom”. In: *Advances in Engineering Software* 32.7 (2001), pp. 511–518.
- [40] Andrew V Knyazev. “Toward the optimal preconditioned eigensolver: Locally optimal block preconditioned conjugate gradient method”. In: *SIAM journal on scientific computing* 23.2 (2001), pp. 517–541.
- [41] Alexander F Vakakis et al. *Normal modes and localization in nonlinear systems*. Springer, 2001.
- [42] Mark Adams. “Evaluation of three unstructured multigrid methods on 3D finite element problems in solid mechanics”. In: *International Journal for Numerical Methods in Engineering* 55.5 (2002), pp. 519–534.
- [43] Pedro Ribeiro. “Periodic vibration of plates with large displacements”. In: *AIAA journal* 40.1 (2002), pp. 185–188.
- [44] Pramod Malatkar. “Nonlinear vibrations of cantilever beams and plates”. PhD thesis. Virginia Polytechnic Institute and State University, 2003.
- [45] Alexander A Muravyov and Stephen A Rizzi. “Determination of nonlinear stiffness with application to random vibration of geometrically nonlinear structures”. In: *Computers & Structures* 81.15 (2003), pp. 1513–1523.
- [46] Mark F Adams et al. “Ultrascale implicit finite element analyses in solid mechanics with over a half a billion degrees of freedom”. In: *SC’04: Proceedings of the 2004 ACM/IEEE conference on Supercomputing*. IEEE, 2004, pp. 34–34.
- [47] Marco Amabili. “Nonlinear vibrations of rectangular plates with different boundary conditions: theory and experiments”. In: *Computers & structures* 82.31-32 (2004), pp. 2587–2605.
- [48] F Ma and CH Ng. “On the orthogonality of natural modes of vibration”. In: *Mechanics Research Communications* 31.3 (2004), pp. 295–299.
- [49] Zu-Qing Qu. *Model Order Reduction Techniques with Applications in Finite Element Analysis: With Applications in Finite Element Analysis*. Springer Science & Business Media, 2004.
- [50] KY Sze, XH Liu, and SH Lo. “Popular benchmark problems for geometric nonlinear analysis of shells”. In: *Finite elements in analysis and design* 40.11 (2004), pp. 1551–1569.
- [51] Marco Amabili. “Non-linear vibrations of doubly curved shallow shells”. In: *International Journal of Non-Linear Mechanics* 40.5 (2005), pp. 683–710.
- [52] Jernej Barbič and Doug L James. “Real-time subspace integration for St. Venant-Kirchhoff deformable models”. In: *ACM transactions on graphics (TOG)* 24.3 (2005), pp. 982–990.
- [53] AC Hindmarsh and LR Petzold. “LSODA, ordinary differential equation solver for stiff or non-stiff system”. In: (2005).
- [54] Gaetan Kerschen et al. “The method of proper orthogonal decomposition for dynamical characterization and order reduction of mechanical systems: an overview”. In: *Nonlinear dynamics* 41.1 (2005), pp. 147–169.
- [55] Rubens Sampaio and Christian Soize. “Remarks on the efficiency of POD for model reduction in non-linear dynamics of continuous elastic systems”. In: *International Journal for numerical methods in Engineering* 72.1 (2007), pp. 22–45.

- [56] Luo ZhangPing and Xiang JinWu. “Novel modal method for efficient calculation of complex eigenvector derivatives”. In: *AIAA journal* 45.6 (2007), pp. 1406–1414.
- [57] Gaëtan Kerschen et al. “Nonlinear normal modes, Part I: A useful framework for the structural dynamicist”. In: *Mechanical systems and signal processing* 23.1 (2009), pp. 170–194.
- [58] Ye Kurylov and Marco Amabili. “Nonlinear vibrations of clamped-free circular cylindrical shells”. In: *Journal of sound and vibration* 330.22 (2011), pp. 5363–5381.
- [59] Paolo Tiso. “Effective modal derivatives based reduction method for geometrically nonlinear structures”. In: *International Design Engineering Technical Conferences and Computers and Information in Engineering Conference*. Vol. 54785. 2011, pp. 399–406.
- [60] Paolo Tiso. “Optimal second order reduction basis selection for nonlinear transient analysis”. In: *Modal Analysis Topics, Volume 3*. Springer, 2011, pp. 27–39.
- [61] Marc P Mignolet et al. “A review of indirect/non-intrusive reduced order modeling of nonlinear geometric structures”. In: *Journal of Sound and Vibration* 332.10 (2013), pp. 2437–2460.
- [62] Gil Ho Yoon et al. “Transient quasi-static Ritz vector (TQSRV) method by Krylov subspaces and eigenvectors for efficient contact dynamic finite element simulation”. In: *Applied Mathematical Modelling* 39.9 (2015), pp. 2740–2762.
- [63] Steven L Brunton, Joshua L Proctor, and J Nathan Kutz. “Discovering governing equations from data by sparse identification of nonlinear dynamical systems”. In: *Proceedings of the national academy of sciences* 113.15 (2016), pp. 3932–3937.
- [64] George Haller and Sten Ponsioen. “Nonlinear normal modes and spectral submanifolds: existence, uniqueness and use in model reduction”. In: *Nonlinear dynamics* 86.3 (2016), pp. 1493–1534.
- [65] J Nathan Kutz et al. *Dynamic mode decomposition: data-driven modeling of complex systems*. SIAM, 2016.
- [66] Long Wu and Paolo Tiso. “Nonlinear model order reduction for flexible multibody dynamics: a modal derivatives approach”. In: *Multibody System Dynamics* 36.4 (2016), pp. 405–425.
- [67] George Haller and Sten Ponsioen. “Exact model reduction by a slow–fast decomposition of nonlinear mechanical systems”. In: *Nonlinear Dynamics* 90.1 (2017), pp. 617–647.
- [68] Bart Holtzer. “Topology Optimization of Geometrically Nonlinear Structures”. In: (2017).
- [69] Shobhit Jain et al. “A quadratic manifold for model order reduction of nonlinear structural dynamics”. In: *Computers & Structures* 188 (2017), pp. 80–94.
- [70] Johannes B Rutzmoser et al. “Generalization of quadratic manifolds for reduced order modeling of nonlinear structural dynamics”. In: *Computers & Structures* 192 (2017), pp. 196–209.
- [71] Robert Szalai, David Ehrhardt, and George Haller. “Nonlinear model identification and spectral submanifolds for multi-degree-of-freedom mechanical vibrations”. In: *Proceedings of the Royal Society A: Mathematical, Physical and Engineering Sciences* 473.2202 (2017), p. 20160759.
- [72] Shobhit Jain and Paolo Tiso. “Simulation-free hyper-reduction for geometrically nonlinear structural dynamics: A quadratic manifold lifting approach”. In: *Journal of Computational and Nonlinear Dynamics* 13.7 (2018).

- [73] Koen Markestein. “Finite element based analysis and validation for nonlinear structural dynamics”. In: (2018).
- [74] Sten Ponsioen, Tiemo Pedergnana, and George Haller. “Automated computation of autonomous spectral submanifolds for nonlinear modal analysis”. In: *Journal of Sound and Vibration* 420 (2018), pp. 269–295.
- [75] Johannes Rutzmoser. “Model order reduction for nonlinear structural dynamics”. PhD thesis. Technische Universität München, 2018.
- [76] Cees SM Sombroek et al. “Numerical computation of nonlinear normal modes in a modal derivative subspace”. In: *Computers & Structures* 195 (2018), pp. 34–46.
- [77] Arthur Givois et al. “On the frequency response computation of geometrically nonlinear flat structures using reduced-order finite element models”. In: *Nonlinear Dynamics* 97.2 (2019), pp. 1747–1781.
- [78] M Cruz Varona et al. “A novel derivation for modal derivatives based on Volterra series representation and its use in nonlinear model order reduction”. In: *Proc. of 7 th ECCOMAS Thematic Conference on Computational Methods in Structural Dynamics and Earthquake Engineering, June*. 2019, pp. 24–26.
- [79] Long Wu et al. “A modal derivatives enhanced Rubin substructuring method for geometrically nonlinear multibody systems”. In: *Multibody system dynamics* 45.1 (2019), pp. 57–85.
- [80] Zijun Wu et al. “Topology optimization of hierarchical lattice structures with substructuring”. In: *Computer Methods in Applied Mechanics and Engineering* 345 (2019), pp. 602–617.
- [81] Steven L Brunton and J Nathan Kutz. “7 Data-driven methods for reduced-order modeling”. In: *Snapshot-Based Methods and Algorithms* (2020), p. 307.
- [82] Sten Ponsioen, Shobhit Jain, and George Haller. “Model reduction to spectral submanifolds and forced-response calculation in high-dimensional mechanical systems”. In: *Journal of Sound and Vibration* 488 (2020), p. 115640.
- [83] Alessandra Vizzaccaro, Loïc Salles, and Cyril Touzé. “Comparison of nonlinear mappings for reduced-order modelling of vibrating structures: normal form theory and quadratic manifold method with modal derivatives”. In: *Nonlinear Dynamics* (2020), pp. 1–36.
- [84] FEA DIANA. “Diana User’s Manual, Release 10.5”. In: *DIANA FEA BV* (2021). URL: <https://dianafea.com/manuals/d105/Diana.html>.
- [85] George Haller. *Fast reduction of nonlinear finite-element models to spectral submanifolds*. NODYCON. 2021.
- [86] Morteza Karamooz Mahdiabadi et al. “A non-intrusive model-order reduction of geometrically nonlinear structural dynamics using modal derivatives”. In: *Mechanical Systems and Signal Processing* 147 (2021), p. 107126.
- [87] Yogesh Kumar Pilania. “Finite element-based model order reduction for nonlinear structural dynamics”. In: (2021).
- [88] Yichang Shen et al. “Comparison of Reduction Methods for Finite Element Geometrically Nonlinear Beam Structures”. In: *Vibration* 4.1 (2021), pp. 175–204.
- [89] Paolo Tiso. Online meeting with Paolo Tiso to discuss computation of Modal Derivatives. Oct. 2021.